New Electrolytes for CO_2 Electrolysis Cells

Mollerup, Pia Lolk

Publication date:
2013

Document Version
Publisher's PDF, also known as Version of record

New Electrolytes for CO_2 Electrolysis Cells

PhD Thesis

Pia Lolk Mollerup

Department of Energy Conversion and Storage
Technical University of Denmark
December 2012

Acknowledgements

The present dissertation is submitted to the Technical University of Denmark and partially fulfills the requirements for the PhD degree. The work has been carried out at the Department of Energy Conversion and Storage with Head of Programme Peter Holtappels as main supervisor and Senior Scientists Peter Blennow and Nikolaos Bonanos as co-supervisors. The PhD scholarship was funded by the Technical University of Denmark as part of the European Graduate School on Sustainable Energy Technology.

First and foremost, I would like to thank all my supervisors for their help and guidance throughout the project and for always being available for questions and inspiring scientific discussions. I would like to thank Research Professor Mogens B. Mogensen for coming up with the idea for the project and for giving me the opportunity to pursue a PhD degree. A special thanks to Peter Holtappels for doing an excellent job in taking over as main supervisor from Mogens B. Mogensen. I would also like to thank Peter Blennow for being a fantastic supervisor and for always being around when I needed help. I hope many PhD students in the future will have the benefit of having him as a supervisor. A special thanks to Nikolaos Bonanos for being an excellent supervisor and for helping me write my very first paper. Also a special thanks to Christodoulos Chatzichristodoulou for helping me with the setups and for

answering my questions whenever I asked.

I would like to thank all the technicians and lab technicians for helping me with setups, equipment and in the various labs. A special thanks to Annelise Mikkelsen and Charlotte Maul for making the ceramic lab an enjoyable place to work.

My fantastic colleges Jonathan Hallinder, Frank Allebrod and Alberto Lapina also deserves to be acknowledged for always being helpful and making my time at Risø extra fun and exciting. A special thanks to Ane S. Christiansen for always smiling no matter how dark the day may seem and for many good discussions in our office.

I would like to thank my family and all my friends for their love and support. A special thanks to Sarah Maria, Christian, Susan and Mette for always being there for me, whenever I needed them. Finally, a very special thanks to my incredible supportive and patient boyfriend Kristian.

Abstract

The aim of this thesis has been to explore the potential of aqueous immobilized K_2CO_3 as a possible electrolyte for co-electrolysis of CO_2 and water at approx. 200 °C. This has been done by exploring the properties of pure K_2CO_3 (aq) and immobilized K_2CO_3 (aq) as well as the properties of the matrix materials $SrTiO_3$ and TiO_2.

Conductivity measurements of aqueous K_2CO_3 have been performed using the van der Pauw technique and a specially designed sample holder with Pt wires as electrodes. The conductivity at ambient temperature was found to increase with concentration up to 30-40 wt% K_2CO_3 (aq), and decline at higher concentrations. Furthermore, the conductivity of 5-30 wt% aqueous K_2CO_3 was measured up to 180-200 °C at 30 bar. The highest conductivity measured was 1.34 S/cm at 172 °C for 30 wt% K_2CO_3 (aq). The conductivity was found to increase with concentration and also temperature for 5-15 wt% K_2CO_3 (aq). For 20 and 30 wt% K_2CO_3 (aq) the conductivity increased with temperature up to 150 and 180 °C, respectively, and then a drop was observed, due to precipitation. The activation energy was obtained by fitting the data to a modified Arrhenius equation and was found to be in the range 0.14-0.17 eV. Furthermore, the activation energy was found not to be concentration dependent.

Thermodynamic equilibrium calculations were conducted using the program FactSage. The calculated concentration limits agreed with the observed experimental limits. It was found that in CO_2 atmosphere the main species in a 10 wt% K_2CO_3 (aq) solution are K^+ and HCO_3^-. The water partial pressure as well as the amount of water vapour at different temperatures, pressures and K_2CO_3 (aq) concentrations was also calculated using FactSage.

K_2CO_3 (aq) was immobilized in both $SrTiO_3$ and TiO_2. It was found that a loss of conductivity occurred when K_2CO_3 (aq) was immobilized, however, by increasing the porosity of the matrix the conductivity could be increased and the loss decreased. Archie's law, with a cementation exponent of 1.6, was found to give a very good fit of the measured conductivity as a function of open porosity at ambient temperature.

The conductivity of K_2CO_3 (aq) immobilized in $SrTiO_3$ or TiO_2 was measured at both ambient and elevated temperatures and pressures. It was found to increase with temperature and concentration unless precipitation occurred. The highest conductivity value measured was 0.21 S/cm at 130 °C for 30 wt% K_2CO_3 (aq) immobilized in $SrTiO_3$, the same value was also obtained for 10 wt% K_2CO_3 (aq) immobilized in $SrTiO_3$ at 175 °C. The highest conductivity value of K_2CO_3 (aq) immobilized in TiO_2 was 0.19 S/cm at 210 °C for 20 wt% K_2CO_3 (aq). The activation energy of K_2CO_3 (aq) immobilized in TiO_2 or $SrTiO_3$ was found to be in the same range as the activation energy of pure K_2CO_3 (aq) and was not concentration dependent.

For measurements in CO_2 atmosphere only TiO_2 could be used without any problems. Using $SrTiO_3$ resulted in undesired formation of the insulator $SrCO_3$. No loss of conductivity was observed for 10 wt% K_2CO_3 immobilized in TiO_2 when changing the atmosphere from N_2 to CO_2.

K_2CO_3 (aq) immobilized in TiO_2 shows good promise as a potential electrolyte for co-electrolysis of CO_2 and water at 200 °C.

Dansk resumé

Formålet med denne afhandling har været at undersøge muligheden for at anvende K_2CO_3 (aq) som elektrolyt til co-elektrolyse af CO_2 og vand ved ca 200 °C. Dette er blevet gjort ved at undersøge egenskaberne af rent K_2CO_3 (aq) og immobiliseret K_2CO_3 (aq) samt egenskaberne af matrix materialerne $SrTiO_3$ og TiO_2.

Ledningsevnemålinger af vandig K_2CO_3 er blevet udført vha. van der Pauw teknikken og en special-designet prøveholder med Pt tråde som elektroder. Ved stuetemperatur blev det observeret at ledningsevnen steg med koncentrationen op til 30-40 wt% K_2CO_3 (aq), men faldt igen ved højere koncentrationer. Ledningsevnen af 5-30 wt% K_2CO_3 (aq) blev også målt op til 180-200 °C ved 30 bar. Den højeste målte ledningsevne var 1.34 S/cm ved 172 °C for 30 wt% K_2CO_3 (aq). Det blev observeret at ledningevnen steg med koncentration og temperatur for 5-15 wt% K_2CO_3 (aq). For 20 og 30 wt% K_2CO_3 (aq) steg ledningsevne med temperaturen op til hhv. 150 og 180 °C, herefter sås et fald grundet udfældning. Aktiveringsenergien blev bestemt vha. en modificeret Arrhenius ligning og var 0,14-0,17 eV. Ydermere sås der ingen sammenhæng mellem koncentrationen og aktiveringsenergien.

Termodynamiske ligevægtsberegninger blev udført ved brug af programmet

FactSage. De beregnede koncentrationsgrænser stemte godt overens med de eksperimentelt observerede. Det blev beregnet at i CO_2 atmosfære er de primære vandige specier i en 10 wt% K_2CO_3 (aq) opløsning hhv. K^+ og $HCO_3{}^-$. Vanddamptrykket samt mængden af vanddamp ved forskellige temperaturer, tryk og K_2CO_3 (aq) koncentrationer blev også beregnet vha. FactSage.

K_2CO_3 (aq) blev immobiliseret i både $SrTiO_3$ og TiO_2. Et tab i ledsningsevnen blev observeret når K_2CO_3 (aq) blev immobiliseret, dog kunne tabet mindskes ved at øge matricens porøsitet. Archies lov med en cementerings eksponent på 1,6 gav et godt fit af den målte ledningsevne som funktion af den åbne porøsitet ved stuetemperatur.

Ledningsevne af K_2CO_3 (aq) immobiliseret i $SrTiO_3$ eller TiO_2 blev målt ved både stuetemperatur og ved øgede temperaturer og tryk. Det blev observeret at ledningevnen steg med temperatur og koncentration såfremt udfældning ikke fandt sted. Den højeste målte ledningsevne var 0.21 S/cm ved 130 °C for 30 wt% K_2CO_3 (aq) immobiliseret i $SrTiO_3$, samme værdi blev også målt for 10 wt% K_2CO_3 (aq) immobiliseret i $SrTiO_3$ ved 175 °C. Den højst målte ledningsevne af K_2CO_3 (aq) immobiliseret i TiO_2 var 0.19 S/cm ved 210 °C for 20 wt% K_2CO_3 (aq). Aktiveringsenergien af K_2CO_3 (aq) immobiliseret i $SrTiO_3$ og TiO_2 var i samme interval som aktiveringsenergien af rent K_2CO_3 (aq) og var ikke koncentrationsafhængig.

Ved målinger i CO_2 atmosfære kan kun TiO_2 anvendes uden problemer. Anvendelse af $SrTiO_3$ resulterer i dannelse af det isolerende stof $SrCO_3$. Intet tab af ledningsevne blev observeret for 10 wt% K_2CO_3 immobiliseret i TiO_2 når atmosfæren blev ændret fra N_2 til CO_2.

K_2CO_3 (aq) immobiliseret i TiO_2 kan finde anvendelse som elektrolyt til co-elektrolyse af CO_2 og vand ved 200 °C.

Publications and Conference Contributions

Publications

I The conductivity of aqueous K_2CO_3 at elevated temperatures and pressures, measured using the AC van der Pauw technique. Pia Lolk Mollerup, Ane Sælland Christiansen, Nikolaos Bonanos and Mogens Mogensen. *Manuscript has been prepared based on Chapter 3 and submitted to Electrochimica Acta.*

II Electrical conductivity measurements of aqueous and immobilized potassium hydroxide. Frank Allebrod, Christodoulos Chatzichristodoulou, Pia Lolk Mollerup and Mogens Bjerg Mogensen, *International Journal of Hydrogen Energy* (2012), **37**, 16505-16514.

III High performance reversible electrochemical cell for H_2O electrolysis or conversion of CO_2 and H_2O to fuel, Frank Allebrod, Christodoulos Chatzichristodoulou, Pia Lolk Mollerup and Mogens Bjerg Mogensen, 2012. Patent Application EP12164019.7

Conference Contributions

I Electrolyte and Electrode Materials for CO_2 Electrolysis Cells at 300 °C. P. L. Mollerup. Oral presentation at the European Graduate School in Sustainable Energy, Spring Meeting, München, Germany, April 7-9, 2010.

II Electrolyte and Electrode Materials for CO_2 Electrolysis Cells at 300 °C. P. L. Mollerup. Oral presentation at meeting held in conjunction with the conference: Sustainable Fuels from CO_2, H_2O, and Carbon-Free Energy, Columbia University, New York, USA, June 4-5, 2010.

III Electrolyte and Electrode Materials for CO_2 Electrolysis Cells at 200-300 °C. Oral presentation at the European Graduate School in Sustainable Energy, winter school, Nyborg Strand, Denmark, December 9-11, 2010.

IV Conductivity of K_2CO_3 (aq) at 25-200 °C. P. Mollerup & M. Mogensen. Poster at Workshop on "Capture and conversion of CO_2 into sustainable hydrocarbon fuels" held at Comwell hotel, Roskilde, Denmark, April 11-15, 2011.

V Conductivity of K_2CO_3 (aq) at 25-200 °C. P. Mollerup & M. Mogensen. Poster at European graduate school (EGS): Summer School "'Energy and Materials from the sun"', Rolduc Abbey, Netherlands, June 20-23, 2011.

VI Conductivity of Aqueous K_2CO_3 up to 200 °C. P. L. Mollerup, A. S. Christiansen, C. Chatzichristodoulou and M. Mogensen. Oral presentation at the 220^{th} ECS meeting, Electrochemical Society, Boston, MA, USA, October 9-14, 2011.

VII Immobilized K_2CO_3 (aq) as a new potential electrolyte for synthetic fuel production. P. L. Mollerup, N. Bonanos, P. Blennow, P. Holtappels and M. Mogensen. Oral presentation at Electrochemistry 2012, Münich, Germany, September 17-19, 2012.

List of Abbreviations

A	Pre-exponential factor
AC	Alternating current
CV	cyclic voltammetry/cyclic voltammogram
DC	Direct current
E_a	Activation Energy
EDX	Energy-dispersive X-ray spectroscopy
EIS	Electrochemical Impedance Spectroscopy
FEG	Field emission gun
GNP	Glycine nitrate combustion process
HER	Hydrogen evolution reaction
PEM	Proton exchange membrane
PFA	Perfluoroalkoxy
RT	Room temperature
SEM	Scanning electron microscope
SOEC	Solid oxide electrolysis cell
SOFC	Solid oxide fuel cell
STN/STN-94	$Sr_{0.94}Ti_{0.9}Nb_{0.1}O_3$
XRPD	X-ray powder diffraction

Contents

Chapter 1

Introduction

The world is focusing more and more on renewable energy sources in order to find alternatives to fossil fuels as these will eventually run out and are also potentially harmful for the environment.[1] Many countries have made initiatives to decrease the amount of fossil fuels and increase the amount of energy from renewable energy sources.[2,3] The Danish government have even made a plan for making Denmark completely free of fossil fuels by 2050. Denmark is highly dependent on fossil fuels with 71% of the electricity being produced from fossil fuels in 2009. However, the remaining electricity is being produced from wind and biomas, 19% and 10%, respectively. By changing from fossil fuels to renewable energies, Denmark will become a greener and more sustainable society.[4]

Changing to renewable energy is, however, a challenge. One very important aspect is the fact that most sources for renewable energy, such as wind and solar energy, do not generate a steady and controllable energy output, but fluctuate.[5] It is therefore necessary to store excess energy so it can be used when needed. One way of storing excess energy is by electrolysis of wa-

ter. For instance, excess electricity can be used to generate hydrogen, which can then later be used to drive e.g. a fuel cell, thereby generating electricity again.[6,7] Another possibility for storing energy is by co-electrolysis of CO_2 and water. Co-electrolysis using solid oxide electrolysis cells (SOEC) results in synthesis gas (H_2 + CO) which can then be reformed into synthetic fuels (hydrocarbons) such as methanol.[8,9] Synthetic fuels made from sustainable energy sources can then directly substitute the fossil fuels that are being used today in for example cars.[9] There is a constant search for materials and improvements that can make more efficient and cheaper electrolysis cells.[6] This will make them more competitive to fossil fuels with respect to price, but highly efficient cells are also necessary to produce the large amounts of synthetic fuels necessary to substitute just parts of the worlds consumption of fossil fuels. The worlds total energy consumption was approx. 97,000 TWh (8,823 Mtoe) in 2010 with approx. 80 % comming from fossil fuels. On top of this the worlds energy consumption is increasing every year.[2]

Different electrolysis cells exist today such as alkaline electrolysis cells, proton exchange membrane (PEM) and the previously mentioned SOEC. SOEC have an oxide ion conducting electrolyte and are typically operated at 800-1000 °C.[8] In PEM electrolysis cells the electrolyte is a proton conducting membrane, hence the name, and they are typically operated below 100 °C.[10] In alkaline electrolysis cells the electrolyte is typically 30 wt% KOH (aq) and they are also typically operated below 100 °C.[9,11] One of the benefits of using KOH (aq) as the electrolyte in alkaline electrolysis cells is its high conductivity. In general, aqueous electrolytes are known for their high conductivity at lower temperatures.[12] One way of making electrolysis more efficient is by increasing the temperatures and thereby taking advantage of the improved electrical efficiency at elevated temperatures.[6] However, in order to use aqueous electrolytes at elevated temperatures pressures must be applied to avoid water evaporation. If no pressure is applied the water will simply boil off above 100 °C, the exact temperature where this occurs depends on the aqueous electrolyte and its concentration.[13,14]

To successfully use aqueous electrolytes at elevated temperatures and under pressure it is necessary to know the electrolyte properties, such as ionic conductivity, thermal expansion, vapor pressure of water, and stability towards phase separation under these conditions. A potential problem with using aqueous electrolytes is handling them, but by immobilizing (fixating) them in a porous matrix the handling can become much easier.

Immobilization of solutions is already used for different applications such as molten carbonate cells and liquid membranes. In molten carbonate cells the melted salt is usually immobilized in a ceramic matrix such as γ-$LiAlO_2$ or α-$LiAlO_2$.[15] Immobilized liquid membranes are typically used for gas/vapour separation and have been researched for more than 30 years.[16] Usually, a polymeric material is used for the immobilization but ceramic materials with ionic liquids have also been investigated.[17] Furthermore, many studies have been made on porous sedimentary rocks containing brine to determine how the porosity, composition, water content and salinity affect the total conductivity as well as other properties of the brine-containing rock.[18]

1.1 Development of a Novel Cell Concept

As mentioned earlier co-electrolysis using SOEC can be used to form synthesis gas, which can then be reformed into hydrocarbons. If it was possible to decrease the temperature to for example 200 °C where most hydrocarbons are stable[12,19] it should in theory be possible to form hydrocarbons directly by co-electrolysis. However, operating a SOEC at 200 °C is not possible due to the materials used. There are no current electrochemical systems that can produce hydrocarbons at 200 °C. In order to explore this potentially exciting field new cell designs and choice of materials need to be developed.

A potential cell for co-electrolysis at approx. 200 °C could consist of an immobilized aqueous electrolyte, to get a high electrolyte conductivity, and gas diffusion electrodes. Gas diffusion electrodes are porous electrodes which can be used for cells where the reactants and/or products are gaseous. Todays gas diffusion electrodes are designed to optimize the contact between

the reactants and the electrolyte.[20] The gas diffusion electrodes have to contain proper catalysts to promote the desired reactions. Large pores makes it easier for the gas to flow and are therefore preferable in outer parts of the electrode. The reaction usually takes place at the interface between electrolyte and electrode, which is why smaller pores are preferred close to the electrolyte in order to increase the contact area between electrolyte, catalyst and gases (reactants).[21]

As the cell is intended for co-electrolysis of CO_2 and water choosing an electrolyte with either HCO_3^- or CO_3^{2-} as the anion appears to be a good choice due to the fact that CO_2 will react with the water in the electrolyte and form the following equilibrium:[22]

$$CO_2\ (g) + H_2O\ (l) \rightleftharpoons HCO_3^-\ (aq) + H^+\ (aq)$$

Which then leads to the following equilibrium:[22]

$$HCO_3^-\ (aq) \rightleftharpoons CO_3^{2-}\ (aq) + H^+\ (aq)$$

$KHCO_3$ (aq) and K_2CO_3 (aq) are already known in literature as electrolytes for reduction of CO_2.[22–26] However, K_2CO_3 (aq) appears to be a better choice as it has a higher conductivity than $KHCO_3$ (aq).[12] Furthermore, the price of K_2CO_3 (s) is very low and its solubility in water at room temperature is high.[12,27] This means that measurements over a large range of concentrations are possible.

The conductivity of 0.5-25 wt% K_2CO_3 (aq) is 7-223 mS/cm at 20 °C.[12] But most likely the conductivity of the immobilized solution will be lower.[28] As a comparison the conductivity of different solid ion conductors can be seen in Figure 1.1. In the typical operating range of SOEC (800-1000 °C) the best electrolytes, according to the Figure, have a conductivity in the range 0.1-1 S/cm. PEM cells with standard and modified Nafion membranes usually have an electrolyte conductivity in the range 0.1-0.4 S/cm. They are, however, not stable at 200 °C, but new materials are being reseached.[29,30] Based on experience from PEM cells and SOEC a good development goal for the immobilized K_2CO_3 (aq) electrolyte is to obtain a conductivity above 0.1 S/cm at 200 °C.

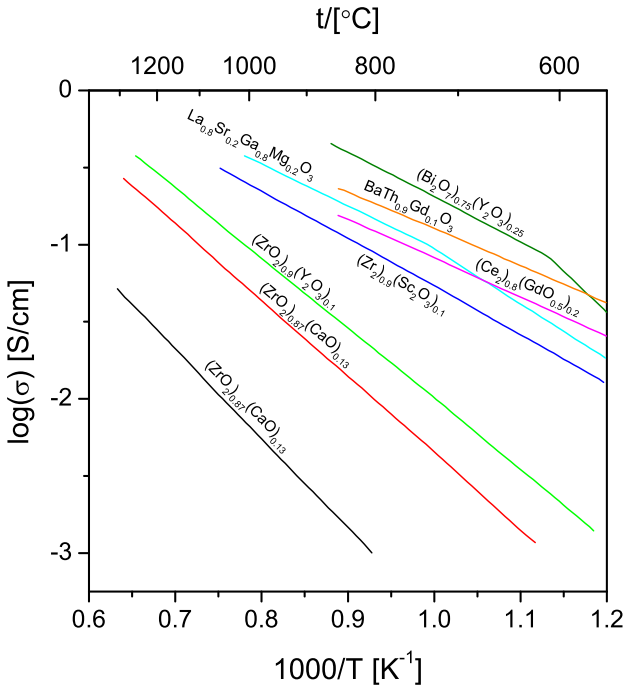

Figure 1.1: Redrawn Figure of the electrical conductivity as a function of 1000/T for different oxide ion conductors.[31]

Many different materials can be used for the immobilization, provided they are chemically stable/compatible. It is important that the material is not electronically conducting. Furthermore, the materials have to be porous and have a variable pore size. The matrix material should also be easy to fabricate and durable. Preferably it should also be cheap. As mentioned earlier ceramic materials are already used in molten carbonate cells for immobilization. In solid oxide cells ceramics are used as solid oxide ion conducting electrolytes but also as gas diffusion electrodes.[32,33] $SrTiO_3$ is known to be chemically stable, robust and non-conducting and the pore size can be varied.[34–36] It can be synthesized but is also commercially available.[37,38] Furthermore, Nb-doped $SrTiO_3$ can be used for gas diffusion electrodes as it becomes electronically

conducting after reduction at high temperatures.[36,39] This makes $SrTiO_3$ a good candidate for the matrix material, with Nb-doped $SrTiO_3$ as a potential electrode material.

It is very important to ensure that the aqueous electrolyte is tightly bound in the matrix, ie. has high capillary forces. By assuming cylindrical pores the capillary forces, ΔP, can be found using the Young-Laplace equation, eq. 1.1, where a is the pore radius, Θ the contact angle and γ_{lv} the liquid-vapour surface tension.[40] The higher the capillary forces the tighter the aqueous electrolyte is bound, meaning a high ΔP is desired.

$$\Delta P = \frac{2\gamma_{lv}}{a}\cos\Theta \tag{1.1}$$

The equation clearly shows that by decreasing the pore radius the capillary forces can be significantly increased. The capillary forces can also be increased by choosing a material that the solution will wet more, ie. has decreased contact angle, and by decreasing the surface tension. The liquid-vapour surface tension for water is 71.99 mN/m at 25 °C.[12] When dissolving salt in water the surface tension increases, however, the surface tension of salt solutions also decreases with temperature. This can be seen in Table 1.1 where the surface tension of K_2CO_3 (aq) from 20-95 °C is shown.

Table 1.1: Surface tension of K_2CO_3 (aq) solutions from 20-95 °C .[41]

Conc./wt%	20 °C	30 °C	40 °C	50 °C	60 °C	70 °C	80 °C	90 °C	95 °C
8.5	73.2	72.4	71.1	69.6	67.5	66.0	63.9		
17.3		75.8	74.5	73.2	71.1	69.8	68.0	66.5	
30.6		81.3	80.3	79.3	78.0	76.6	75.1		
36.4		86.3	84.7	83.7	82.1	81.1	79.5	78.0	
42.9	94.8	93.3	91.7	90.2	88.6	87.1	86.1	85.0	84.0

The contact angle and surface tension are further explained in Chapter 2.

A sketch of an ideal, hyphothesized cell can be seen in Figure 1.2. K_2CO_3 (aq) is shown as the aqueous immobilized electrolyte and the hydrocarbon formed is methanol. The reactions and mechanisms of the hyphothesized cell are unknown.

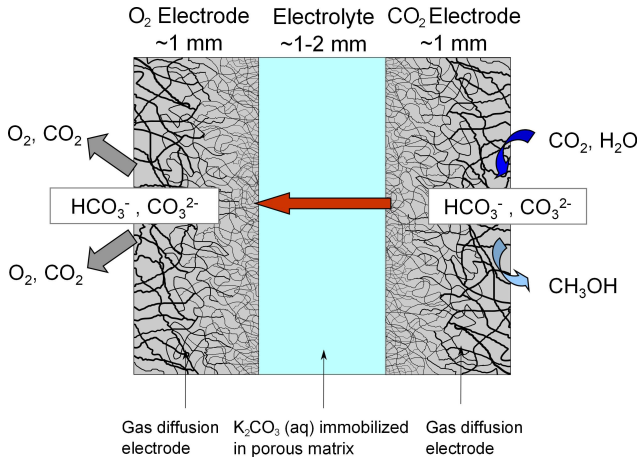

Figure 1.2: Sketch of ideal hypothesized co-electrolysis cell with immobilized K_2CO_3 (aq) as the electrolyte and with gas diffusion electrodes. The cell is fed with CO_2 and water on one side where methanol is formed and on the other side O_2 evolution occurs as well as some CO_2 formation. HCO_3^- and CO_3^{2-} are shown as the charge carriers.

1.2 CO_2 Reduction

In order to make a cell that can perform co-electrolysis of CO_2 and water and generate hydrocarbons it is necessary to find suitable catalysts. Without a catalyst that can reduce CO_2 the cell cannot produce hydrocarbons. The most widely mentioned catalyst in the literature for reduction of CO_2 to hydrocarbons in heterogeneous catalysis is Cu but ceramic materials such as $La_{1.8}Sr_{0.2}CuO_4$ have also been reported.[22,42] Many other metals such as Pb, Sn, Au, Zn, Ni and Pt have also been tested but it has been found that they either primarily form CO or $HCOO^-$ when using aqueous electrolytes.[22,43,44]

If the catalyst material is electronically conducting it can potentially also be used as an electrode material. Reduction of CO_2 using Cu electrodes has already been successfully carried out using $KHCO_3$ (aq) as the electrolyte at room temperature.[22] Furthermore, $La_{1.8}Sr_{0.2}CuO_4$ has been used as gas diffusion electrodes (and catalyst) for CO_2 reduction.[42] It has also been reported that gas diffusion electrodes in general enhances the reaction rate of

CO_2 reduction.[45–48] The products formed when reducing CO_2 using aqueous electrolytes vary with both electrolyte concentration, pressure, anionic specie and temperature, so predicting which products will be formed under given conditions is extremely difficult.[22]

Using K_2CO_3 (aq) as the electrolyte for CO_2 reduction results in a very complicated system with many different equilibriums. When exposing the K_2CO_3 (aq) solution to CO_2 (g) the following equilibrium sets in:[22]

$$CO_2\ (g) + H_2O\ (l) + {CO_3}^{2-}\ (aq) \rightleftharpoons 2\ {HCO_3}^{-}\ (aq) \tag{1.2}$$

The equilibrium shows that exposing a solution with ${CO_3}^{2-}$ ions (such as K_2CO_3 (aq)) to CO_2 a conversion to ${HCO_3}^{-}$ ions will occur to some extent. It also clearly shows that by increasing the partial pressure of CO_2 the equilibrium is shifted to the right, which means that the amount of ${HCO_3}^{-}$ ions increases and the amount of ${CO_3}^{2-}$ ions decreases. This also means that the CO_2 partial pressure affect the possible charge carriers in the aqueous solution.

Some other important, and previously mentioned, equilibriums are:

$$CO_2\ (g) + H_2O\ (l) \rightleftharpoons {HCO_3}^{-}\ (aq) + H^+\ (aq) \qquad pK_{a1} = 6.35\ (25\ °C) \tag{1.3}$$

$$HCO_3^{-}\ (aq) \rightleftharpoons {CO_3}^{2-}\ (aq) + H^+\ (aq) \qquad pK_{a2} = 10.33\ (25\ °C) \tag{1.4}$$

The equilibriums show that the pH (H^+ concentration) is affected by the different equilibriums which means that it can change depending on the measurement conditions.

According to Hori[22] OH^- is generated when CO_2 is reduced in an aqueous solution, due to the involvement of H_2O in the reduction. If the product is ethanol the reaction is as follows:

$$2\ CO_2 + 9\ H_2O + 12\ e^- \rightleftharpoons C_2H_5OH + 12\ OH^- \tag{1.5}$$

The formation of OH^- then leads to the following equilibriums:

$$OH^-\ (aq) + {HCO_3}^{-}\ (aq) \rightleftharpoons H_2O\ (l) + {CO_3}^{2-}\ (aq) \tag{1.6}$$

$$CO_2\ (g) + OH^-\ (aq) \rightleftharpoons {HCO_3}^{-}\ (aq) \tag{1.7}$$

Hori[22] has also stated that reaching equilibrium for eq. 1.6 is instantaneous but for eq. 1.7 it is slow.

One of the limiting factors for reducing CO_2 is the supply of CO_2. The solubility of CO_2 is very low in $KHCO_3$ (aq), but using gas diffusion electrodes should help ensure that enough CO_2 is present at the reaction sites. Increased pressure will also increase the solubility of CO_2 which should also increase reaction rates.[49,50]

Hydrogen evolution reaction (HER) is a competing reaction that can be expected to take place when reducing CO_2 using aqueous electrolytes. It is therefore important to choose conditions that suppress the reaction whenever possible. In acidic solutions the standard potential for HER is lower than for CO_2 reduction but at pH > 7 the potentials are very similar. Furthermore, HER has been reported to increase with $KHCO_3$ concentration.[22]

To summarize it should be possible to reduce CO_2 using immobilized K_2CO_3 (aq) as the electrolyte and Cu as catalyst at least at room temperature. It is, however, impossible to predict which products will be formed at elevated temperatures and pressures.

1.3 Thesis Purpose and Outline

The purpose of this thesis is to explore the potential of immobilized K_2CO_3 (aq) as a possible electrolyte for co-electrolysis of CO_2 and water at approx. 200 °C. This has been done by first exploring the properties of pure K_2CO_3 (aq) and then immobilized K_2CO_3 (aq) at temperatures from ambient to 200 °C and pressures from ambient to 50 bar in both N_2 and CO_2 atmosphere. Different matrix materials, $SrTiO_3$ and TiO_2, have been used for the immobilization and the properties of the matrix materials have also been studied. Furthermore, the changes in water partial pressure and water vapour content at elevated temperatures and pressures have been investigated in order to understand how the system behaves at elevated temperatures and pressures. As part of the general proof of concept initial studies of some electrodes (Ag,

Pt, Cu and Nb-doped $SrTiO_3$) have been made to explore the performance potential.

This first Chapter has given an introduction to the subject and illustrated the background and motivation. In Chapter 2 all the techniques used in the project are explained. This is then followed by several Chapters with results and discussion of the experimental work. Chapter 3 covers the properties of pure K_2CO_3 (aq). Results from equilibrium calculations as well as experimental results at both ambient conditions as well as elevated temperatures and pressures are reported and discussed. The Chapter is intended to give the reader a good understanding of the properties of pure K_2CO_3 (aq) and its possible limitations. Chapter 4 deals with the water management issues that have been identified at elevated temperatures and pressures. Equilibrium calculation results are reported and prevention of water evaporation at elevated temperatures is discussed. In Chapter 5 the two different matrix materials, $SrTiO_3$ and TiO_2, are compared and experimental results, at both ambient conditions and elevated temperatures and pressures, are reported and discussed. The microstructure of the two matrix materials are compared as well as their pore size and pore size distribution. The conductivity of K_2CO_3 (aq) immobilized in the two different materials is also reported and compared. Chapter 6 contains a summary of the presented work as well as concluding remarks. In Chapter 7 a future outlook is given.

Chapter 2

Experimental Techniques and Models

This chapter gives an overview of the fabrication of the matrix materials including powders synthesis. Furthermore, the different characterization techniques as well as setups and sample holders are described. Finally, several models that can be used to describe the conductivity of an immobilized aqueous solution are discussed.

2.1 Powder Synthesis

2.1.1 Strontium Titanate, $SrTiO_3$

$SrTiO_3$ powder (with the desired ratio Sr/Ti=1) has been prepared from strontium nitrate, titanium lactate, glycine, ammonium nitrate and citric acid by the modified glycine nitrate combustion process (GNP) developed by Blennow *et al.*[37] For safety reasons (as it is a combustion process) the batch size was limited to approx. 5.5 g $SrTiO_3$. The prepared powder was calcined at 350 °C in order to remove any unreacted materials and carbon containing compounds.

The resulting powder was white. Part of the powder was further calcined at higher temperatures, 900–1200 °C and it was found that the particle size increased with calcination temperature.

2.1.2 Niobium-doped Strontium Titanate, STN

Nb-doped strontium titanate (STN) was also prepared using the modified GNP as described in Section 2.1.1 but with addition of Nb-oxalate to introduce niobium to the material.[37] Again the batch size was limited to approx. 5.5 g. Furthermore, the material was prepared with a non-stoichiometric ratio, $Sr_{0.94}Ti_{0.9}Nb_{0.1}O_3$, as this material has been reported to have a high electronic conductivity after reduction in hydrogen at high temperature.[39] To get a more complete combustion up to 2 g extra ammonium nitrate was added. The synthesis of the STN powder was very similar to the $SrTiO_3$ synthesis, however the formed powder was gray instead of white, see Figure 2.1.

Figure 2.1: STN powder before calcination.

The powder was calcined at both 350, 900 and 1100 °C. X-ray powder diffraction (XRPD) diffractograms were obtained after each calcination, see Figure 2.2, and show that the powder contained $SrCO_3$ until calcination at 1100 °C. After calcination at 900 °C the powder changed color from gray to pure white. The $SrCO_3$ formation could have been caused by the powder containing SrO phases which could have reacted with CO_2 and formed $SrCO_3$. $SrCO_3$ is an insulator and therefore highly undesired in a material intended for electrodes.

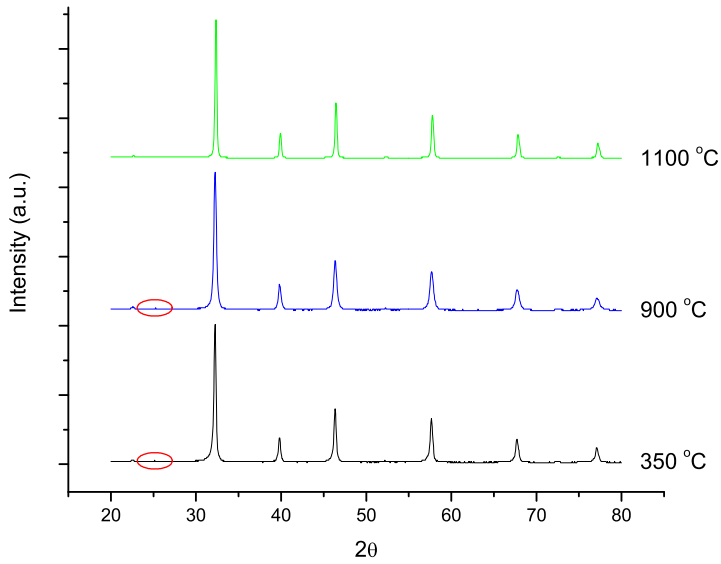

Figure 2.2: XRPD diffractograms of STN powder calcined at 350, 900 and 1100 °C, at both 350 and 900 °C a small peak from $SrCO_3$ can be seen indicated by the red ring.

2.1.3 Precipitation Synthesis

As an alternative to the $SrTiO_3$ powder produced by the GNP synthesis a precipitation synthesis was carried out. The starting materials were $Sr(NO_3)_2$ (anhydrous), NaOH, $TiCl_3$ solution (10 wt% in 30 wt% HCl), ethanol and conc. NH_4OH (aq). The synthesis was performed under N_2 gas as much as possible until the precipitation had taken place. The powder was calcined at 400, 600 and 900 °C and XRPD diffractograms were obtained after each calcination, see Figure 2.3. The Figure clearly shows that the material is not phase pure not even after calcination at 900 °C. It was therefore concluded that the synthesis was not a suitable alternative to the GNP synthesis.

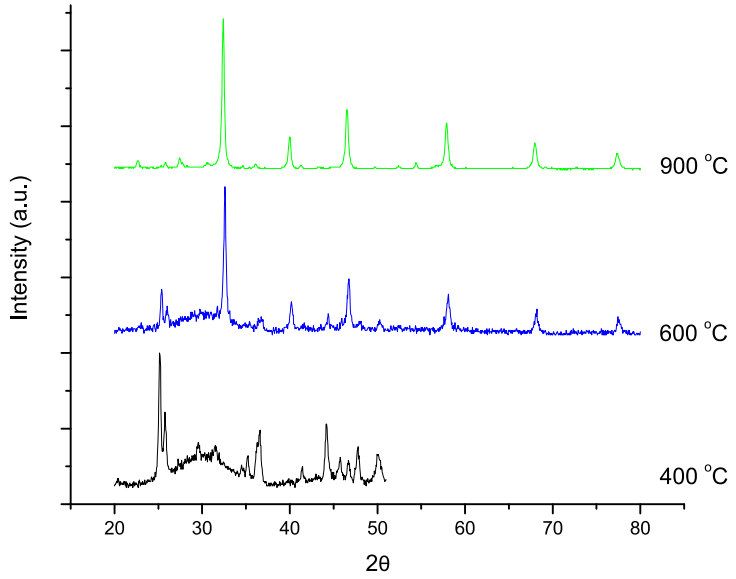

Figure 2.3: XRPD diffractograms of $SrTiO_3$ prepared by precipitation synthesis and calcined at 400, 600 and 900 °C.

2.2 Pellet Fabrication

$SrTiO_3$ pellets were fabricated using powder from the GNP synthesis and from Inframat Advanced Materials, USA. Powder was bought from Inframat Advanced Materials in order to get one large batch of $SrTiO_3$ powder and thereby minimize the difference between pellets. The powder from Inframat Advanced Materials had a particle size (diameter) of approx. 100 nm. The particle size was specified by the manufacturer but also confirmed with scanning electron microscopy (SEM).

Due to problems with $SrCO_3$ formation when using $SrTiO_3$ in CO_2 atmosphere, see Section 5.3.3.1, pellets made of TiO_2 were also fabricated. The pellets were fabricated using powder (Sigma Aldrich, trace metals basis) with a particle size (diameter) of approx. 100-200 nm. The particle size was found using SEM.

All pellets were pressed uniaxially with a pressure of 130 MPa for 20-30 seconds and isostatically (in water) with a pressure of 250 MPa for 20 seconds. The pellets were sintered at 1000 °C for 12 hours unless otherwise stated. The pellets had a diameter of approx. 10.7-11.5 mm and a height of approx. 2.2-5.5 mm after sintering at 1000 °C.

2.2.1 Electrodes

Cells for two electrode measurements were fabricated using STN, STN+Ag, Cu, Pt or Ag ink. Both Cu, Pt, Ag and Ag+STN electrodes were painted on sintered $SrTiO_3$ pellets. The Ag electrodes were made using a Ag paste (ESL ElectroScience) mixed with a few drops of ethanol. The Ag+STN electrodes were made by adding 10 wt% STN powder to the Ag paste and then a little ethanol to get a good consistency for painting. The cells were heat treated in air at 400-415 °C for 1 hour in order to remove solvents etc. The Pt electrodes were made using an ink from Ferro and heat treated in air at 800 °C for 1 hour. The Cu electrodes were made with two different inks both prepared in house using fine copper powder from Alfa Aesar. The cells were heat treated at approx. 400 °C in air to remove solvents etc. and at 600-700 °C in 9% H_2/Ar to prevent oxidation of Cu. STN ink was prepared in house using STN powder, solvents, fillers and binders. The electrodes were sprayed on and then heat treated at 1000 °C in air, in order to sinter them, and at 1200 °C in 9% H_2/Ar for 3 hours in order to reduce them and make them electronically conducting.

2.3 X-ray Powder Diffraction

X-ray powder diffraction (XRPD) is a technique where a powder sample is hit with a beam of X-rays and the diffracted X-rays are detected. It can be used to identify the crystalline compounds or phases in a material. The technique cannot be used for detecting amorphous products or impurities of less than approx. 5%.[51,52]

Basic Principles in X-ray Powder Diffraction

X-rays are electromagnetic radiation with wavelengths in the range of 1 Å. X-rays are produced when high-energy charged particles, such as electrons accelerated through 30,000 V, collide with matter. Usually monochromatic X-rays are used for experiments and they are produced by accelerating a beam of electrons and letting them strike a metal target, often Cu. The electrons ionize some of the Cu 1s electrons, and then an electron from an outer orbital (2p or 3p) drops down and fills the vacancy thereby emitting $K\alpha$ or $K\beta$ radiation. The 2p $\rightarrow$ 1s transition occurs more often wherefore $K\alpha$ radiation is most common. The $K\alpha$ transition is a doublet with both $K\alpha_1$ = 1.54051 Å and $K\alpha_2$ = 1.54433 Å radiation. The latter can be removed to obtain monochromatic X-rays, which result in better data when measuring X-ray powder diffraction spectra.[52]

Diffraction by Crystals

Crystals can be seen as made up of small building blocks called unit cells. A unit cell is the smallest repeating unit, which shows the full symmetry of the crystal structure. All crystals can be classified into one of the 7 crystal systems, which are based on their angles and side lengths. Lattice planes are often used when describing a given crystal structure. The spacing between parallel planes are called d. Crystals are due to their regularly repeating structure able to diffract radiation when the wavelength is similar to the interatomic separation, which is usually 2–3 Å. There are two different approaches when dealing with diffraction by crystals, there are the Laue equations and Bragg's law. The former is rarely used in solid state chemistry since it is much more complicated to use than Bragg's law. However, Laue's equations describes the phenomenon of scattering better.[52]

Bragg's Law

Bragg's law, eq. 2.1, is based on seeing crystals as built up in layers or planes, each acting as a semi-transparent mirror. Some of the X-rays are deflected by the plane while others pass through and can then later be deflected by other layers. When an X-ray is deflected the angle of the incoming X-ray beam is

the same as the one for the deflected beam.[52] Bragg's law states:

$$2d \sin\theta = n\lambda \tag{2.1}$$

where d is the spacing between parallel planes, θ is the Bragg angle, n is an integer and λ is the wavelenght. When Bragg's law is satisfied the reflected beams are in phase and interfere constructively. At angles different from the Bragg angle, the reflected beams are out of phase and destructive interference or cancellation occurs.[52]

A finely powdered sample ideally has crystals arranged in every possible orientation, wherefore the various lattice planes are also present in every possible direction. For each set of planes there must be crystals oriented at the Bragg angle to the incident beam resulting in diffraction. The diffraction is cone shaped and each set of planes gives its own cone of radiation. A detector is used to measure the intensities and the angles, and then a diffraction pattern can be made, by plotting the intensities as a function of the angle. The peaks at the lower angles correspond to the planes with the largest distances in the crystal.[52]

The X-ray diffraction patterns can be used for identifying materials by measuring and comparing to a database with known diffraction patterns. If the crystal structure is known it is also possible to calculate a powder diffraction pattern, but minor differences may occur compared to measured patterns. If two materials have the same composition except for one element, and they have the same crystal structure, the X-ray powder diffraction patterns will be very similar. They will only vary slightly since changing an atom may change the unit cell parameters slightly, resulting in a small shift in the peaks. The substitution may also affect the structure factors resulting in differences in intensities. If the crystal system is known the unit cell parameters can be determined with good accuracy from the diffraction pattern.

X-ray powder diffraction was performed on both powders and pellets in order to determine the phase purity of the materials. The measurements were

performed using a STOE Theta-Theta X-ray diffractometer with Cu Kα radiation and a Bruker D8 Advance X-ray diffractometer with Cu Kα radiation.

2.4 Scanning Electron Microscopy

A scanning electron microscope (SEM) can be used to visualize the surface of a sample, at very high magnifications. In a SEM electrons are used to image the surface and the sample must therefore be conducting to avoid a charge building up at the surface. If the sample or the surface is not conducting this can be achieved by coating the sample with a conducting material such as carbon or gold.

A SEM consist of many different parts such as an electron gun, lenses and detectors. The electron gun generates the primary electrons used to image the sample. Several different electron guns exist; the most common are the tungsten filaments, LaB_6 and the field emission gun (FEG).[53,54]

Tungsten filament guns are the cheapest, but they also have the lowest brightness. A LaB_6 gun has approx. 10 times better brightness, than the tungsten filament. Both the tungsten filament and the LaB_6 gun are based on thermionic emission, where heating the filament to around 2700 K is used to emit electrons. The electrons have an energy spread of 1-2 eV.[53,54]

The field emission gun (FEG) has about a factor 1000 higher brightness and emits electrons by subjecting a metal surface, such as tungsten, to an extremely high electric field. The metal has to be formed as a sharp tip in order to apply such a high field. An extractor electrode is used to generate the electric field, causing electrons to be emitted. Since the tip function as a cathode, an anode is required; the anode sets the acceleration voltage, of the electrons. The beam booster increases the voltage of the electron beam to a higher value than the acceleration voltage. This reduces the sensitivity of the electron beam to magnetic stray fields. The field emission gun has a small energy spread of less than 0.5 eV. The tip consists of a tungsten crystal tip with a ZrO reservoir. This is known as a Schottky-emitter. The tip is heated

to around 1800 K, and therefore a suppressor electrode is used to avoid the emission of thermal electrons that are not emitted from the tip.[53,54]

A FEG requires a very low pressure (vacuum) to avoid ions hitting the very fine tip. The vacuum must be lower than 10^{-7} Pa, which is known as ultra high vacuum. Thermionic guns, such as tungsten and LaB_6, only require a vacuum of 10^{-2}-10^{-3} Pa.[53]

To prevent the electron beam from being deflected by ions/molecules in the specimen chamber it is also evacuated. Usually pressures below 10^{-7} Pa are used for normal SEM.[54]

Furthermore, the SEM has a lot of lenses in order to focus the beam on the sample, and help collect reflected electrons, which is essential to obtain good high-resolution images. Both electromagnetic and electrostatic lenses exist.[54]

The SEM is also equipped with one or more detectors used to detect the different types of scattered electrons, explained in Section 2.4.1. Detectors for secondary electrons and backscattered electrons are the most commonly used. Detectors for secondary electrons can be placed near the sample surface or in the beam path.

2.4.1 Scattering of Electrons

When the primary electron beam hits the specimen, electrons are scattered, see Figure 2.4. Two different types of scattering can take place, elastic and inelastic. When an electron is elastically scattered, it maintains its energy although it might change direction. Inelastic scattering is the opposite, meaning that the electron changes energy and maybe also direction.[53] The scattered electrons can be divided into different categories, and contain different information about the sample. The volume from which the scattered electrons arise is called the interaction volume.[54]

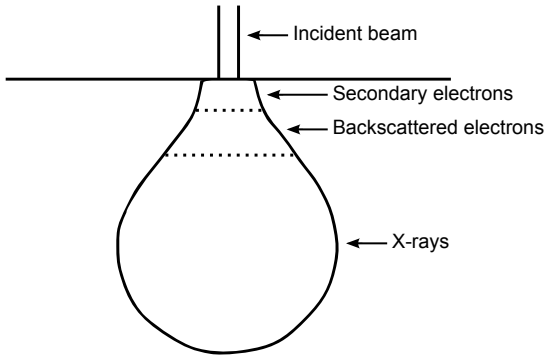

Figure 2.4: Redrawn image of the interaction volume also showing the different types of scattered electrons.[53]

The most important scattered electrons are the secondary electrons, the backscattered electrons and the X-rays. The first two are primarily used for imaging and the latter for material identification. Secondary electrons are generated by inelastic scattering, and are therefore low in energy. Backscattered electrons, on the other hand, come from elastically scattered electron, and are high in energy. They come from deeper within the sample (big interaction volume), and contain information about the material but are also used for imaging. The X-rays come from even deeper within the sample (very large interaction volume), and are used for identifying different materials in the sample.[54]

In this project two different SEM have been used, a Hitachi TM-1000 and a more advanced Zeiss Supra 35. Both powder and sintered pellets have been investigated. Some samples have been coated with gold or carbon. The microstructure of both fractured and polished pellet crosssections have been investigated. The polished crosssections have been obtained by embedding pellets in epoxy and polishing the surface.

2.4.2 Energy Dispersive X-ray Spectroscopy

Energy Dispersive X-ray spectroscopy (EDX) is a technique where the X-rays are used for determining the elements in the sample as well as the composi-

tion. It is possible to do measurements on spots, line scans and whole images (element mapping).[53]

In this project EDX has been performed on a few samples using the Zeiss Supra 35 scanning electron microscope.

2.5 Mercury Porosimetry

Mercury porosimetry is a method used to dermine the porous properties of solids and is based on the capillary rise phenomenon inside the pores/capillaries of a solid. As mercury is a non-wetting liquid ($\Theta > 90°$) a pressure must be applied to force the liquid to flow up the capillary (pore). According to the Young-Laplace equation, see eq. 2.2, the pressure difference across a capillary interface is directly proportional to the curvature of the surface.

$$\Delta P = \gamma_{lv} \left(\frac{1}{R_1} + \frac{1}{R_2} \right) \tag{2.2}$$

where ΔP is the pressure difference between the two phases (liquid and air), γ_{lv} is the surface tension of the liquid and R_1 and R_2 are the two different radii of a non-spherical droplet. If the capillary is small and circular then the surface of the liquid becomes a hemisphere and therefore $R_1 = R_2 = R$. This then reduces the equation to eq. 2.3, which is normally used for mercury porosimetry.[40] It can also be written as a function of pore radius and contact angle, see eq. 1.1 in Section 1.1.

$$\Delta P = \frac{2\gamma_{lv}}{R} \tag{2.3}$$

The pore size as well as the open and closed porosity of several $SrTiO_3$ and TiO_2 pellets were determined using a Micromeritics Autopore IV Hg Porosimeter.

2.6 Contact Angle and Surface Tension

As mentioned in Chapter 1 the surface tension as well as the contact angle are very important properties when immobilizing an aqueous solution such

as K_2CO_3 (aq) in a porous ceramic matrix.

Contact angle measurements are typically performed on smooth surfaces but the surface of a ceramic matrix can be expected to be rough. The wetting of rough surfaces can be different from the wetting of smooth surfaces, which means that the contact angle between a K_2CO_3 (aq) solution and a ceramic matrix can vary depending on the surface-roughness of the matrix. To determine the contact angle on rough surfaces both the advancing and receeding contact angle is typically measured.[55]

Several models exist to explain how a rough surface is wetted. Among these are the Wenzel and the Cassie model, see fig 2.5 and 2.6.

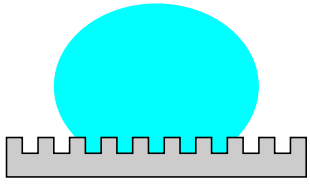

Figure 2.5: Illustration of the Wenzel model, where the void beneath the droplet is filled with liquid.

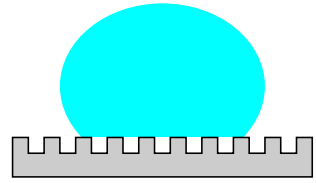

Figure 2.6: Illustration of the Cassie model, where the void beneath the droplet is filled with air.

The Wenzel model assumes that the void beneath the droplet is filled with solution (homogeneous wetting) and predicts that the contact angle increases on hydrophobic surfaces but decreases on hydrophilip surfaces. The Cassie model assumes that the void beneath the droplet is filled with air (heterogeneous wetting) and predicts that the surface becomes more hydrophobic and the contact angle increases.[56] Furthermore, the surface of the matrix can contain impurities/contaminations which can also affect the wetting.

The surface tension is related to the contact angle by the Young equation:

$$\gamma_{sv} = \gamma_{sl} + \gamma_{lv} cos\Theta \tag{2.4}$$

where γ_{sv}, γ_{sl} and γ_{lv} is the solid-vapour, solid-liquid and liquid-vapour surface tension, respectively. As previously mentioned the liquid-vapour surface

tension of K_2CO_3 (aq) solutions increases with concentration but decreases with temperature.[41]

2.7 Setups for Electrochemical Characterization

In order to measure the conductivity of K_2CO_3 (aq) at elevated temperatures and pressures a specially designed setup was used. The majority of the results reported in this thesis have been obtained using this setup. Furthermore, two different setups were used to perform measurements at ambient temperature, one with gas flow and one without. Construction of the pressurized setup as well as the ambient temperature setup without gas flow was not part of this project.

2.7.1 Pressurized Setup

Conductivity measurements under pressure and at elevated temperatures were performed in a Parr autoclave type 4760 with 600 ml volume and a Teflon liner. The autoclave was made of Inconel 600 which is known to be very corrosion resistant in alkaline media[57] and also a suitable material when using a steam and carbon dioxide containing atmosphere.[58,59] The autoclave was pressurized using nitrogen, carbon dioxide or synthetic air. A J-type thermo well was used to measure the temperature inside the autoclave. A drawing of the setup can be seen in Figure 2.7.

An aqueous solution of K_2CO_3 with a concentration lower that the one being measured was placed in the bottom of the autoclave in the Teflon liner during tests. This reservoir was intended to prevent water loss from the solution being measured. The water partial pressure increases with temperature and, due to the system being closed, the water can only come from the reservoir or the solution being measured. However, the water partial pressure above an aqueous solution decreases with concentration.[60,61] The water partial pressure above the reservoir should, therefore, be higher than above the solution being measured and water should, therefore, evaporate from the reservoir

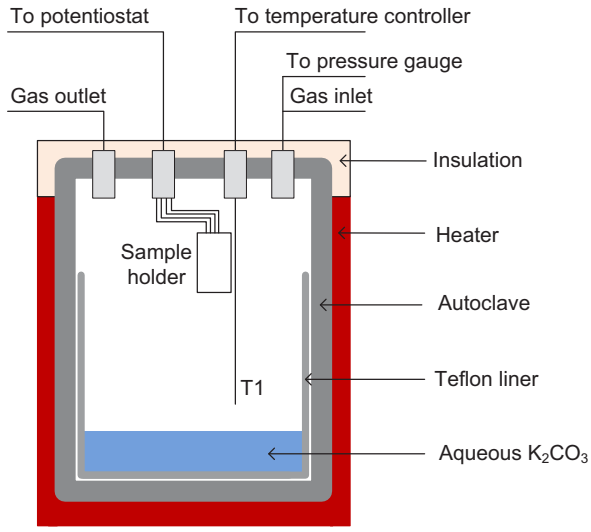

Figure 2.7: Drawing of setup, T1 = J-type thermo well.

instead from the solution being measured. Water management during tests is discussed further in Chapter 4.

2.7.2 Non-pressurized Setups

A few measurements were performed using a non-pressurized setup with gas flow. The setup consisted of a 500 ml PFA (perfluoroalkoxy) container with gas inlet and outlet as well as a thermocouple. The inlet gas was passed through a water bottle to humidify the gas before it entered the container. If the inlet gas is not humidified the solution being measured will dry over time as it is loosing water by humidifying the inlet gas in order to reach the equilibrium water partial pressure above the solution. K_2CO_3 (aq) solution with the same concentration as the solution being measured was placed in the bottom of the container during tests. This solution was intended as an alternative to the water bottle as it was possible to bubble the inlet gas through the solution, this was however never done.

Measurements were made in different CO_2 and N_2 gas mixtures with a flow of 50 ml/min. The measurements were performed at ambient temperature on 10 and 30 wt% K_2CO_3 (aq) immobilized in $SrTiO_3$.

A two electrode setup was also used to perform measurements at ambient temperature and pressure in air on immobilized K_2CO_3 (aq). This setup had a Pt mesh as current collector and a load to ensure good contact.

2.8 The van der Pauw Technique

The measurement of the ionic conductivity of aqueous solutions is usually performed in a dip cell with parallel electrodes made of platinum foil. However, with concentrated solutions of high conductivity, lead resistances introduce errors, especially at high temperatures. One way to address this issue is with four terminal measurements, e.g. as illustrated by Landviser.[62]

Alternatively, the conductivity can be measured using the van der Pauw technique, commonly associated with conductivity measurements on semiconductors and metals.[63] The method involves placing four probes at the edge of the sample, as shown in Fig. 2.8. For the technique to work, the contacts must be sufficiently small and the sample of homogenous thickness and simply connected (i.e. free of holes). Two adjacent electrodes are used for supplying the current and the other two for measuring the voltage. After this, the connections are rotated 90°, A→B, B→C, C→D and D→A. The voltage/current ratios for the two cases will then be $R_{AB,CD}$ and $R_{BC,DA}$. The measurement does not stipulate that the sample be cylindrical or the electrodes equally spaced around the sample, however this geometry is often chosen for convenience.[63]

The specific resistance of the sample, ρ, is related to $R_{AB,CD}$, $R_{BC,DA}$ and the height of the sample, d, as follows:[63]

$$\exp\left(\frac{-\pi d R_{AB,CD}}{\rho}\right) + \exp\left(\frac{-\pi d R_{BC,DA}}{\rho}\right) = 1 \tag{2.5}$$

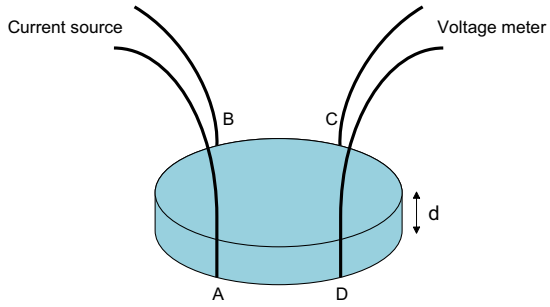

Figure 2.8: Sample with four contacts. Current source and voltage meter are shown on the Figure.

If $R_{AB,CD}$ = $R_{BC,DA}$ = R the equation has an explicit solution:

$$\rho = \frac{\pi d}{\ln 2} R \tag{2.6}$$

However, if $R_{AB,CD} \neq R_{BC,DA}$ the specific resistance can be calculated using the following equation:[63]

$$\rho = \frac{\pi d}{\ln 2} \frac{R_{AB,CD} + R_{BC,DA}}{2} f \tag{2.7}$$

where the correction factor, f, is a function of the ratio $R_{AB,CD}/R_{BC,DA}$ and can be approximated by the following equation:[63]

$$f \approx 1 - \left(\frac{R_{AB,CD} - R_{BC,DA}}{R_{AB,CD} + R_{BC,DA}} \right)^2 \frac{\ln 2}{2} - \left(\frac{R_{AB,CD} - R_{BC,DA}}{R_{AB,CD} + R_{BC,DA}} \right)^4 \left(\frac{(\ln 2)^2}{4} - \frac{(\ln 2)^3}{12} \right) \tag{2.8}$$

If $R_{AB,CD}$ = $R_{BC,DA}$ then f = 1, but even if the difference between $R_{AB,CD}$ and $R_{BC,DA}$ is 20 % the correction factor decreases less than 1 %, see Figure 2.9.

Therefore, if $R_{AB,CD} \approx R_{BC,DA}$ the following equation can be used:

$$\rho = \frac{\pi d}{\ln 2} \frac{R_{AB,CD} + R_{BC,DA}}{2} \tag{2.9}$$

The specific conductivity is the inverse of the specific resistance:

$$\sigma = \frac{1}{\rho} \tag{2.10}$$

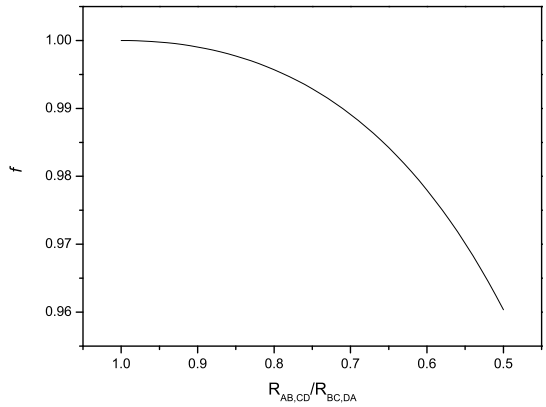

Figure 2.9: Correction factor, f, as a function of the ratio $R_{AB,CD}/R_{BC,DA}$.

The advantage of the van der Pauw technique is that the resistance obtained is free of any contribution from the electrodes. Although most applications of the technique have been on electronic conductors, using DC, the technique has also been proven to work on aqueous electrolytes[28,64] and solid electrolytes,[65] using AC.

The conductivity of pure K_2CO_3 (aq) as well as K_2CO_3 (aq) immobilized in $SrTiO_3$ have been measured using the van der Pauw technique. Measurements at ambient temperature were performed in all 4 possible configurations (where half have identical resistances), by rotating the wires 90° between each measurement. For measurements at elevated temperature the correction factor, f, was first determined by measuring the resistance in the two different configurations ($R_{AB,CD}$ and $R_{BC,DA}$) at room temperature and then all measurements at elevated temperature were performed using only one configuration, $R_{AB,CD}$.

2.9 Electrochemical Impedance Spectroscopy

When performing impedance measurements on an electrochemical system a small sinusoidal potential or current is applied, the frequency is varied and

from the response an impedance spectrum is obtained. By varying the measurement conditions information about the given electrochemical system can be obtained. The impedance response is defined as:[66]

$$Z = \frac{\Delta V}{\Delta I} \tag{2.11}$$

And it consists of a real and an imaginary part:

$$Z = Z_r + jZ_j \tag{2.12}$$

When the input and output are in phase the impedance only consist of a real part and when they are completely out of phase it only consist of an imaginary part. The relation between the complex impedance and the phase angle can be seen clearly on a phasor diagram, see Figure 2.10, and it can also be expressed as:[66]

$$Z = |Z|\, exp(j\phi) \tag{2.13}$$

where $|Z|$ is the magnitude of the impedance vector (the modulus) and ϕ the phase angle.

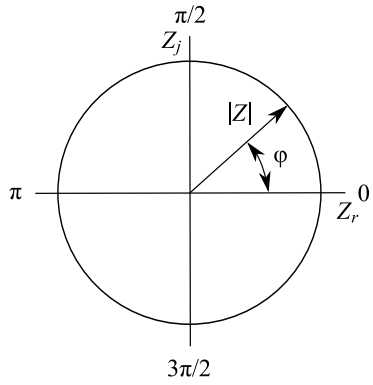

Figure 2.10: Phasor diagram.[66]

A Gamry reference 600 or 3000 potentiostat[67] has been used to perform AC impedance measurements on both pure and immobilized K_2CO_3 (aq) solutions in order to determine their conductivity.

2.9.1 Two Electrode Measurements

Two electrode measurements were performed on K_2CO_3 (aq) immobilized in both $SrTiO_3$ and TiO_2. The sample holder shown in Figure 2.11 was used for measurements at elevated temperature and pressure. The sample holder consists of two inconel tubes in a PFA tube fitting. Springs are used to press the two inconel cylinders together in order to ensure good contact during the measurements. Furthermore, Pt mesh are used as current collector.

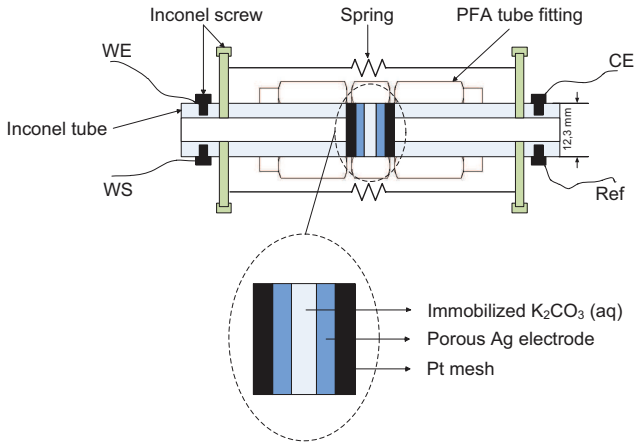

Figure 2.11: Two electrode sample holder used for measurements at elevated temperature and pressure. WE = Working electrode, WS = Working sense, CE = counter electrode and ref = reference electrode.

The resistance of the samples were measured over a frequency range. The electrolyte resistance is usually found in the high frequency range when Z_{imag} is zero (or very close to).[66] But as the Z_{imag} value never came close to zero at lower frequencies the resistance of the electrolyte was simple taken to be the average of the real part of the impedance (Z_{real}) for those measurements for which the imaginary part (Z_{imag}) was smaller than a certain limit, $\pm$0.1-1 Ω or simply the value were the imaginary part was smallest. The specific resistance was found using the following equation:

$$\rho = R\frac{A}{d} \tag{2.14}$$

where d is the thickness of the sample, A the area of the electrode and R the resistance of the sample. The specific conductivity was then found using eq. 2.10

2.9.2 Four Electrode Measurements

Several sample holders were used for conductivity measurements using the van der Pauw technique. In Figure 2.12 the sample holder for measurements of pure K_2CO_3 (aq) can be seen. The sample holder is made of Teflon and has a Teflon pellet in the bottom to fixate the Pt wires (electrodes). Furthermore, it has a Teflon lid with a hole to allow for expansion and compression of the the solution upon heating and cooling.

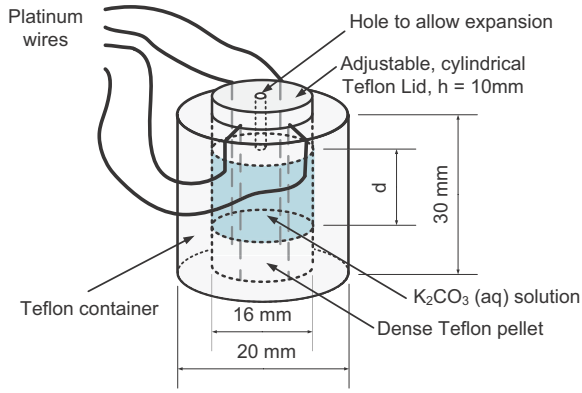

Figure 2.12: Drawing of sample holder used for conductivity measurements on pure K_2CO_3 (aq).

Figure 2.13 shows the sample holder used for measuring the conductivity of K_2CO_3 (aq) immobilized in $SrTiO_3$. The sample holder is also made of Teflon and also has Pt wires as electrodes. The sample holder also has a slit (not shown on Figure) to be able to expand and compress the sample holder and thereby ensure good contact.

As the van der Pauw method eliminates the contribution from the wires the impedance measurements should in theory result in the same Z_{real} value

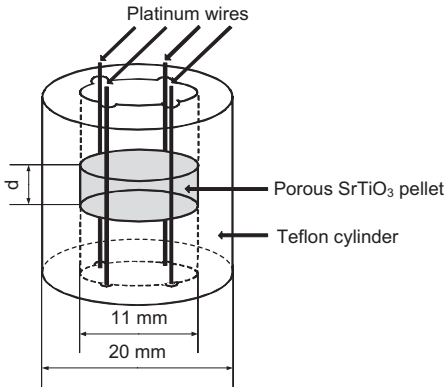

Figure 2.13: Sample holder used for 4 electrode measurements on K_2CO_3 (aq) immobilized in $SrTiO_3$.

over the whole frequency range with Z_{imag} always being zero.[66] This was almost the case for the measurements, however, a little variation in Z_{imag} and Z_{real} was seen. Therefore, for the four electrode measurements on pure K_2CO_3 (aq) the resistance was taken to be the mean of the modulus of the impedance (Z_{mod}) for those measurements for which the phase angle was smaller than $\pm 0.5°$ for ambient temperature and smaller than $\pm 1°$ for elevated temperature. For the measurements on immobilized K_2CO_3 (aq) the resistance was taken to be the average of the real part of the impedance (Z_{real}) for those measurements for which the imaginary part (Z_{imag}) was smaller than a certain limit, $\pm$0.1-1 Ω.

2.10 Thermodynamic Calculations

FactSage[68] is a program that can be used to make thermodynamic calculations. It calculates (predicts) chemical equilibria through Gibbs energy minimization. Calculations are therefore based on assuming complete equilibrium. Data from available databases are used in the calculations.

Phase diagrams have been calculated using FactSage.[68] The database Fact53 was used for the calculations and both liquids (except for plasmas), solids,

gas and aqueous species were allowed in the calculations. Gases were assumed to be real and not ideal. Available molar volume data was also included. Calculations were made for 0-100 wt% K_2CO_3 in H_2O at 0-300 °C at different pressures. Phase diagrams with CO_2 (g) were also calculated.

Equilibrium calculations were also made on systems containing K_2CO_3 + H_2O and K_2CO_3 + H_2O + CO_2. The calculations were based on the volume being fixed and with an inital pressure of 10-50 bars. Furthermore, equilibrium calculations were made in order to determine which species were present under given conditions.

2.11 Conductivity Models for Porous Systems

There are several models that can be used for calculating the conductivity of a system consisting of two phases with different conductivities, such as an aqueous electrolyte immobilized in a porous matrix. Among these are the Bruggeman asymmetric and symmetric models as well as Archie's law.[18,69,70]

The three models have been compared with results from conductivity measurements at ambient temperature on 10 wt% K_2CO_3 (aq) immobilized in both $SrTiO_3$ and TiO_2.

2.11.1 Bruggeman Asymmetric Model

The Bruggeman asymmetric model treats a continuous phase of conductivity σ_1 with an embedded discontinuous phase σ_2 and a volume fraction of x_2.[69,70]

$$\frac{\sigma_1}{\sigma_m}\left(\frac{\sigma_m-\sigma_2}{\sigma_1-\sigma_2}\right)^3=(1-x_2)^3 \tag{2.15}$$

where σ_m is the total conductivity of the dispersion and x_1, x_2 is the volume fraction of the continuous and the discontinuous phase, respectively.

If the discontinuous phase is non-conducting (σ_2 = 0) then σ_m can be found

using the simpler equation:

$$\sigma_m = \sigma_1 \left(1 - x_2\right)^{3/2} \tag{2.16}$$

2.11.2 Bruggeman Symmetric Model

The Bruggeman symmetric model makes no distinction between continuous and discontinuous phase.[69,70]

$$\sigma_m = \frac{1}{4}\left(q + \left(q^2 + 8\sigma_1\sigma_2\right)^{1/2}\right) \tag{2.17}$$

where

$$q = \left(3x_1 - 1\right)\sigma_1 + \left(3x_2 - 1\right)\sigma_2 \tag{2.18}$$

and

$$x_1 + x_2 = 1 \tag{2.19}$$

If σ_2 = 0 then σ_m can be found using the following equation:

$$\sigma_m = \frac{1}{4}\left(q + |q|\right) \tag{2.20}$$

and

$$q = \left(3x_1 - 1\right)\sigma_1 \tag{2.21}$$

The symmetric model predicts zero conductivity until 33.3 % porosity and then the conductivity follows a straight line with slope $3\sigma_1/2$. The model is therefore only valid for porosities above 33.3 % or if the conductivity is zero (or very close to) at porosities below 33.3 %.

2.11.3 Archie's Law

Archie's law is often used in petrophysics and relates the conductivity of a sedimentary rock to its porosity.[18]

$$\sigma_m = \sigma_1 \theta^m \tag{2.22}$$

where σ_m is the total conductivity of the rock (solution containing matrix), σ_1 is the conductivity of the pure solution, m is the cementation exponent (which is usually between 1 and 2) and θ is the porosity.

If θ is substituted with (1 - x_2) (the notation from the Bruggeman model) then the equation can be written as:

$$\sigma_m = \sigma_1 \left(1 - x_2\right)^m \tag{2.23}$$

which is identical to equation 2.16 for m = 1.5

Chapter 3

Properties of Bulk Electrolyte

3.1 Introduction

The properties of the electrolyte are very important, therefore, the first part of the project focused on the properties of pure K_2CO_3 (aq). The literature was searched for relevant properties of K_2CO_3 (aq) and the program FactSage[68] was used for calculating both phase diagrams and species present in the solution under different conditions.

A very important property is the conductivity, however, very little information could be found in the literature. Therefore, the first experimental part of the project focused on measuring the conductivity of pure K_2CO_3 (aq). The conductivity was measured at various concentrations and at both ambient and elevated temperature and pressure. All measurements were performed using the van der Pauw technique, see Section 2.8.

Highlights from this chapter have been submitted as a paper to Electrochimica Acta.

3.2 Experimental

The K_2CO_3 (aq) solutions were prepared from Milli-Q water and K_2CO_3 powder (Sigma-Aldrich, ACS reagent). Measurements were performed using the van der Pauw technique, described in Section 2.8 and the sample holder described in Section 2.9.2. A Gamry[67] potentiostat was used to perform the measurements. Measurements at ambient temperature and pressure were made in galvanostatic mode with 10 mA amplitude in the range 10 Hz - 10 kHz. The measurements were performed in all four possible configurations (where half have identical resistances), by rotating the wires 90° between each measurement. All measurements at elevated temperature and pressure were performed using the setup described in Section 2.7. The measurements were performed in potentiostatic mode and with 10 mV amplitude and in the range 100 Hz - 100 kHz. The measurements were performed with two different configurations at room temperature by making one measurement and then rotating the wires 90°. The measurements at elevated temperature were made with one configuration where the resistance was $R_{AB,CD}$.

The resistance was taken to be the mean of the modulus of the impedance (Z_{mod}) for those measurements for which the phase angle was smaller than $\pm 0.5°$ for ambient temperature and pressure and smaller than $\pm 1°$ for elevated temperature and pressure (see e.g. Figure 3.8).

3.3 Results

3.3.1 Solubility, Phase Diagrams and Species

It is very important to know how different conditions affect the K_2CO_3 (aq) electrolyte and which conditions that are optimal for the intended application: co-electrolysis at 200 °C. To study this, phase diagrams and equilibrium calculations have been carried out using FactSage.[68] One very important factor is to ensure that the solution stays aqueous and that K_2CO_3 does not precipitate as this would decrease the conductivity of the solution. In Figure 3.1 a phase diagram for 0-100 wt% K_2CO_3 (aq) at 0-300 °C can be seen. The database Fact53 was used for the calculations and both liquids (except for

plasmas), solids, gas and aqueous species were allowed in the calculations. Initially only K_2CO_3 and H_2O were assumed to be present at 30 bar. The calculations assume complete equilibrium. Gasses were assumed to be real and not ideal. Available molar volume data was also included. The different regions have been labelled. It can clearly be seen that there are limits both with respect to concentration and temperature. If the concentration becomes too high precipitation occurs and if the temperature becomes too high both precipitation and gas formation (mainly H_2O (g)) can occur. If the temperature is kept below 200 °C concentrations up to approx. 20 wt% K_2CO_3 (aq) can be used. The highest concentration that can be used at 25 °C is approx. 53 wt% which matches the solubility limit reported in the literature, 52.7 wt%.[12]

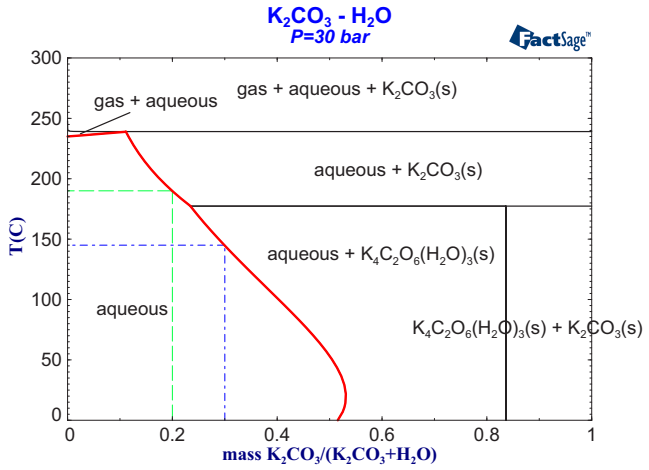

Figure 3.1: Calculated phase diagram for K_2CO_3 and H_2O at 0-300 °C and 30 bar. The dashed and dash-dot line indicates at which temperature precipitation occurs for 20 and 30 wt% K_2CO_3 (aq) respectively. The thick line shows the limit for the aqueous region. The phase diagram has been calculated using FactSage.[68]

In Figure 3.2 it can be seen which temperatures and pressures are needed for keeping a 10 wt% K_2CO_3 (aq) solution completely aqueous. The calculations have been made with a N_2 partial pressure of 10 bar. N_2 was included as it is almost completely inert and in order to have some gas present in the calculations. It can be seen that increasing the pressure increases the aqueous

region so the solution will stay aqueous at higher temperatures, however at temperatures above 250 °C precipitation will occur no matter the pressure.

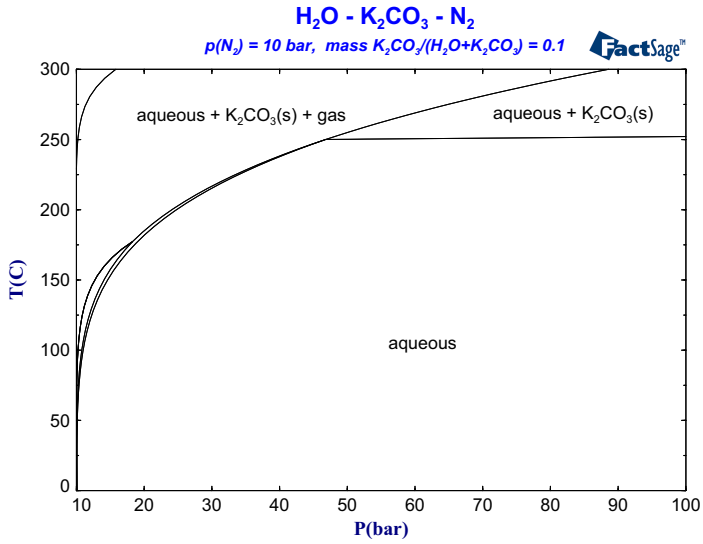

Figure 3.2: Calculated phase diagram for 10 wt% K_2CO_3 (aq) from 0-300 °C and 10-100 bar. The partial pressure of N_2 is 10 bar and the different regions have been labelled. The phase diagram has been calculated using FactSage. [68]

If the atmosphere also contains CO_2 the phase diagram changes, see Figure 3.3. The phase diagram shows the different regions for 0-100 wt% K_2CO_3 (aq) from 0-300 °C in 1 bar of CO_2 and a total pressure of 30 or 100 bar. The aqueous region is much smaller when measuring in a CO_2 containing atmosphere than in a N_2 atmosphere, see Figure 3.1, especially at lower temperatures. This significantly limits the concentration range that can be used for measurements/applications in CO_2 atmosphere. Only concentrations of 10 wt% or less can be used from 25 °C to approx. 225 °C without the risk of precipitation with a total pressure of 30 bar. If the pressure is 100 bar it should theoretically be possible to go up to almost 300 °C, based on the thermodymic calculations. It can be seen that increasing the pressure moves the line where gas formation occurs up to higher temperatures, it does however not affect

the concentration range at lower temperatures. Increasing the partial pressure of CO_2 does not a significant effect on the aqueous region below 200 °C, see Appendix A.

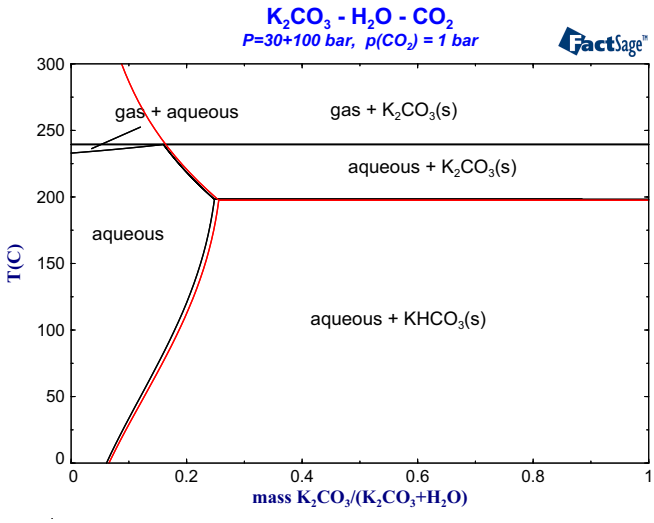

Figure 3.3: Calculated phase diagram for K_2CO_3 and H_2O at 0-300 °C and 1 bar of CO_2. The black lines are for a total pressure of 30 bar and the red line are for 100 bar. The phase diagram has been calculated using FactSage.[68]

The species in 10 wt% K_2CO_3 (aq) at 30 bar in N_2 and in CO_2 have been calculated using FactSage,[68] see Figure 3.4 and 3.5. The calculations have been made on 20 g of solution from 20 to 200 °C. The calculations are based on a fixed volume of 0.6 L and constant pressure. The pressure was kept constant by allowing the the amount of N_2 and CO_2 to vary with temperature. It can be seen that in N_2 atmosphere there is a change in aqueous species when the temperature increases. The change is from CO_3^{2-} to HCO_3^- and OH^- species. This indicates that reaction 1.6 in Section 1.2 is exothermic, wherefore, an increase in temperature will push the equilibrium to the left. At 200 °C approx. half of the CO_3^{2-} ions are converted to HCO_3^- and OH^-. The amount of H^+ is almost zero for the whole temperature range.

In CO_2 atmosphere different species are predicted to be present. Below 40 °C it can be seen that some precipitation of $KHCO_3$ (s) occurs which is consistent with the solubility limit indicated on Figure 3.3. From 40-200 °C the $KHCO_3$ (s) is redissolved which also correlates well with Figure 3.3. The amount of K^+ and HCO_3^- species is the same for the whole temperature range and these are the main species in the solution. The concentration of H^+, OH^- and CO_3^{2-} is almost zero for the whole temperature range.

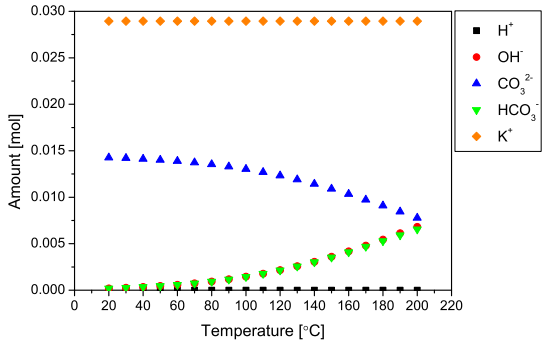

Figure 3.4: Aqueous species in 10 wt% K_2CO_3 (aq) from 20-200 °C at 30 bar in N_2 atmosphere calculated using FactSage.[68] The calculations have been made on 20 g of solution and with a fixed volume of 0.6 L.

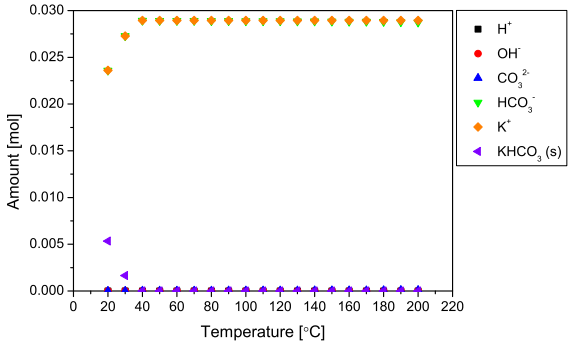

Figure 3.5: Aqueous species in 10 wt% K_2CO_3 (aq) from 20-200 °C at 30 bar in CO_2 atmosphere calculated using FactSage.[68] The amount of $KHCO_3$ (s) is also shown. The calculations have been made on 20 g of solution and with a fixed volume of 0.6 L.

3.3.2 Conductivity at Ambient Pressure and Temperature

The conductivity of 10-50 wt% aqueous K_2CO_3 at ambient temperature and pressure was measured and compared to literature values,[12,71] see Figure 3.6 and 3.7. The resistance was found to be almost identical for the four different configurations so the conductivity was calculated using equation 2.6 and 2.10 in Section 2.8. The average of the conductivity found for each of the four different configurations was defined as the sample conductivity.

The measured values were in good agreement with the literature values. The conductivity appeared to increase non-linearly with concentration and reached a maximum at 30-40 wt% K_2CO_3 (aq). At higher concentration the conductivity decreased again.

It was also found that the conductivity was highly temperature sensitive as a change of only a few degrees had significant effect on the conductivity. In Figure 3.7 the conductivity of an aqueous solution with 0-7.5 wt% K_2CO_3 is shown. In this case there was good agreement between the literature values.

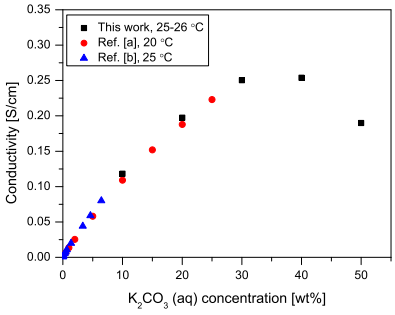

Figure 3.6: Conductivity of 0.01-50 wt% K_2CO_3 (aq) at ambient temperature. [a][12] and [b].[71]

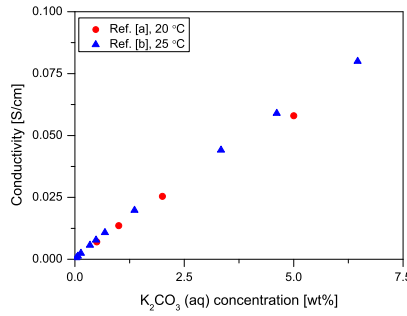

Figure 3.7: Low concentration region of Fig. 3.6. [a][12] and [b].[71]

3.3.3 Conductivity at Elevated Pressure and Temperature

The conductivity of 5-30 wt% K_2CO_3 (aq) was also measured from ambient temperature up to 180-200 °C at 30 bar. The difference between the two re-

sistances $R_{AB,CD}$ and $R_{BC,DA}$ measured at ambient temperature was found to be small enough for 5-20 wt% K_2CO_3 (aq) to allow the correction factor, f, to be one. The difference was, however, larger for 30 wt% K_2CO_3 (aq), wherefore the correction factor was found, using equation 2.8 in Section 2.8, and applied to the data for 30 wt% K_2CO_3 (aq). The specific measured resistance, $\rho_{measured}$ was found by taking the average of Z_{mod} for all frequencies where the phase angle was smaller than $\pm 1°$ and then using equation 2.7 or 2.9 (assumming $R_{AB,CD} = R_{BC,DA}$) and 2.10 in Section 2.8. The corrected specific resistance ($\rho_{correct}$) was found by multiplying the specific measured resistance with the average of $R_{AB,CD}$ and $R_{BC,DA}$, divided by $R_{AB,CD}$, all measured at room temperature:

$$\rho_{corrected} = \rho_{measured} \cdot \frac{R_{average}}{R_{AB,CD}} \tag{3.1}$$

Finally the specific conductivity was found using eq. 2.10 in Section 2.8.

The Z_{mod} and phase angle of a typical measurement can be seen in Figure 3.8. It can be seen that Z_{mod} was very stable over the whole frequency range. The Figure also shows that the phase angle was smaller than $\pm 2°$ for the whole frequency range and smaller than $\pm 0.5°$ in the range 100-20000 Hz.

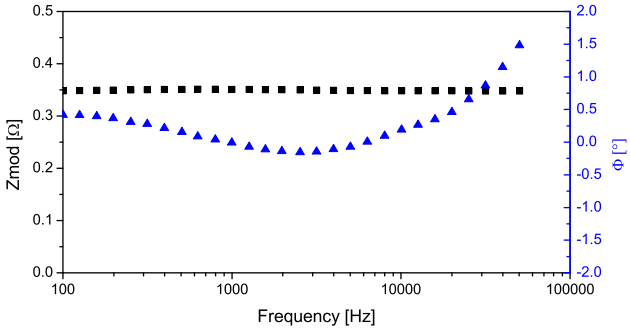

Figure 3.8: Z_{mod} (■ left) and phase angle (▲ right) as a function of frequency for a typical measurement.

Figure 3.9 shows the conductivity of 5-30 wt% K_2CO_3 (aq) at elevated temperature and pressure. It can be seen that the conductivity increased almost

linearly with temperature up to 100-120 °C. The conductivity also increased with concentration. For 30 wt% K_2CO_3 (aq) a drop in conductivity was seen above 180 °C and for 20 wt% a small drop was seen at 150 °C. The highest conductivity measured was 1.34 S/cm at 172 °C for 30 wt% K_2CO_3 (aq).

The conductivities for 5-30 wt% K_2CO_3 (aq) from ambient temperature to 180 °C have been fitted using a third order polynomial, see Figure 3.9. The fits have no particular physical meaning but can be used for estimating conductivities at other temperatures and concentrations than the measured. The estimated conductivity at a range of temperatures can be found in Table 3.1.

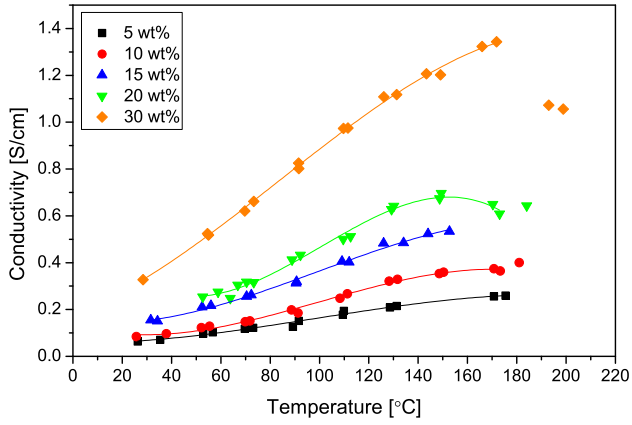

Figure 3.9: Conductivity of 5-30 wt% K_2CO_3 (aq) from ambient temperature to 180-200 °C. All measurements were performed at 30 bar. The lines are third order polynomial fits made for each concentration from ambient temperature to 180 °C.

Table 3.1: Conductivity of 5-30 wt% K_2CO_3 (aq) at various temperatures, calculated from third order polynomial fits.

	20 °C	40 °C	60 °C	80 °C	100 °C	120 °C	140 °C	160 °C	180 °C	200 °C
5 wt%	0.06	0.08	0.10	0.13	0.16	0.20	0.23	0.25	0.26	0.26
10 wt%	0.10	0.10	0.13	0.17	0.23	0.29	0.34	0.37	0.37	0.33
15 wt%	0.14	0.17	0.22	0.29	0.36	0.44	0.51	0.56	0.58	0.57
20 wt%	0.37	0.27	0.27	0.35	0.47	0.58	0.66	0.67	0.58	0.33
30 wt%	0.28	0.41	0.56	0.72	0.88	1.04	1.18	1.29	1.36	1.39

The phase diagram in Figure 3.1 shows that precipitation of $K_4C_2O_6(H_2O)_3$ ($(K_2CO_3)_2(H_2O)_3$) occurs for 30 wt% K_2CO_3 (aq) above 145 °C and that precipitation of K_2CO_3 occurs for 20 wt% K_2CO_3 (aq) above 190 °C. Precipitation would result in fewer charge carriers and therefore a drop in conductivity as seen in Fig. 3.9. The phase diagram, Fig. 3.1, also shows that precipitation of $K_4C_2O_6(H_2O)_3$ ($(K_2CO_3)_2(H_2O)_3$) occurs at concentrations above approx. 50 wt% at room temperature and that the precipitation takes place at lower concentrations with increasing temperature.

Activation Energy

The activation energy for conductivity can be found using the modified Arrhenius equation:[30,72]

$$\sigma = \frac{A}{T} e^{-E_a/RT} \tag{3.2}$$

where A is the pre-exponential factor, E_a the activation energy and R the gas constant. Although the application of this equation to liquids is not entirely consistent with current theory of liquid transport, it is found to provide a good description of the data. A plot of ln(σT) as a function of 1/T will have the slope $-E_a/R$. Figure 3.10 shows ln(σT) as a function of 1/T for 5-30 wt% K_2CO_3 (aq) for temperatures below 150 °C and the corresponding linear fits. The pre-exponential factor (A) and the activation energy (E_a) can be found in Table 3.2. The fit appears to describe the data well and the activation energy was the in range 0.14-0.17 eV for all the measured concentrations. It can be seen that the activation energy was similar for 5, 15 and 30 wt% K_2CO_3 (aq) and higher for both 10 and 20 wt%. Furthermore, the pre-exponential factor for 15 wt% K_2CO_3 (aq) is very close to the value for 10 wt% K_2CO_3 (aq) and therefore lower than expected if the values are following a trend.

Table 3.2: Pre-exponential factor and activation energy including standard error for 5-30 wt% K_2CO_3 (aq). Calculated from a linear fit of ln(σT) as a function of 1/T using y = a + bx.

	5 wt%	10 wt%	15 wt%	20 wt%	30 wt%
A/(K·S/cm)	6800±1200	14800±2100	16200±1400	28300±5000	34500±3900
E_a/eV	0.152±0.005	0.166±0.004	0.154±0.003	0.165±0.006	0.149±0.004

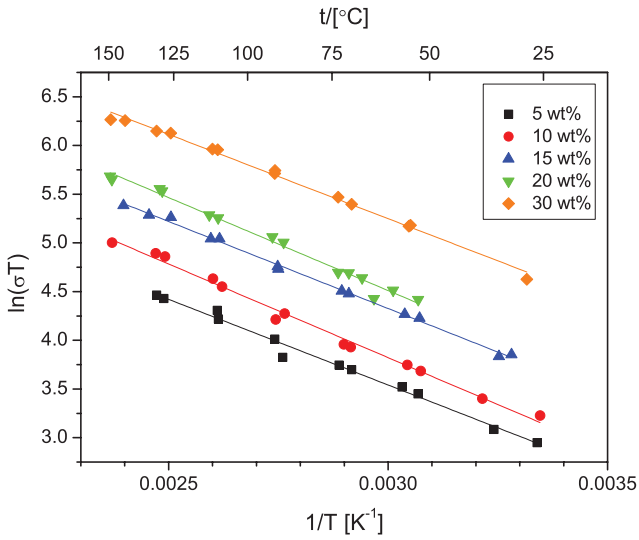

Figure 3.10: Arrhenius plot showing ln(σT) as a function of 1/T for 5-30 wt% K_2CO_3 (aq). The lines show the linear fits.

3.4 Discussion

The solubility of K_2CO_3 (s) in water is 52.7 wt% at 25 °C.[12] This sets the limit for how strong concentrations that can be made and measured at RT in air (or an inert gas).

The fact that Figure 3.3 does not change significantly below 200 °C when the CO_2 partial pressure is increased indicates that equilibrium 1.2 in Section 1.2 has been shifted as much as possible to the right and therefore, increasing the CO_2 partial pressure (and thereby possibly the CO_2 (aq) concentration) has no significant effect.

Figure 3.4 shows that there is a change in aqueous species from CO_3^{2-} to HCO_3^- and OH^- when the temperature increases. This indicates that reaction 1.6 in Section 1.2 is exothermic, wherefore, an increase in temperature will push the equilibrium to the left.

The fact that K^+ and HCO_3^- are the main species in a 10 wt% K_2CO_3 (aq) solution in CO_2 atmopshere from 40-200 °C fits well with equilibrium 1.2 in Section 1.2 which should be pushed to the right when the partial pressure of CO_2 increases, as this should increase the CO_2 concentration. This also indicates that the main charge carriers for a 10 wt% K_2CO_3 (aq) electrolyte being used in CO_2 atmosphere is K^+ and HCO_3^-.

The difference between the measured conductivity values and the values found in the literature, see Figure 3.6, can be explained by the difference in temperature. The drop in conductivity for 30 wt% K_2CO_3 (aq) seen in Fig. 3.9 can be partly explained by the calculated phase diagram seen in Fig. 3.1. According to the calculated phase diagram, precipitation should occur above 145 °C and not 172 °C as seen in Fig. 3.9. One possible explanation is that the system was not at equilibrium or that the measured temperature was not the actual sample temperature. This would lead to precipitation at a higher temperature than expected.

For 20 wt% K_2CO_3 (aq) there appeared to be a decrease in conductivity above 150 °C, see Figure 3.9, which was not expected since the phase diagram indicates that precipitation occurs above 190 °C for 20 wt% K_2CO_3 (aq). The heating of the sample was not stable but overshooting often and therefore cooling occurred before measuring at the desired temperature. It is possible that the temperature had been above 200 °C and precipitation had occurred and that the precipitation was still present at the time of measurement. Furthermore, if the thermo well is measuring lower temperatures than expected and maybe also cooling faster than the liquid the measured temperature will be lower than the sample temperature. Another possibility is that water has been evaporating from the liquid which would cause higher local concentrations and therefore precipitation and again loss of conductivity.

Another possible explanation is that the conductivity is reaching a limiting factor such as a maximum mobility at higher temperatures. However, this tendency is not seen in all cases. Another limiting factor could be blocking of the electrodes. Due to the increasing temperature, gas had to be let out of

the autoclave to keep the pressure constant and when this happened a quick drop of less than 1 bar in the total pressure occurred. This could have lead to bubble formation on the electrodes and also on the sample holder walls. Even a small bubble would be relatively big on the small electrode wires and therefore blocking a substantial part of the electrode.

When the autoclave is pressurized a slight compression of the liquid takes place. This results in more charge carriers per volume of liquid and therefore a possible change in conductivity when comparing to ambient pressure data. However, the adiabatic compressibility of 3 wt% K_2CO_3 (aq) at 25 °C is $41.757 \cdot 10^{-10}$ Pa^{-1} and for water it is $44.7 \cdot 10^{-10}$ Pa^{-1}.[73] For higher concentrations of K_2CO_3 (aq) the compressibility should be even smaller which means that the error would be negligible. Upon heating, thermal expansion occurs which would result in fewer charge carriers per volume and, therefore, a possible loss of conductivity. The thermal expansion of a 27 wt% K_2CO_3 aqueous solution from -15 to 40 °C is less than 2 % and less than 0.5 % for water.[74] During cooling the liquid is compressed and the height of the liquid therefore decreases. However, liquid is placed in the hole of the lid so when the liquid is compressed extra liquid is available, thereby minimizing the change in height of the liquid. The increase in conductivity from 25 to 50 °C is however around 50 %, which makes the up to 1 % change due to thermal expansion negligible.

The Arrhenius fits were good and the activation energy was found to be quite low, 0.14-0.17 eV, and did not appear to be dependent on concentration in this case. The values are similar to the values found for Nafion® membranes (approx. 0.1 eV) and for other aqueous solutions[30,75] and much lower than the values found for typical solid electrolytes, based on zirconium and cerium oxides (0.6-1.0 eV).[76] The fit was limited to conductivity values obtained below 150 °C due to the loss of conductivity for 20 wt% K_2CO_3 (aq) seen above this temperature. The low pre-exponential factor found for 15 wt% K_2CO_3 (aq) can be explained by the measured temperature being lower than the actual sample temperature due to using a thermo well. This would increase both the pre-exponential factor and also the activation energy. An increased activation energy for 15 wt% K_2CO_3 (aq) would also mean that the activa-

tion energy peaks at 15 wt% K_2CO_3 (aq) and would thus be dependent on concentration.

3.5 Conclusion

If the concentration is kept below 20 wt% then aqueous K_2CO_3 can be used as an electrolyte from ambient temperature up to 200 °C with a pressure of 30 bar leading to conductivities up to 0.6 S/cm.

The main charge carriers for 10 wt% K_2CO_3 (aq) used in CO_2 atmosphere are most likely K^+ and $HCO_3{}^-$.

K_2CO_3 (aq) has good potential as an electrolyte. The small temperature dependence makes pressurized K_2CO_3 (aq) an interesting candidate as a new potential electrolyte at elevated temperatures.

Chapter 4

Water Management at Elevated Temperature and Pressure

4.1 Introduction

Measuring the conductivity of immobilized aqueous solutions at elevated temperatures and pressures can lead to unforeseen problems. It is therefore essential to evaluate the method used to conduct the measurements. This chapter describes problems observed during the pressurized tests on immobilized K_2CO_3 (aq) and analyses possible ways to mitigate setup-introduced errors.

The pressurised setup described in Section 2.7 has been used for all measurements presented in this chapter.

Equilibrium calculations have been performed using FactSage.[68] The water partial pressure and water vapour content at different measurement conditions has been calculated.

4.2 Results

4.2.1 Conductivity Measurement Problems

In many tests the pellets with immobilized K_2CO_3 (aq) stopped working at 90-120 °C or showed a significant drop in conductivity, see Figure 4.1. In most cases this occurred suddenly with the resistance increasing from a few ohms or less to kΩ or MΩ from one measurement to the next. This problem was never observed for the measurements on pure K_2CO_3 (aq) solutions, see Figure 3.9 in Chapter 3. After the tests the pellets appeared dry and would regain conductivity if water was added, indicating that they had "dried out" during test.

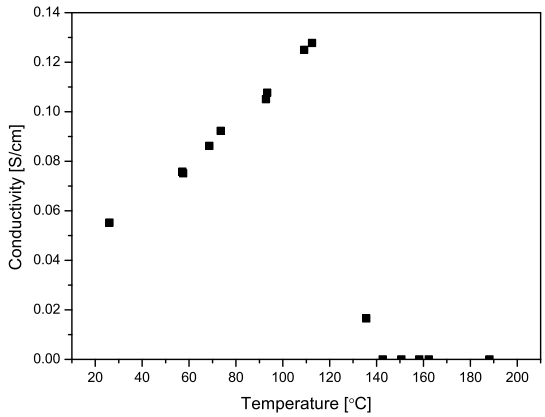

Figure 4.1: Conductivity of 10 wt% K_2CO_3 (aq) immobilized in $SrTiO_3$ from ambient temperature to 190 °C. The measurements was performed at 30 bar using a four electrode sample holder.

The pressurized setup did not allow for humidified inlet gases so all water management had to be included into the pressurized part. Therefore, a reservoir with a lower concentration was included in the setup as mentioned in Section 2.7. The reservoir was supposed to avoid water evaporation from the immobilized solution due to its lower concentration, see Section 2.7, as it should be more favorable to evaporate water from the lower concentration reservoir than from the immobilized solution. Many tests were performed to

figure out exactly why the pellets were "drying out". No temperature gradients were found in the autoclave that could explain the problem. The size and position of the sample holder as well as varying the sample height appeared to have no effect. Neither did changing the total pressure or letting the pressure increase with temperature instead of keeping it constant. The problem seemed present for all measured concentrations of K_2CO_3 (aq) immobilized in both $SrTiO_3$ and TiO_2. Changing the atmosphere from N_2 to CO_2 did not have any effect either. Decreasing the ramp rate appeared to have some positive effect on the stability, see Figure 4.2. But unfortunately this effect was not consistent. Furthermore, it was observed that the conductivity for increasing temperature was lower when using a slower ramp rate.

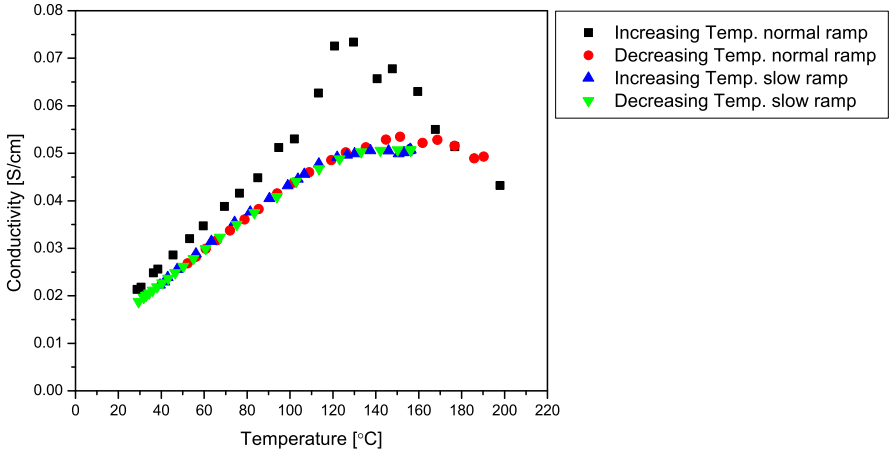

Figure 4.2: Conductivity as a function of temperature for a cell consisting of 10 wt% immobilized K_2CO_3 (aq) immobilized in $SrTiO_3$ and STN electrodes. The cell was tested in N_2. The normal ramp rate of the heating mantle consisted of ramping 30 °C within 30 min and then holding the temperature for 30 min, up to 270 °C. The slow ramp rate was different from 150 °C and up, where the ramping and holding time was changed from 30 min to 1 hour. The ramp only went up to 210 °C and was kept there for 5 hours. Four bad data points at 180-200 °C have been removed from the normal ramp rate data set.

In some tests part of the conductivity was regained after longer times at a constant temperature or when ramping down in temperature. In two tests in a row the problem never occurred, see Figure 5.10 in Section 5.3.3.1. This

result could however never be reproduced, not even using the same pellet, sample holder and heating ramp program.

One test indicated that the problem was caused by the large surface area between the immobilized solution and the gas since the problem appeared to be smaller when $SrCO_3$ formation partly blocked the surface of the electrodes, see Section 5.3.3.1. This caused the conductivity to flatten out at elevated temperatures but the cell continued to work.

4.2.2 Thermodynamic Calculations

In Figure 4.3 the water partial pressure and amount of water in the gas phase as a function of temperature for a 10 wt% K_2CO_3 (aq) solution in N_2 atmosphere can be seen. The calculations were based on 30 g of solution and a constant pressure of 30 bar. This is very similar to the conditions of many of the conductivity measurements performed during the project. 30 g of solution is similar to the total amount of solution in the reservoir and pellet. The Figure shows that the partial pressure increased with temperature as expected. It can also be seen that the amount of water in the gas phase was more than 1 gram above 130 °C and approx. 4 g at 200 °C.

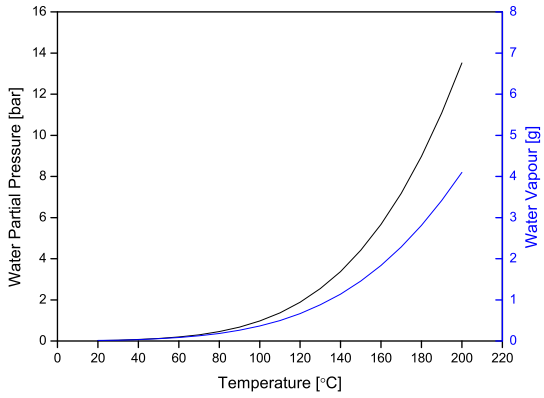

Figure 4.3: Water partial pressure and amount of water in the gas phase as a function of temperature for 10 wt% K_2CO_3 (aq) in N_2 atmosphere with a constant pressure of 30 bar. Calculations have been made in 10 °C steps on a 0.6 L volume using FactSage.[68]

Figure 4.4 shows the water partial pressure as a function of temperature for 0-30 wt% K_2CO_3 (aq) in N_2 atmosphere with a constant pressure of 30 bar. It can be seen that the partial pressure only decreased slightly with increasing concentration. The difference between pure water (0 wt% K_2CO_3 (aq)) and 30 wt% K_2CO_3 (aq) was less than 2 bars at 200 °C and between pure water and 10 wt% K_2CO_3 (aq) it was less than 1 bar at 200 °C.

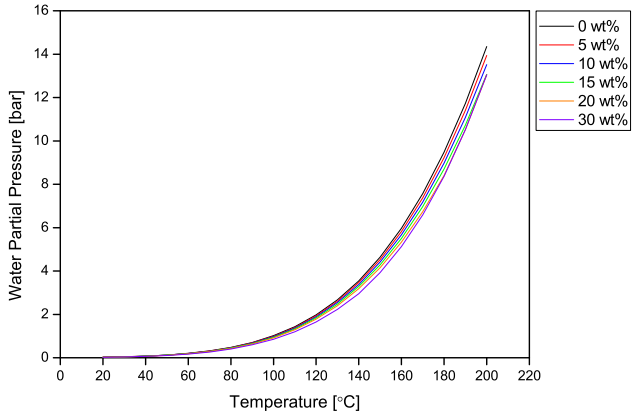

Figure 4.4: Water partial pressure as a function of temperature for 0-30 wt% K_2CO_3 (aq) in N_2 atmosphere with a constant pressure of 30 bar. Calculations have been made in 10 °C steps on a 0.6 L volume using FactSage.[68]

In Figure 4.5 and 4.6 it can be seen how the water partial pressure varied with the total pressure for a 10 wt% K_2CO_3 (aq) solution in N_2 and CO_2 atmosphere. Comparing the two graphs, it can be seen that increasing the total pressure increased the water partial pressure slightly as expected since there was more gas to humidify. It can also be seen that the difference between N_2 and CO_2 atmosphere was negligible.

Figure 4.7 shows the partial pressure and total pressure as a function of temperature for 10 wt% K_2CO_3 (aq) in N_2 atmosphere. The inital pressure was 30 bar and the pressure was allowed to increase with temperature. It can be

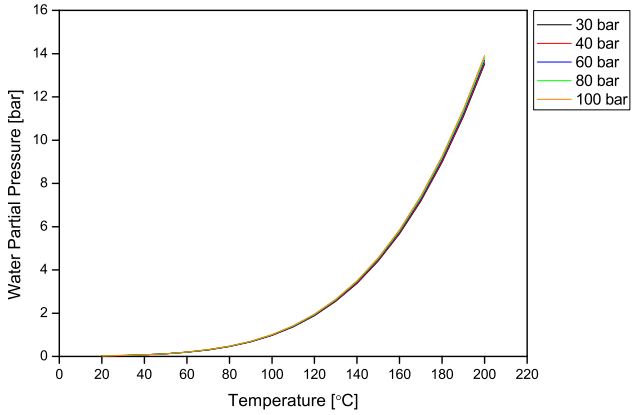

Figure 4.5: Water partial pressure as a function of temperature for 10 wt% K_2CO_3 (aq) in N_2 atmosphere with a constant pressure of 30-100 bar. Calculations have been made in 10 °C steps on a 0.6 L volume using FactSage.[68]

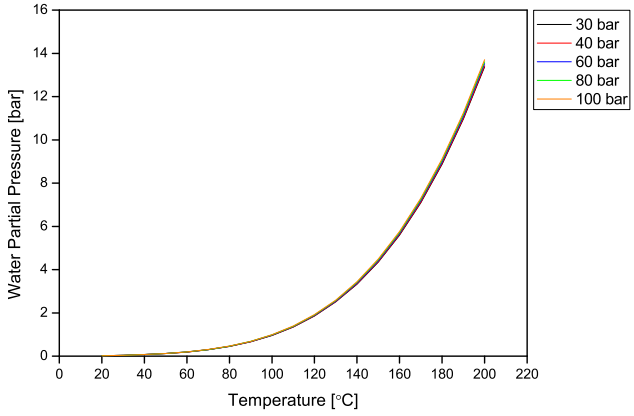

Figure 4.6: Water partial pressure as a function of temperature for 10 wt% K_2CO_3 (aq) in CO_2 atmosphere with a constant pressure of 30-100 bar. Calculations have been made in 10 °C steps on a 0.6 L volume using FactSage.[68]

seen that the water partial pressure difference between keeping a constant pressure, Figure 4.3, and letting it increase with temperature was negligible which was expected looking at Figure 4.5.

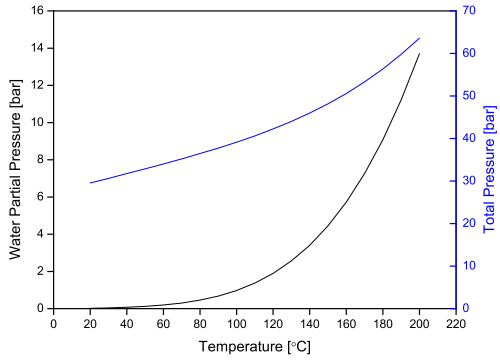

Figure 4.7: Water partial pressure and total pressure as a function of temperature for 10 wt% K_2CO_3 (aq) in N_2 atmosphere with an initial pressure of 30 bar. Calculations have been made in 10 °C steps on a 0.6 L volume using FactSage.[68]

In Figure 4.8 the amount of water in the gas phase for a 10 wt% K_2CO_3 (aq) solution can be seen. The calculations have been made on 30 g of solution in N_2 atmosphere and a volume of 0.6 and 0.25 L, respectively. It can be seen that the amount of water in the gas phase decreased significantly when the volume was decreased. This was as expected since there was less gas to humidify.

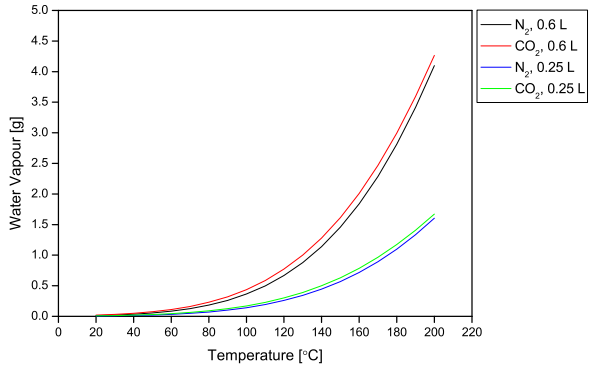

Figure 4.8: Amount of water in the gas phase as a function of temperature for 10 wt% K_2CO_3 (aq) in N_2 and CO_2 atmosphere with a constant pressure of 30 bar. Calculations have been made in 10 °C steps on a 0.6 and 0.25 L volume using FactSage.[68]

4.2.3 Measurements on Modified Setup

Conductivity measurements were also performed using pure water in the reservoir (instead of an K_2CO_3 (aq) solution) and with a decreased autoclave volume, see Figure 4.9. If the pellet was "drying out" due to water evaporation from the pellet instead of the reservoir this should decrease the problem and result in more stable measurements, as indicated by the results in Section 4.2.2. The Figure clearly shows that the conductivity was much more stable than in Figure 4.1.

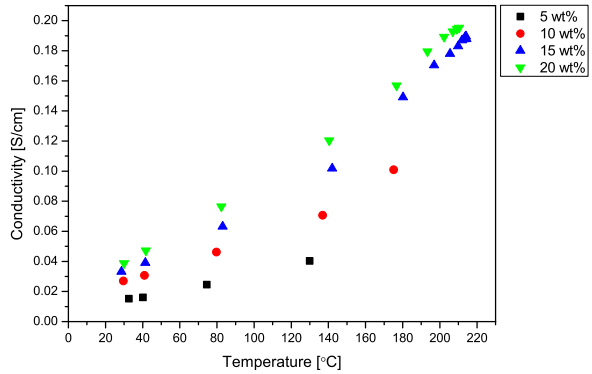

Figure 4.9: Conductivity of 5-20 wt% K_2CO_3 (aq) immobilized in TiO_2 from ambient temperature to max. 215 °C. All measurements were performed on the same pellet. All measurements were performed with an initial pressure of 30 bar and the pressure was allowed to increase with temperature.

4.3 Discussion

As problems with water evaporation from the solution was not observed when measuring on pure solution, see Figure 3.9 in Chapter 3, it indicated that the problem was related to the immobilization or the smaller amount of solution in the pellets compared to the amount used for pure solution measurements, 0.1-0.3 mL and 2 mL, respectively.

Figure 4.4 shows that the driving force for evaporating water from the reservoir instead of the pellet became very small if the reservoir only had a slightly

lower concentration than the solution in the pellet. Even using pure water in the reservoir when measuring 10 wt% K_2CO_3 (aq) would not result in a very strong driving force.

The results in Section 4.2.2 clearly showed that the water loss above 100 °C was significant especially when looking at the small amount of solution in the pellets; 0.1-0.3 mL. If just 10 % of the water loss came from the pellet then it would be enough to cause the surface of the pellet to dry out, in some cases the whole pellet. Precipitation could also be occuring if the concentration becomes too high due to the water loss, as seen in the calculated phase diagrams in Section 3.3.1. Minimizing the amount of gas will decrease the amount of water being evaporated, as there is less gas to humidify, and should therefore reduce the problem. Increasing the surface area between the reservoir and the gas should also make evaporation from the reservoir more favorable.

These considerations lead to new measurements, see Figure 4.9, where the volume of the autoclave was decreased from 0.6 L to approx. 0.25 L by adding ceramic zirconia beads. The beads were added to the Teflon liner and the liner was filled all the way up to the sample holder. Water was also used in the reservoir instead of a K_2CO_3 (aq) solution to make the driving force for evaporating water from the reservoir instead of the pellet as strong as possible. Water was added up to approx. 1 cm from the top of the beads, to wet the top beads and thereby increase the surface area. Choosing pure water in the reservoir would in theory (based on thermodynamics) cause the pellet to be flooded when the system approaches equilibrium, since equilibrium will mean that the pellet and the reservoir have the same concentration. However, the previous measurements indicated that the equilibrium of the system is approached very slowly as it was never reached within the time frame of the measurements. Therefore, the system appeared to have kinetic limitations. Figure 4.9 clearly showed that the modifications to the setup improved the results, especially at concentrations above 5 wt% K_2CO_3 (aq). It can, however, also be seen that the system is not completely stable and appears to be trying to approach equilibrium, as the difference in conductivity between 15 and 20 wt% K_2CO_3 (aq) appears to be very small at elevated temperatures.

The best way to avoid the "drying of the pellet" is naturally to humidify the inlet gas. Such a substantial change to the setup was, however, not possible within the scope of the project. The easiest way to get the correct humidification is to pass the inlet gas through a solution identical to the one being measured under the exact same conditions. This, however, is quite complicated when using a pressurized setup and would require a different setup e.g. with flow. Steam can also be added using a catalytic burner, but the amount of steam produced has to be varied with temperature as the water partial pressure varies with temperature. If the added amount of steam is too small the pellet will dry out but if the amount is too large the pellet will be flooded instead. Since it is hard to add more solution to the pellet during a test it should be more favorable to run the test with slightly too little steam. If the pellet starts "drying" more steam can be added which should cause the pellet to regain conductivity, however the time this takes is unknown.

4.4 Conclusion

Problems with water evaporation from the immobilized K_2CO_3 (aq) solutions at elevated temperature and pressure have been encountered during the course of the project. Decreasing the volume of the autoclave and using pure water in the reservoir appeared to significantly improve the stability of the tests. It is, however, only a compromise for tests running over longer times since the pellet should be flooded over time when the system approaches equilibrium. A better solution is to use a setup with a flow and humidify the inlet gas. However, this is complicated as the water partial pressure changes with temperature but if achieved it should make long-term testing possible. Due to time limitations such improvements to the setup was not possible during the course of the project.

As water evaporation from the immobilized solution usually lead to a rapid drop in conductivity data up to this point should be relatively reliable. Thus, in the following chapters only reliable data are presented.

Chapter 5

Immobilized K_2CO_3 (aq)

5.1 Introduction

After determining the conductivity of pure K_2CO_3 (aq) under various conditions and verifying it as a potential electrolyte material, the project moved on to focus on immobilized K_2CO_3 (aq). Initial measurements and studies were performed on $SrTiO_3$ pellets (with immobilized K_2CO_3 (aq)) made with powder from the modified glycine nitrate combustion process, described in Section 2.1.1. These studies showed that the solution could be immobilized easily and that measurements of the conductivity was possible. All measurements presented in this chapter on K_2CO_3 (aq) immobilized in $SrTiO_3$ have, however, been made on $SrTiO_3$ pellets made from powder from Inframat Advanced Materials, USA. As all the $SrTiO_3$ powder from Inframat Advanced Materials come from the same batch, this should result in similar pellets. Measurements were also performed on K_2CO_3 (aq) immobilized in TiO_2, these pellets were also made using powder from the same batch from Sigma-Aldrich.

In this chapter the conductivity of K_2CO_3 (aq) immobilized in both $SrTiO_3$ and TiO_2 is presented. Values at both ambient and elevated temperature and pressure are given as well as results from measurements in CO_2 atmosphere. Furthermore, the microstructure of two different matrix materials and their effect on the conductivity are compared.

5.2 Experimental

$SrTiO_3$ and TiO_2 pellets were made using the method described in Section 2.2. All pellets were sintered for 12 hours at 1000 °C unless otherwise stated.

The K_2CO_3 (aq) solutions were prepared from Milli-Q water and K_2CO_3 powder (Sigma-Aldrich, ACS reagent). The K_2CO_3 (aq) solutions were immobilized by submerging/soaking the $SrTiO_3$ and TiO_2 pellets in the solution for min. 5 min.

Conductivity measurements were performed on 0.001-30 wt% K_2CO_3 (aq) immobilized in $SrTiO_3$ and 0.001-20 wt% K_2CO_3 (aq) immobilized in TiO_2.

Measurements at ambient temperature and pressure were performed using two different setups, one with and one without gas flow. The measurements performed using the setup without gas flow were made in potentiostatic mode with 10 mV amplitude in the range 1 Hz - 1 MHz. The resistance was found as described in Section 2.9.1 with a Z_{imag} limit of ± 1 Ω for measurements with varying porosity. For the measurements with varying concentration the Z_{imag} limit was ± 50 Ω for measurements with concentrations below 5 wt% and ± 5 Ω for the other concentrations. Furthermore, the data were corrected for inductance, which was less than 1 %. In most cases two measurements were performed on each pellet and the difference was negligible wherefore the average of the two measurements was used.

The non-pressurized setup, described in Section 2.7, was used to perform measurements with gas flow. The measurements were performed at ambient temperature using the van der Pauw method, described in Section 2.8. A four

electrode sample holder, described in Section 2.9.2, was used for the measurements which were made in potentistatic mode in the range 100 Hz - 100 kHz. The amplitude was 10 mV for the measurements on 10 wt% K_2CO_3 (aq) immobilized in $SrTiO_3$ and 5 mV for the measurements on 30 wt% K_2CO_3 (aq) immobilized in $SrTiO_3$. The resistance was found by taking the average of Z_{real} for those measurements for which Z_{imag} was smaller than $\pm 0.1\ \Omega$.

Measurements on K_2CO_3 (aq) immobilized in $SrTiO_3$ at elevated temperature and pressure have been made using both a four electrode sample holder and a two electrode sample holder. The pressurized setup described in Section 2.7 was used for the tests. The measurements conducted using a four electrode sample holder, described in Section 2.9.2, were made in potentiostatic mode with 10 mV amplitude in the range 100 Hz - 100 kHz. Except for 5 wt% K_2CO_3 (aq) immobilized in $SrTiO_3$ which was measured with 5 mV amplitude. The measurements were made with a constant pressure of 30 bar except for 20 wt% immobilized K_2CO_3 (aq) which was measured at 40 bar. The measurements at elevated temperature were made with one configuration and corrected as described in Chapter 3. The resistance was found by taking the average of Z_{real} for those measurements for which Z_{imag} was smaller than $\pm 0.1\ \Omega$. The measurements made using the two electrode sample holder, described in Section 2.9.1, were made in potentiostatic mode with 5 mV amplitude in the range 10 Hz - 100 kHz or 100 Hz - 100 kHz. The measurements were performed with an initial pressure of 30 bar and the pressure was then allowed to increase with temperature. The resistance was found by taking the average of Z_{real} for those measurements for which Z_{imag} was smaller than $\pm 0.1\ \Omega$.

The measurements on K_2CO_3 (aq) immobilized in TiO_2 pellets at elevated temperature and pressure were made using a two electrode sample holder, described in Section 2.9.1. The measurements were conducted in potentiostatic mode with 50 mV amplitude in the range 0.1 Hz - 1 MHz. The measurements were made with an initial pressure of 30 bar and the pressure was allowed to increase with temperature. The resistance was found by taking the Z_{real} value for the measurement for which Z_{imag} was smallest. The pres-

surized setup described in Section 2.7 and the sample holder described in Section 2.9.1 was used for the measurements.

The differences in applied potential and frequency range is mainly due to using different Gamry potentiostats.[67] As the electrolyte resistance is found in the high frequency range, the variation in low range should not have any influence on the conductivity results.[66] As the applied potentials are low they should not have a significant influence on the results either.[66]

5.3 Results

5.3.1 Matrix Characterization

Before any $SrTiO_3$ pellets were made, the phase purity of the powders was confirmed with XRPD, described in Section 2.3. In Figure 5.1 the XRPD diffractogram of the powder from Inframat Advanced Materials, USA, can be seen. The diffractogram shows that the powder was phase pure within the detection limit (5%). The powders from the glycine nitrate combustion process (GNP) were also checked and the XRPD diffractograms of these can be seen in Section 2.1.2 and Appendix B.

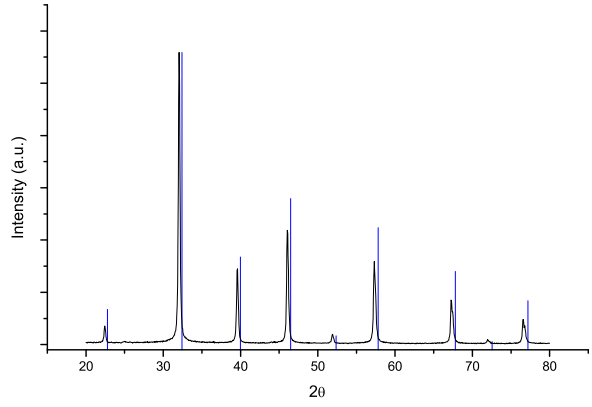

Figure 5.1: XRPD diffractogram of $SrTiO_3$ from Inframat Advanced Materials, USA. The blue lines indicate $SrTiO_3$ peaks. The peaks are slightly shifted due to the sample not being properly aligned during the measurement.

Due to problems using $SrTiO_3$ pellets in CO_2 atmosphere, see Section 5.3.3.1, the phase purity of a TiO_2 pellet after test in CO_2 was checked before any conductivity measurements were performed. The XRPD diffractogram can be seen in Figure 5.2.

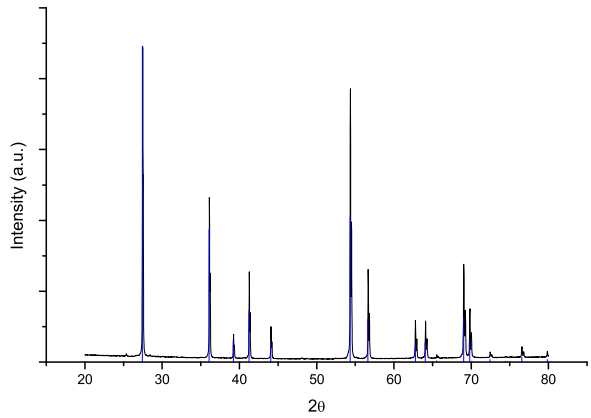

Figure 5.2: XRPD diffractogram of TiO_2 after test in CO_2. The blue lines indicate TiO_2 (rutile) peaks. The pellet was rinsed several times with water to remove the K_2CO_3 (aq) before the XRPD measurement. The peaks for rutile TiO_2 are shown.

In Figure 5.3 a polished cross section of a $SrTiO_3$ pellet can be seen. The pellet was sintered for 12 hours at 1000 °C. It can be seen that the microstructure is quite porous and the pores are sub micron size.

Figure 5.4 shows a fractured surface of a TiO_2 pellet also sintered for 12 hours at 1000 °C. It can be seen that the microstructure was porous but the TiO_2 particles and pores appeared to be larger than in the $SrTiO_3$ pellet.

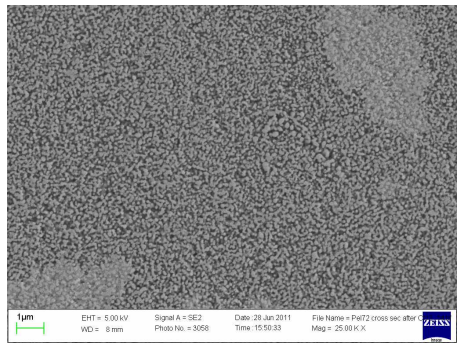

Figure 5.3: SEM image of polished $SrTiO_3$ cross section. The pellet has been sintered for 12 hours at 1000 °C.

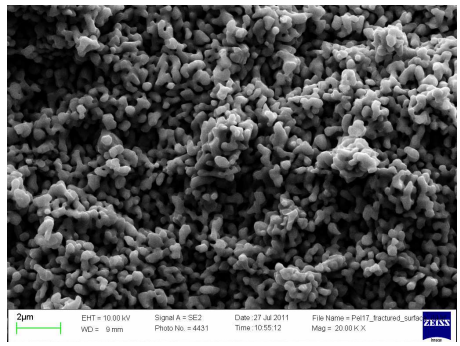

Figure 5.4: SEM image of fractured TiO_2 surface. The pellet has been sintered for 12 hours at 1000 °C.

The open porosity of several $SrTiO_3$ and TiO_2 pellets sintered at 1000-1150 °C has been measured using Hg porosimetry. The technique was explained in Section 2.5. In Figure 5.5 the pore size distribution can be seen and in Table 5.1 the open porosity and amount of closed pores are shown. It can be seen that the pore size and porosity was much smaller for $SrTiO_3$ than for TiO_2. Furthermore, it can be seen that the pore size almost did not change with sintering temperature for $SrTiO_3$ but increased with sintering temperature for TiO_2. The pore size distribution appeared to be relatively narrow for both materials. The porosity was found to decrease with increasing sintering temperature except for TiO_2 sintered at 1000 °C.

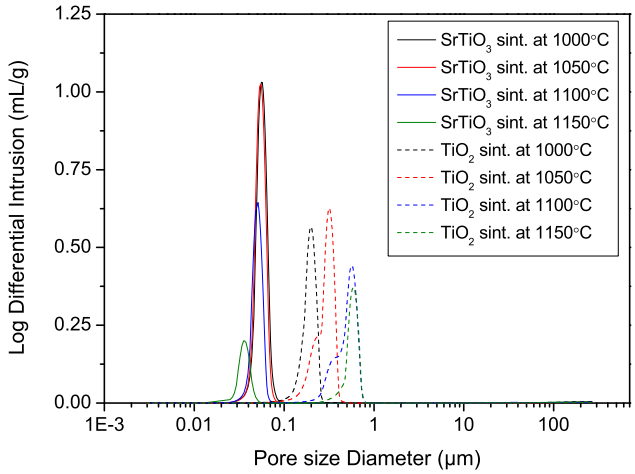

Figure 5.5: Pore size distribution for $SrTiO_3$ and TiO_2 pellets sintered at various temperatures.

Table 5.1: Open porosity and amount of closed pores for $SrTiO_3$ and TiO_2 pellets sintered at various temperatures. * indicates samples that are outside the recommended measuring range of the Micromeritics Autopore IV Hg Porosimeter used for the measurements.

Sintering temp.	Material	Avg. pore diameter/nm	Open porosity/%	Closed pores/%
1000 °C	$SrTiO_3$	56	40.8	12.7
	TiO_2	187	27.3	5.1
1050 °C	$SrTiO_3$	54	40.5	9.3
	TiO_2	268	33.9	0.5
1100 °C	$SrTiO_3$	51	30.3	8.1
	TiO_2*	461	28.6	1.9
1150 °C	$SrTiO_3$*	38	14.0	4.0
	TiO_2*	557	19.6	-

5.3.2 Conductivity at Ambient Conditions

The conductivity of 10 wt% K_2CO_3 (aq) immobilized in $SrTiO_3$ and TiO_2 pellets sintered at 1000-1150 °C as a function of open porosity can be seen in Figure 5.6. The Figure also shows the conductivity predicted by both the symmetric and asymmetric Bruggeman model as well as Archie's law,[18,69,70] explained in Section 2.11. The conductivity value used for the Bruggeman models and Archie's law came from a third order polynomial fit of the values for pure K_2CO_3 (aq) seen in Figure 5.21.

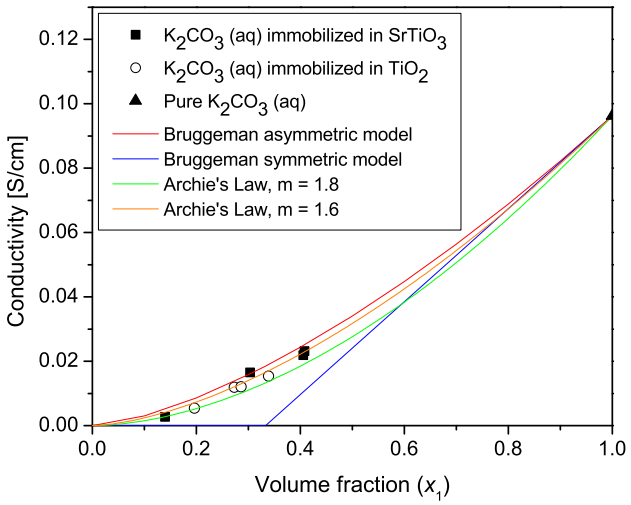

Figure 5.6: Conductivity as a function of open porosity for 10 wt% pure and immobilized K_2CO_3 (aq). The $SrTiO_3$ pellets were approx. 5 mm thick and the TiO_2 pellets were approx. 4 mm thick. The measurements were performed at 19-21 °C. The plot also shows the conductivity predicted by the Bruggeman models and Archie's law.[18,69,70] The conductivity value for pure 10 wt% K_2CO_3 (aq) solution used for the Bruggeman models and Archie's law has been found by fitting of the pure solution data in Figure 5.21.

The conductivity increased with the porosity for immobilized K_2CO_3 (aq). Despite the difference in pore size and distribution between the two matrix materials, the conductivity did not appear to be matrix dependent in this case, but only depended on the volume fraction of open pores. In both cases the Bruggeman symmetric model was very far from the measured values. The asymmetric model appeared to fit much better but predicted higher values than measured. Archie's law gave the best fit, with a cementation exponent, m, of 1.6. At very low porosities Archie's law, with m = 1.6, was predicting higher conductivities than measured.

In Figure 5.7 a log-log plot of the conductivity of immobilized K_2CO_3 (aq) as a function of K_2CO_3 (aq) concentration at ambient temperature can be seen. The measurements were performed on K_2CO_3 (aq) solutions immobilized in a $SrTiO_3$ and a TiO_2 pellet. The pellets were sintered at 1000 °C for 12 hours

and were from the same batches as the pellets sintered at 1000 °C in Table 5.1. The values were corrected for inductance; the change was, however, negligible since it was less than 0.1%.

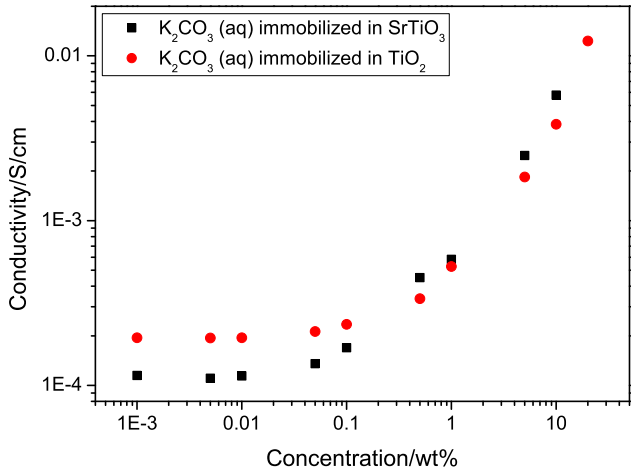

Figure 5.7: Log-log plot of the conductivity as a function of K_2CO_3 (aq) concentration at ambient temperature. Both TiO_2 and $SrTiO_3$ were used to immobilize the K_2CO_3 (aq) solutions. The measurements were performed at 22-23 °C.

From Figure 5.7 it can be seen that for very low concentrations, below 0.01 wt%, the conductivity became independent of concentration. Furthermore, it can be seen that at the very low concentrations the conductivity appeared to be higher when using TiO_2 compared to $SrTiO_3$ for immobilization. At higher concentrations the conductivity increased with concentration, it did, however, not reach the same level at 10 wt% K_2CO_3 (aq) as seen in Figure 5.6. The conductivity of the water used to make the K_2CO_3 (aq) solutions was measured to be $5.8{\cdot}10^{-5}$ S/cm when immobilized in the TiO_2 pellet. The pellets were exposed to normal air during measurements and the K_2CO_3 (aq) solutions should therefore have been affected by the CO_2 in the air, which should also give rise to some conductivity. As the $SrTiO_3$ and TiO_2 pellet came from the same batch as the pellets sintered at 1000 °C in Table 5.1, the predicted open porosity of the TiO_2 pellet was lower than the predicted open porosity of the $SrTiO_3$ pellet. This could explain the higher conductivity when using

$SrTiO_3$ for immobilizing K_2CO_3 (aq) solution with concentrations above 0.5 wt%.

5.3.2.1 Conductivity Measurements with Gas Flow

The conductivity of 10 and 30 wt% K_2CO_3 (aq) immobilized in $SrTiO_3$ was measured at ambient temperature and pressure in a setup with gas flow. In Figure 5.8 the results for 10 wt% K_2CO_3 (aq) immobilized in $SrTiO_3$ can be seen. The conductivity was measured for 7 days in both pure N_2 flow, N_2/CO_2 mixtures and in pure CO_2 flow. The conductivity was a little unstable in the beginning but then appeared to stabilize. A small drop in conductivity was observed when CO_2 was added to the gas flow, but no further drop was observed when the CO_2 content in the N_2/CO_2 mixture was increased. Later the conductivity in pure CO_2 flow was lower than in the N_2/CO_2 mixture. Finally, the gas was changed back to pure N_2 which did not have any effect on the conductivity during the length of the test.

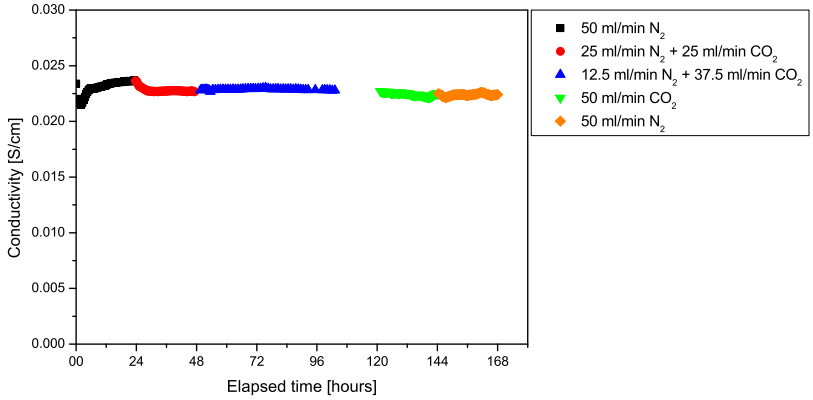

Figure 5.8: Conductivity as a function of elapsed time for 10 wt% K_2CO_3 (aq) immobilized in $SrTiO_3$. The measurements were performed at ambient temperature and pressure in different N_2/CO_2 mixtures.

Figure 5.9 shows the conductivity of 30 wt% K_2CO_3 (aq) immobilized in $SrTiO_3$ at ambient temperature and pressure in N_2 and CO_2 flow. The conductivity appeared to be unstable in the beginning but then appeared to sta-

bilize. When the gas flow was changed to CO_2 a large drop in conductivity was observed; from approx. 0.065 to 0.040 S/cm. The conductivity did, however, increase again after approx. 42 hours in CO_2 flow (60 hours in total). A small increase was seen when the gas flow was changed back to N_2 but the conductivity appeared to stabilize at the end of the test.

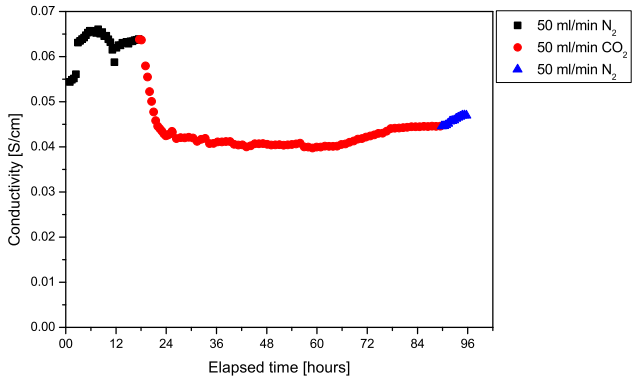

Figure 5.9: Conductivity as a function of elapsed time for 30 wt% K_2CO_3 (aq) immobilized in $SrTiO_3$. The measurements were performed at ambient temperature and pressure in both N_2 and CO_2 flow.

5.3.3 Conductivity at Elevated Temp. and Pressure

5.3.3.1 $SrTiO_3$ as Matrix

Figure 5.10 shows the conductivity of 10 wt% K_2CO_3 (aq) immobilized in $SrTiO_3$ from ambient temperature to max. 200 °C. Two measurements were made right after each other on the same pellet. The initial pressure was 30 bar N_2 and the pressure was allowed to increase with temperature. The measurements were performed using a two electrode sample holder, see Section 2.9.1. The Figure shows an almost linear increase in conductivity as a function of temperature. The curves appear to bend a little at elevated temperatures. Up to approx. 140 °C the conductivity appeared to be the same in both measurements for both increasing and decreasing temperature. Above 140 °C the conductivity varied a little more.

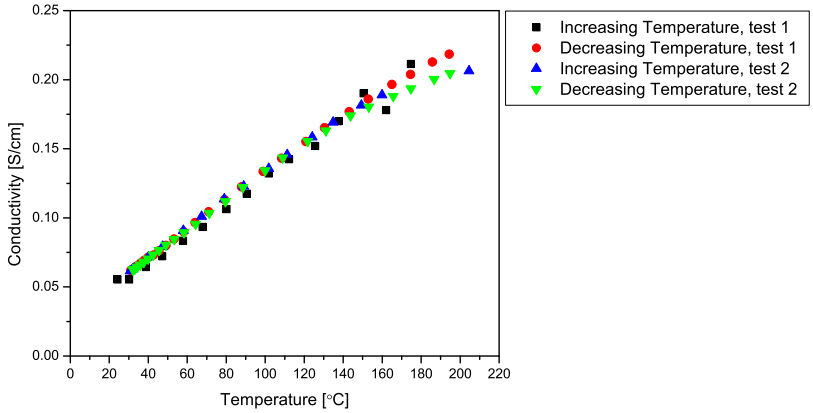

Figure 5.10: Conductivity of 10 wt% K_2CO_3 (aq) immobilized in $SrTiO_3$ from ambient temperature to max. 200 °C. Two test were made right after each other without opening the autoclave. The initial pressure was 30 bar N_2 and the pressure was allowed to increase with temperature. A two electrode sample holder was used for the measurements.

Figure 5.11 shows the conductivity of 5-30 wt% K_2CO_3 (aq) immobilized in $SrTiO_3$ from ambient temperature up to max. 180 °C. The measurements were performed at a constant pressure of 30 bar. Different $SrTiO_3$ pellets were used for the different concentrations, but they all had an estimated porosity of 49-50%. It can be seen that the conductivity increased with temperature and in general also with concentration of K_2CO_3 (aq). At ambient temperature it appeared as if 15 wt% K_2CO_3 (aq) immobilized in $SrTiO_3$ had a higher conductivity than 10 and 20 wt%, which had a similar conductivity. Above approx. 80 °C this was no longer the case and the conductivity generally increased with concentration. It can be seen that the conductivity was higher than 0.1 S/cm for all concentrations above 115 °C, but for 10-30 wt% K_2CO_3 (aq) immobilized in $SrTiO_3$ this occurred already at 90 °C.

In Figure 5.12, an Arrhenius plot of the data presented in Figure 5.11 can be seen. The temperature dependence can be described using equation 3.2 shown in Section 3.3.3. In Table 5.2 the activation energy (E_a) and the pre-exponential factor (A) are shown. The activation energy and the pre-exponential factor varied for the different concentrations. Both the activation energy and

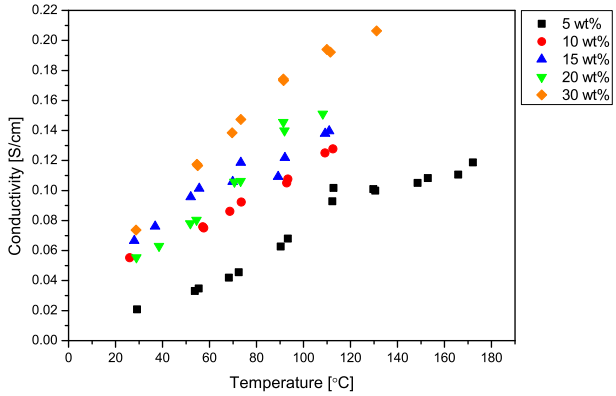

Figure 5.11: Conductivity of 5-30 wt% K_2CO_3 (aq) immobilized in $SrTiO_3$ from ambient temperature to max. 180 °C. All measurements were performed at 30 bar using a four electrode sample holder. The data are for increasing temperature.

the pre-exponential factor were smallest for 10 and 15 wt% K_2CO_3 (aq) immobilized in $SrTiO_3$. For 5, 20 and 30 wt% the pre-exponential factor and the activation energy decreased with increasing concentration. The activation energy was found to be in the range 0.11-0.22 eV.

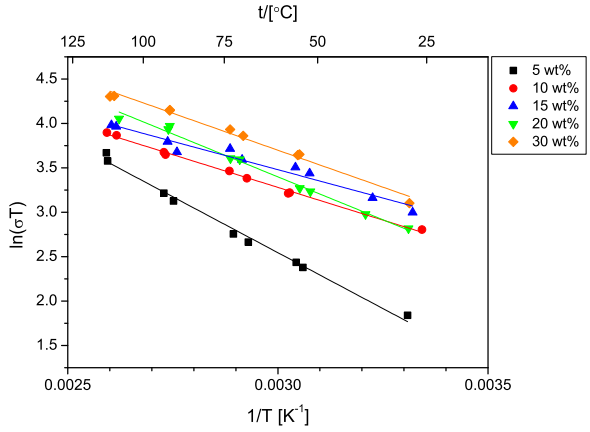

Figure 5.12: Arrhenius plot of Figure 5.11 showing ln(σT) as a function of 1/T for 5-30 wt% K_2CO_3 (aq) immobilized in $SrTiO_3$. The lines show the linear fits. All measurements were performed at 30 bar using a four electrode sample holder.

Table 5.2: Pre-exponential factor and activation energy including standard error for 5-30 wt% K_2CO_3 (aq) immobilized in $SrTiO_3$. Calculated from a linear fit of $\ln(\sigma T)$ as a function of $1/T$.

	5 wt%	10 wt%	15 wt%	20 wt%	30 wt%
A	25000 ± 6200	2200 ± 250	1550 ± 410	10070 ± 2060	6080 ± 1280
E_a/eV	0.217 ± 0.007	0.127 ± 0.003	0.110 ± 0.008	0.167 ± 0.006	0.143 ± 0.006

Measurements in CO_2 Atmosphere

A symmetrical cell with 10 wt% K_2CO_3 (aq) immobilized in $SrTiO_3$ and STN-94 ($Sr_{0.94}Ti_{0.9}Nb_{0.1}O_3$) electrodes was tested first in N_2 and then in CO_2, see Figure 5.13. The conductivity followed the same trend during heating and

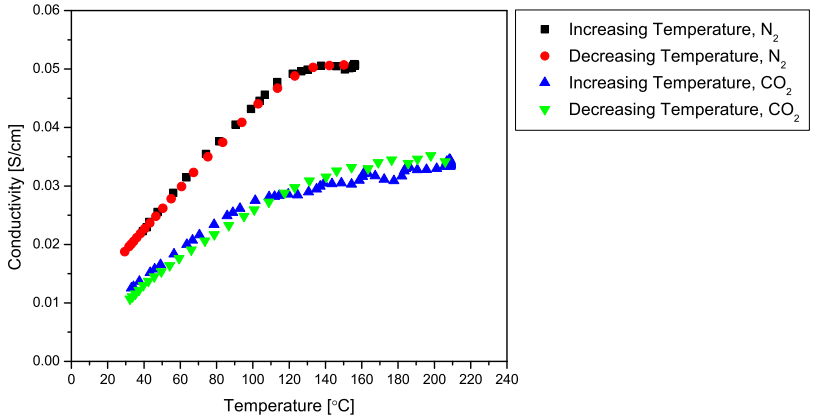

Figure 5.13: Conductivity of 10 wt% K_2CO_3 (aq) immobilized in $SrTiO_3$ with STN-94 electrodes, measured from ambient temperature to 160-210 °C. First tested in N_2 and then in CO_2. The initial pressure was approx. 30 bar and the pressure was allowed to increase with temperature. The results for both increasing and decreasing temperature are shown. The measurements were performed using a two electrode sample holder.

cooling and appeared to flatten out at higher temperatures. The conductivity was found to be lower in CO_2 than in N_2, which was initially believed to be caused by the change in charge carriers and possible precipitation, see Section 3.3.1. However, after the test in CO_2 the colour of the STN electrodes had changed from dark grey to light grey and their conductivity was nearly zero. The sample was therefore measured using XRPD which showed that $SrCO_3$ was now present in the sample, see Figure 5.14. The sample was then

investigated using SEM and EDX, see Figure 5.15, 5.16 and 5.17. The SEM images showed that large particles were present on the surface of the sample and the EDX results, see Figure 5.17, showed that the large particles consisted mainly of Sr, C and O. Peaks for Ti could be identified but were found to be very small. The smaller particles contained Sr, Ti, Nb and O as expected and also K, which indicated that the sample still contained some K_2CO_3. Formation of $SrCO_3$ on the surface of the cell could have caused blocking or partly blocking of the electrodes, since $SrCO_3$ is an electrical insulator.

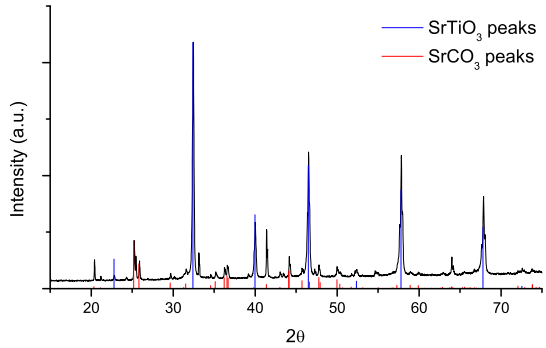

Figure 5.14: XRPD diffractogram of a $SrTiO_3$ cell with STN-94 electrodes after test in CO_2. The cell was rinsed several times with water to remove the K_2CO_3 (aq) before the XRPD measurement. The peaks for both $SrTiO_3$ and $SrCO_3$ are shown.

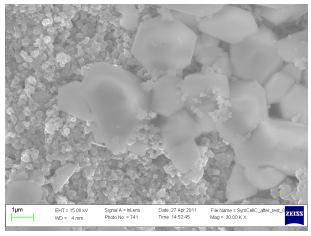

Figure 5.15: SEM image of the surface of a $SrTiO_3$ cell with STN-94 electrodes after test in CO_2. The acceleration voltage was 15 kV and the working distance 4 mm.

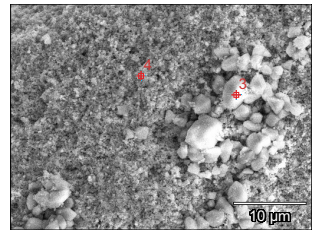

Figure 5.16: SEM image used for EDX showing the surface of a $SrTiO_3$ cell with STN-94 electrodes after test in CO_2. Two points (3 and 4) are indicated on the image.

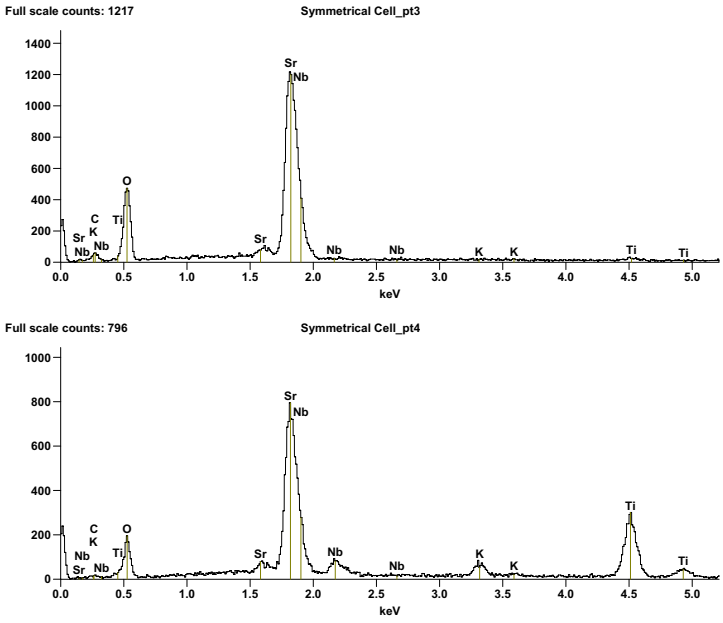

Figure 5.17: EDX spectra of point 3 and 4 shown on Figure 5.16. Peaks for C, O, Sr, Ti, Nb and K have been identified in the range 0-5 keV.

$SrCO_3$ formation should not occur if $SrTiO_3$ is completely stoichiometric, since CO_2 does not react with $SrTiO_3$.[77,78] CO_2 can however react with SrO and form $SrCO_3$, $\Delta G^{\ominus}$ = -183.8 kJ/mol, indicating that the powder used for the pellets is slightly overstoichiometric with respect to Sr and, therefore, contains SrO. This was proven by taking a Sr-deficient sample, $Sr_{0.95}TiO_3$, soaking it in K_2CO_3 (aq) and running the same test again in CO_2. The sample did not form $SrCO_3$, see Appendix C. Further tests also indicated that the formation of $SrCO_3$ was significantly more pronounced when the material was soaked in K_2CO_3 (aq) (ie. used for immobilization) prior to the test in CO_2. It was also found that the $SrCO_3$ formation was not caused by the STN-94 electrodes since they were Sr-deficient and no $SrCO_3$ formation was seen on a sample consisting only of STN-94 that had been soaked in K_2CO_3 (aq) prior to test in CO_2. The XRPD diffractogram of a sample that has not been

soaked prior to test in CO_2 as well as the XRPD diffractograms of $Sr_{0.95}TiO_3$ and STN-94 after test in CO_2 can be seen in Appendix C.

5.3.3.2 TiO_2 as Matrix

In Figure 5.18 the conductivity of 5-20 wt% K_2CO_3 (aq) immobilized in TiO_2 is shown. The conductivity was measured from ambient temperature to max. 215 °C with an initial pressure of 30 bar. All measurements were made on the same TiO_2 pellet. Data at higher temperatures have been excluded for 5 and 10 wt% K_2CO_3 (aq) immobilized in TiO_2 due to a significant drop in the conductivity, caused by water management issues discussed in Chapter 4. It can be seen that the conductivity increased with both temperature and concentration. The conductivity for 15 and 20 wt% K_2CO_3 (aq) immobilized in TiO_2 appeared to be very similar at 215 °C. The highest conductivity measured was 0.2 S/cm at 210 °C on 20 wt% K_2CO_3 (aq) immobilized in TiO_2.

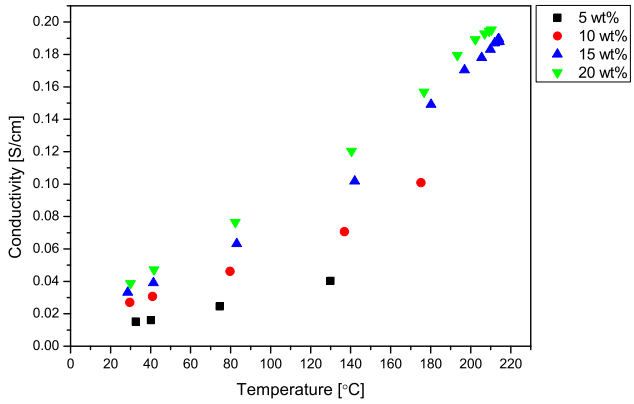

Figure 5.18: Conductivity of 5-20 wt% K_2CO_3 (aq) immobilized in TiO_2 from ambient temperature to max. 215 °C. All measurements were performed on the same pellet. All measurements were performed with an initial pressure of 30 bar and the pressure was allowed to increase with temperature.

Figure 5.19 shows ln(σT) as a function of 1/T for the data presented in Figure 5.18. The pre-exponential factor (A) and the activation energy (E_a) can be found in Table 5.3. The linear fits appeared to describe the experimental

data well and the activation energy was in the range 0.13-0.15 eV for all the measured concentrations. 15 wt% K_2CO_3 (aq) immobilized in TiO_2 had the highest pre-exponential factor (A) and activation energy (E_a).

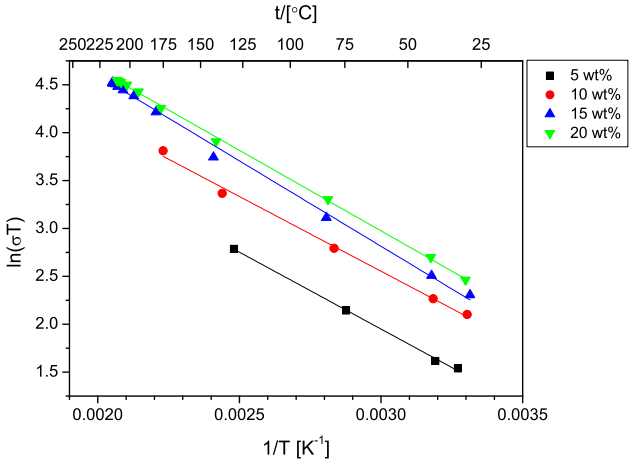

Figure 5.19: Arrhenius plot of Figure 5.18 showing ln(σT) as a function of 1/T for 5-20 wt% K_2CO_3 (aq) immobilized in TiO_2. The lines show the linear fits. All measurements were performed on the same pellet. All measurements were performed with an initial pressure of 30 bar and the pressure was allowed to increase with temperature.

Table 5.3: Pre-exponential factor and activation energy including standard error for 5-20 wt% K_2CO_3 (aq) immobilized in TiO_2. Calculated from a linear fit of ln(σT) as a function of 1/T.

	5 wt%	10 wt%	15 wt%	20 wt%
A	870 ± 110	1400 ± 230	3520 ± 250	3050 ± 120
E_a/eV	0.138 ± 0.003	0.134 ± 0.005	0.154 ± 0.002	0.145 ± 0.001

Measurements in CO_2 Atmosphere

The conductivity of 10 wt% K_2CO_3 (aq) immobilized in TiO_2 was measured in both N_2 and CO_2 atmosphere, see Figure 5.20. The same TiO_2 pellet was used for both measurements, which were performed right after each other. The initial pressure was 30 bar and the pressure was then allowed to increase with temperature. It can be seen that the conductivity increased with temperature and the difference between the two measurements was very small.

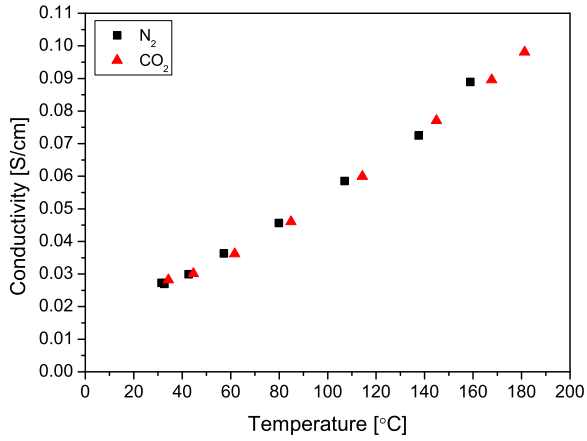

Figure 5.20: 10 wt% K_2CO_3 (aq) immobilized in a TiO_2 pellet; first tested in N_2 atmosphere and then in CO_2 atmosphere. The pellet was not moved between the tests. The initial pressure was 30 bar for both measurements and the pressure was allowed to increase with temperature.

According to the calculated phase diagram, Figure 3.3 in Section 3.3.1, only 10 wt% K_2CO_3 (aq) or less appears to be completely aqueous at room temperature in a CO_2 containing atmosphere. At higher concentrations $KHCO_3$ (s) will precipitate according to the phase diagram. At temperatures up to 200 °C the purely aqueous region broadens to include higher concentrations; at 200 °C 20 wt% K_2CO_3 (aq) will be completely aqueous. At temperatures above 200 °C the region shrinks again. The difference between 30 and 100 bar of total pressure appears to be at which temperature gas formation (and precipitation of K_2CO_3 (s)) occurs. At 30 bar it occurs at 240 °C but at 100 bar it occurs above 300 °C.

The solubility of $KHCO_3$ in water is much lower than K_2CO_3.[12] Having CO_2 gas present during test therefore decreases the size of the aqueous region, compared to tests without CO_2, and limits the possible concentration region.

5.3.3.3 Comparison of $SrTiO_3$ and TiO_2 as Matrix

The conductivity of pure 10 wt% K_2CO_3 (aq) and 10 wt% K_2CO_3 (aq) immobilized in $SrTiO_3$ and TiO_2 can be seen in Figure 5.21. The conductivity was

measured at 30-40 bar from ambient temperature up to 110-185 °C. It can be seen that the conductivity increased with temperature in all cases and that the conductivity of 10 wt% K_2CO_3 (aq) immobilized in $SrTiO_3$ was higher than for 10 wt% K_2CO_3 (aq) immobilized in TiO_2. The conductivity of pure K_2CO_3 (aq) was higher than immobilized K_2CO_3 (aq), as expected due to the porous structure.

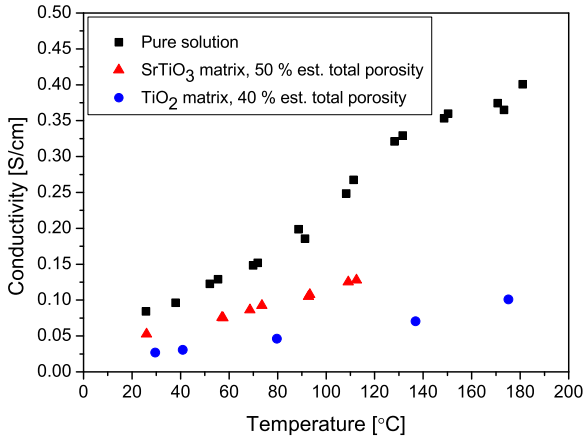

Figure 5.21: Conductivity of 10 wt% K_2CO_3 (aq) both pure and immobilized in $SrTiO_3$ and TiO_2, from ambient temperature up to 185 °C. The initial pressure was 30 bar in all tests and the pressure was kept constant during the test where $SrTiO_3$ was used for immobilization and allowed to increase with the temperature in the other tests. The conductivity of pure K_2CO_3 (aq) and K_2CO_3 (aq) immobilized in $SrTiO_3$ was measured using a four electrode setup.

Figure 5.22 shows the conductivity of pure as well as immobilized 5-30 wt% K_2CO_3 (aq) at 100 and 150 °C. Several $SrTiO_3$ pellets and one TiO_2 pellet have been used for the immobilization. The measurements on pure K_2CO_3 (aq) and K_2CO_3 (aq) immobilized in $SrTiO_3$ pellets were carried out at 30 bar, except for 15 wt% K_2CO_3 (aq) and 20 wt% K_2CO_3 (aq) immobilized in $SrTiO_3$, which were measured at 40 bar. The measurements on K_2CO_3 (aq) immobilized in the TiO_2 pellet were carried out with an initial pressure of 30 bar and the pressure was allowed to increase with temperature. The conductivity increased with concentration in all cases and was highest for pure K_2CO_3 (aq) and lowest when TiO_2 was used for the immobilization. The difference be-

tween pure K_2CO_3 (aq) and K_2CO_3 (aq) immobilized in $SrTiO_3$ appeared to increase with concentration. At 100 °C for 5 and 10 wt% K_2CO_3 (aq) the loss when using $SrTiO_3$ for immobilization appeared to be around 50% and at higher concentrations it was more than 50%. For TiO_2 the loss was much greater for all concentrations at both 100 and 150 °C, but did not appear to vary with concentration. Despite the significant loss when immobilizing, and TiO_2 being the poorest matrix choice, the conductivity of 15 wt% K_2CO_3 (aq) immobilized in TiO_2 was still above 0.1 S/cm at 150 °C.

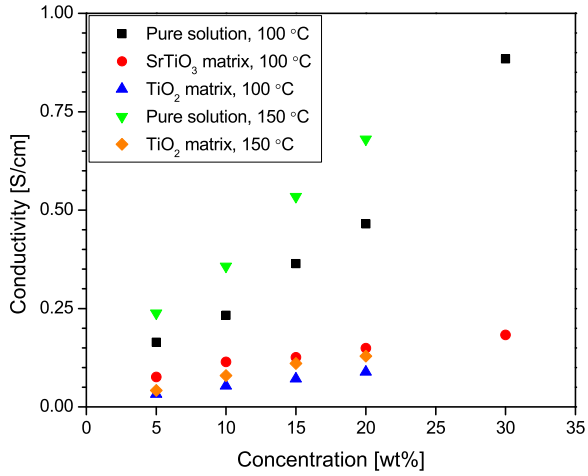

Figure 5.22: Conductivity comparison between pure K_2CO_3 (aq) and K_2CO_3 (aq) immobilized in $SrTiO_3$ and TiO_2 at 100 and 150 °C. The porosity has been estimated to be 50% for the $SrTiO_3$ matrix and 40% for the TiO_2 matrix. The values have been obtained from third order polynomial fits of the measured values from ambient temperature up to 180 °C. Pure K_2CO_3 (aq) and K_2CO_3 (aq) immobilized in $SrTiO_3$ was measured using a 4 electrode setup. The measurements of pure K_2CO_3 (aq) and K_2CO_3 (aq) immobilized in $SrTiO_3$ were carried out at 30 bar, except for 15 wt% pure K_2CO_3 (aq) and 20 wt% immobilized K_2CO_3 which were measured at 40 bar. The measurements of K_2CO_3 (aq) immobilized in TiO_2 were carried out with an initial pressure of 30 bar and the pressure was allowed to increase with temperature.

Conductivity measurements using a two electrode sample holder, see Section 2.9.1, have been performed on $SrTiO_3$ and TiO_2 pellets with different electrodes, as mentioned in Section 2.2. Ag was used as it is known to be a good catalyst for oxygen evolution[79] and Cu was used as it is believed to be

a possible catalyst for hydrocarbon formation, see Section 1.2. In Figure 5.23 the conductivity can be seen for two $SrTiO_3$ pellets with Pt and Ag+STN electrodes, respectively. The Figure shows that the conductivity of the solution immobilized in the two pellets was very similar. The pellet with Ag+STN electrodes appeared to be slightly better than the pellet with Pt electrodes. Both pellets were prepared the same way but came from different batches, so minor microstructure differences can be expected. Their estimated porosity was 50%.

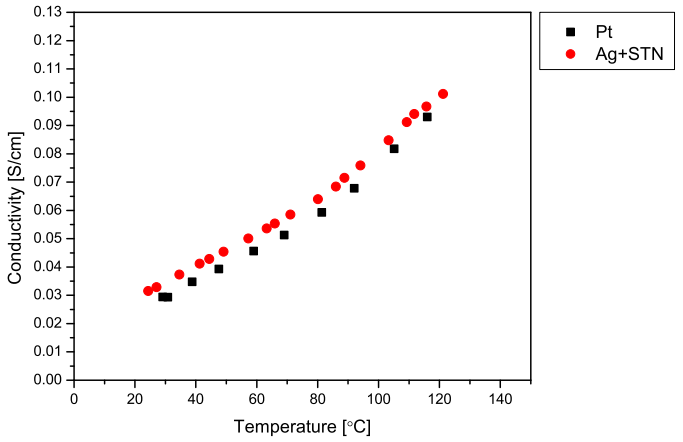

Figure 5.23: Conductivity as a function of temperature for 10 wt% K_2CO_3 (aq) immobilized in two different $SrTiO_3$ pellets, with Pt and Ag+STN electrodes, respectively. The pellets were tested in N_2 atmosphere and in both cases the inital pressure was 30 bar and the pressure was allowed to increase with temperature.

In several cases complete delamination of metal electrodes (Pt, Ag, Ag+STN, Cu) was observed after test, however, it was never clear from the conductivity measurement when it had occurred. The cell would continue to work as the sample holder ensured it was kept together and contact between the K_2CO_3 (aq) solution and the electrode never appeared to be a problem. It was, however, not possible to remove a cell with delaminated electrodes from the sample holder without damaging the delaminated electrodes as they were quite fragile without the support of the matrix. Therefore, once the cell was

removed from the sample holder further tests on the cell was not possible. Delamination was seen more often when using $SrTiO_3$ as the matrix than when using TiO_2. Delamination of Ag electrodes was almost never observed when using TiO_2 as the matrix material. Delamination was never observed with STN electrodes on $SrTiO_3$.

5.4 Discussion

5.4.1 Matrix Comparison

Figure 5.5 shows that $SrTiO_3$ and TiO_2 sinter very different. When the sintering temperature was increased the pore size remained almost unchanged for $SrTiO_3$. This means that some pores completely disappeared when the sintering temperature was increased and that the remaining pores were unchanged. TiO_2, however, showed an increase in pore size when the sintering temperature was increased, this means that the pores grew at the expense of the smaller pores.

Table 5.1 shows that the pore size of $SrTiO_3$ was much smaller than the pore size of TiO_2. This means that the capillary forces, see Section 1.1, are much larger when using $SrTiO_3$ as the matrix compared to TiO_2, as the contact angle of the two materials is similar.[80,81] Large capillary forces are an advantage as it makes the solution tighter bound in pores of the matrix which is essential especially when measuring at elevated pressures in a two atmosphere setup with potential pressure gradients.

5.4.2 Conductivity at Ambient Conditions

Figure 5.6 shows that there was no apparent difference between using $SrTiO_3$ and TiO_2 for immobilizing 10 wt% K_2CO_3 (aq) at ambient temperature and pressure. The conductivity seemed to only depend on the volume fraction of open pores and also fitted perfectly with the conductivity value for 100% porosity (pure liquid). The differences between $SrTiO_3$ and TiO_2 observed in Figure 5.21 can, therefore, be attributed to the differences in porosity and no further influence of the matrix material on the conductivity was indicated.

Furthermore, the porosities of the pellets, used for the measurements shown in Figure 5.21, have only been estimated and the volume fraction of closed pores is unknown. This is due to the fact that Hg porosimetry is a destructive method, and thus the actually tested pellets could not be investigated. The observed differences can be explained by assuming 1 and 10% closed pores in the $SrTiO_3$ and TiO_2 pellet, respectively.

In Figure 5.6 it can be seen that Archie's law, see Section 2.11.3, gave the best fit with a cementation exponent, m, of 1.6. The cementation exponent is a measure of how much the matrix (pore network) increases the resistivity. In order to get a more accurate m-value, data over a wider porosity range are necessary. Pellets with a higher porosity can be fabricated using for example pore formers. Both the asymmetrical Bruggeman model and Archie's law predicts that the conductivity is zero at zero porosity. Figure 5.6 does however indicate that zero conductivity is reached before zero porosity. This could be because at very low porosities it can be difficult to obtain a percolated porosity. Without a percolated porosity conduction through the material is impossible and the measured conductivity would therefore be zero. It is, however, still possible that the material contains open pores, which would lead to zero conductivity before zero open porosity.

The conductivity at very low concentrations was higher when using TiO_2 for immobilization compared to $SrTiO_3$, as seen in Figure 5.7. This could be due to the two materials having a different composition, which could be affecting the conduction mechanism differently.[80,82] The surface of $SrTiO_3$ is, most likely, terminated by SrO and TiO_2 layers and is therefore different from the surface of TiO_2.[83,84] Furthermore, the difference in pore size could also affect the conductivity at very low concentrations.[85] Since very small amounts of impurities can have a large effect on the conductivity at very low concentrations it is hard to determine how much of the conductivity at very low concentrations that can be attributed to impurities in the water used to make the solutions. Part of the conductivity at very low concentrations should be coming from the CO_2 in the air reacting with the water and forming carbonic acid, see equilibrium 1.3 in Section 1.2. For pure water a conductiv-

ity of around $1{\cdot}10^{-6}$ S/cm is obtained due to the CO_2 in the atmosphere.[86] The measured conductivity of the water, used for the solutions, was however $5.8{\cdot}10^{-5}$ S/cm when immobilized in TiO_2, indicating that the water was not completely pure. This value is significantly lower than the conductivity measured at very low K_2CO_3 (aq) concentrations. Therefore, the difference between using $SrTiO_3$ and TiO_2 for the immobilization at these low concentrations is most likely caused by the difference in material composition.

In Figure 5.7 the conductivity for 10 wt% K_2CO_3 (aq) did not reach the same level as seen in Figure 5.6. This could be because the pellet did not contain 10 wt% K_2CO_3 (aq), but a slightly lower concentration. The measurements were performed with increasing concentration, so it is possible that the pellet was not rinsed enough with the 10 wt% solution and was therefore still partly filled with 5 wt% solution. However, since the procedure for rinsing the pellets were the same for both pellets the relative potential error should be the same for both materials, comparing the two materials should therefore still be possible.

From the ambient temperature and pressure results presented in Figure 5.8 and 5.9 it can clearly be seen that the effect of CO_2 was very low on 10 wt% K_2CO_3 (aq) immobilized in $SrTiO_3$ but significant on 30 wt%. There was a small drop in conductivity for 10 wt% when CO_2 was added to the gas stream. According to phase diagrams calculated by FactSage, see Figure 3.3 in Section 3.3.1, 10 wt% K_2CO_3 (aq) in CO_2 atmosphere is on the line between purely aqueous and aqueous + precipitation, so it is indeed possible that precipitation (of $KHCO_3$) occurred, however, it should not have been very pronounced. Precipitation will naturally cause a decrease in charge carriers and therefore a drop in conductivty. It is furthermore possible that the concentration at the surface is slightly higher due to evaporation of water which will make precipitation even more likely.

The large drop in conductivity seen for 30 wt% K_2CO_3 (aq) in Figure 5.9 is expected based on the phase diagram, Figure 3.3, since 30 wt% K_2CO_3 (aq) is well within the region where precipition of $KHCO_3$ occurs. The conduc-

tivity seemed somewhat unstable during the measurements, which could indicate that the system needs time to equilibrate. The increased conductivity, after the initial drop, during CO_2 flow could indicate that some precipitated $KHCO_3$ (s) was re-dissolved. It could, however, also be caused by a variation in the laboratory temperature. The temperature in the lab can change 1-3 °C within a day and the conductivity is highly temperature dependent, as shown in Figure 3.6 in Section 3.3.2. Changing the gas flow back to pure N_2 appeared to have only a little effect. The conductivity did increase slightly, but then appeared to stabilize. In order to regain the lost conductivity the precipitated $KHCO_3$ (s) has to be re-dissolved. However, when the system was exposed to CO_2 a change in charge carriers occurred, see equilibrium 1.2 in Section 1.2. The precipitation of $KHCO_3$ (s) occurred due to the lower solubility of $KHCO_3$ (s) compared K_2CO_3 (s).[12] In order to re-dissolve the $KHCO_3$ (s) a conversion back to K_2CO_3 (s) is therefore necessary. This, however, is unlikely to occur simply by changing the flow back to N_2, as this should have a very limited affect on the equilibrium, if any. As only a minor increase was seen it indicates that this conversion does not occur or only to a very limited extent. Dissolving K_2CO_3 (s) in water is usually very fast, and is not expected to limit the process significantly. However, running the test for a longer time would have indicated if any conversion does occur within a reasonable time frame.

5.4.3 Conductivity at Elevated Temp. and Pressure

Figure 5.11 clearly shows instabilities during measurements of K_2CO_3 (aq) immobilized in $SrTiO_3$ at elevated temperature and pressure unlike Figure 5.10, which shows a very stable conductivity for 10 wt% K_2CO_3 (aq) immobilized in $SrTiO_3$. The instabilities could be caused by water management issues, previously discussed in Chapter 4. If the pellets were loosing and gaining water this would affect the conductivity and thus might explain why the conductivity lines for the different concentrations cross each other in Figure 5.11. The pellets with 10, 15 and 20 wt% K_2CO_3 (aq) immobilized in $SrTiO_3$ simply stopped working at approx. 110 °C due to drying out. After the tests the pellets looked dry and adding a few drops of water made it

possible to measure again. Due to the conductivities not being very stable the activation energy and pre-exponential factor also varied a bit. Figure 5.12 shows that the values still followed a linear trend. It is, however, not possible from the plot to determine if the activation energy was concentration dependent or not. The activation energy was found to be 0.11-0.22 eV which is in the same range as the activation energy found for pure K_2CO_3 (aq), 0.14-0.17 eV, see Section 3.3.3.

From Figure 5.13 it can clearly be seen that a change occurred when the atmosphere was changed from N_2 to CO_2. The test was started right after the gas was changed to CO_2 and even at that point the conductivity was much lower than when the test in N_2 ended. This indicates that the cell was quickly affected by the CO_2. The shape of the conductivity curve is somewhat different in CO_2 atmosphere compared to the one in N_2 atmosphere. The conductivity in N_2 appeared to flatten out which could be due to water evaporation causing precipitation and therefore loss of charge carriers. The XRPD and EDX results together with the SEM images clearly show that $SrCO_3$ had formed on the surface of the cell. The lower conductivity can be explained by the blocked electrodes which makes current collection difficult and furthermore, the $SrCO_3$ could have been blocking the pores and thereby preventing the K_2CO_3 (aq) solution from being in contact with the electrodes. The fact that the cell was able to work up to a high temperature in CO_2 atmosphere could support the theory that the $SrCO_3$ was partly blocking the pores. By blocking the pores the surface area between the K_2CO_3 (aq) solution and the gas was decreased and therefore water evaporation was less likely to occur.

The change in colour of the STN-94 electrodes after the test in CO_2 atmosphere could be caused by the $SrCO_3$ layer on the surface, it is also possible that the STN-94 layer itself was affected but this was not found relevant for the purpose of this study and was therefore not investigated further.

From Figure 5.2 it can be seen that there was no problem with using TiO_2 in CO_2 atmosphere. Figure 5.18 does, however, indicate some instabilities, due to the water management issue discussed in Chapter 4, when measur-

ing the conductivity of K_2CO_3 (aq) immobilized in TiO_2 in N_2 atmosphere. The relative difference in conductivity between the measured concentrations vary as a function of temperature. This could be due to the solution loosing or gaining a little amount of water. It could appear as if the 15 and 20 wt% solutions were trying to reach the same conductivity value and therefore the same equilibrium concentration. In order to stabilize the measurements, as discussed in Chapter 4, all tests on TiO_2 were performed with a significantly smaller autoclave volume compared to earlier tests on K_2CO_3 (aq) immobilized in $SrTiO_3$. Furthermore, the tests were made with only water in the bottom of the autoclave. If the system was trying to reach equilibrium the solution in the TiO_2 pellet should be gaining water in an effort to reach the concentration of the reservoir (0 wt%). It can clearly be seen that the system did not reach equilibrium, but that the concentration was affected.

It can also be seen that in most cases it was possible to have a high conductivity, of K_2CO_3 (aq) immobilized in TiO_2, up to 180 °C which is a significant improvement compared to earlier measurements on K_2CO_3 (aq) immobilized in $SrTiO_3$, see Figure 5.11. It was in all cases possible to continue the measurement but for 5 and 10 wt% K_2CO_3 (aq) immobilized in TiO_2 there was a significant drop in conductivity at the higher temperatures. The conductivity did, however, improve for 5 and 10 wt% K_2CO_3 (aq) during cooling, see Appendix D.

The activation energy for 5-20 wt% K_2CO_3 (aq) immobilized in TiO_2 was found to be very narrow, 0.13-0.15 eV, and in the same range as the activation energy of pure K_2CO_3 (aq) and K_2CO_3 (aq) immobilized in $SrTiO_3$; 0.14-0.17 eV and 0.11-0.22 eV, respectively. Again no clear correlation between activation energy and concentration could be found.

Figure 5.20 shows that 10 wt% K_2CO_3 (aq) immobilized in TiO_2 can be used in CO_2 atmosphere without conductivity loss. The CO_3^{2-} ions should to a large extend be converted to HCO_3^- ions when the solution is exposed to a high pressure of CO_2, see equilibrium 1.2 in Section 1.2. Calculations by FactSage[68] show that during tests with an initial CO_2 pressure of 30 bar the con-

centration of HCO_3^- ions is at least 1000 times higher than the concentration of CO_3^{2-} ion in the temperature range 20-200 °C. This also fits with the results for constant pressure presented in Figure 3.5 in Section 3.3.1. 10 wt% K_2CO_3 corresponds to 14 wt% $KHCO_3$ (if all ions are converted) and the conductivity values for 10 wt% K_2CO_3 and 15 wt% $KHCO_3$ are very similar; 0.109 compared to 0.101 S/cm.[12] This explains why the conductivity remained the same when changing from N_2 to CO_2 atmosphere as the change in the type of charge carrier only has a small effect on the conductivity.

Figure 5.21 shows that there was a difference between using $SrTiO_3$ and TiO_2 pellets for immobilization of 10 wt% K_2CO_3 (aq) from ambient temperature up to 185 °C. At higher temperatures, the difference in conductivity between 10 wt% K_2CO_3 (aq) immobilized in $SrTiO_3$ and TiO_2 increased. The pellets did, however, have different estimated porosities, with $SrTiO_3$ having the highest estimated porosity. Both the Bruggeman asymmetrical model and Archie's law indicate that the affect of porosity was not linear. According to the models the loss of conductivity is larger than the loss of solution volume when immobilizing. It was therefore expected that the loss when using TiO_2 for the immobilization was larger than when using $SrTiO_3$, due to their different estimated porosities.

From Figure 5.21 it can, however, be seen that the value for 10 wt% K_2CO_3 (aq) immobilized in $SrTiO_3$ at ambient temperature does not fit with Archie's law, with a cementation exponent of 1.6 (previosly determined), as the conductivity was approx. 50% of the conductivity of pure K_2CO_3 (aq). Assuming the estimated porosity is correct, Archie's law predicts a conductivity for the immobilized solution of only 33% of the pure solution. If the open porosity was only 40%, as indicated in Table 5.1, Archie's law predicts a conductivity of only 23% of the pure solution. The ambient conductivity value for 10 wt% K_2CO_3 (aq) immobilized in TiO_2 does, however, fit quite well with Archie's law, assuming the estimated porosity is correct. The conductivity is approx. 26% of the conductivity of pure K_2CO_3 (aq) (found by extrapolating the data to 25 °C) and Archie's law predicts 23%. However, if the open porosity was only 27% as indicated by Table 5.1, Archie's law indicates a con-

ductivity of only 15% of the conductivity of pure K_2CO_3 (aq). As Archie's law has been found to fit very well (with m = 1.6) at ambient temperature for a range of $SrTiO_3$ and TiO_2 pellets sintered at different temperatures, see Figure 5.6, and the conductivity was not found to change upon pressurization it seems unlikely that Archie's law does not apply to the ambient temperature data in Figure 5.21. It is, therefore, most likely that the estimated porosity of TiO_2 is correct as this value fits with Archie's law. The measured conductivity of 10 wt% K_2CO_3 (aq) immobilized in $SrTiO_3$ was higher than predicted by Archie's law, which could indicate that concentration of the solution was higher than 10 wt%. The concentration could have increased if extra solution was present during mounting of the sample, ie. a drop of solution on top of the pellet, and water evaporation occurred. Water evaporation was observed when a soaked pellet was left in open air for several minutes as the surface of the sample dried out.

Figure 5.21 also shows that the conductivity difference between 10 wt% pure K_2CO_3 (aq) and 10 wt% K_2CO_3 (aq) immobilized in $SrTiO_3$ and TiO_2 increased with temperature. According to Stroemich *et al.*[87] Archie's law is valid at elevated temperatures and pressure for a 0.09 M NaCl (aq) solution. This indicates that either Archie's law is not valid for stronger solutions at elevated temperatures or that the water management issues, discussed in Chapter 4, were effecting the conductivity at elevated temperatures. Measuring the conductivity at elevated temperatures of 10 wt% K_2CO_3 (aq) immobilized in $SrTiO_3$ and TiO_2 pellets with different porosities (as has been done at ambient temperature) should make it possible to determine if Archie's law can be used at elevated temperatures in this case and if so how it is dependent on temperature.

Another possible explanation for the observed difference in conductivity between K_2CO_3 (aq) immobilized in $SrTiO_3$ and TiO_2 at elevated temperatures is the previously mentioned difference in composition and pore size. In order to determine if the pore size has an affect on the conductivity at elevated temperatures samples of $SrTiO_3$ and TiO_2 with similar pore size and distribution can be fabricated and measured.

Figure 5.22 show that the relative loss when immobilizing K_2CO_3 (aq) in $SrTiO_3$ increased with concentration. This was, however, not seen when using TiO_2 as the matrix. All measurements on K_2CO_3 (aq) immobilized in TiO_2 were performed after modifying the setup in order to minimize the water managements issues, described in Chapter 4. It is therefore very likely that water management issues were the reason for the increased conductivity loss with increasing concentration of K_2CO_3 (aq) immobilized in $SrTiO_3$.

5.5 Conclusion

Both $SrTiO_3$ and TiO_2 have successfully been used for immobilization of K_2CO_3 (aq). A conductivity loss occurs, compared to pure K_2CO_3 (aq), when K_2CO_3 (aq) is immobilized using either porous $SrTiO_3$ or TiO_2, however, by increasing the porosity of the matrix the conductivity can be increased and the loss decreased. Archie's law, with a cementation exponent of 1.6, was found to give a very good fit for ambient temperature measurements. Further studies are, however, necessary to determine if Archie's law is also applicable at elevated temperatures in this case.

The porosity of $SrTiO_3$ was found to be higher than the porosity of TiO_2 for pellets sintered at the same temperature. Furthermore, the average pore size was found to be smaller in $SrTiO_3$ compared to TiO_2.

The conductivity of K_2CO_3 (aq) immobilized in $SrTiO_3$ or TiO_2 increased with temperature and concentration unless precipitation occurred. The conductivity did not appear to depend on the type of matrix material in this study.The highest conductivity value measured in N_2 atmosphere was 0.21 S/cm at 130 °C for 30 wt% K_2CO_3 (aq) immobilized in $SrTiO_3$, the same value was also obtained for 10 wt% K_2CO_3 (aq) immobilized in $SrTiO_3$ at 175 °C. The highest conductivity measured using TiO_2 as the matrix material was 0.2 S/cm at 210 °C on 20 wt% K_2CO_3 (aq) immobilized in TiO_2. These conductivity values are well above the aim, mentioned in Section 1.1, of 0.1 S/cm at 200 °C for an immobilized K_2CO_3 (aq) electrolyte. This illustrates that the

concept of using immobilized aqueous electrolytes is promising, which was the aim of this project. The activation energy of K_2CO_3 (aq) immobilized in TiO_2 or $SrTiO_3$ was found to be in the range 0.13-0.15 eV and 0.11-0.22 eV, respectively. No clear concentration dependence could be found.

For tests and applications in CO_2 atmosphere, $SrTiO_3$ has to be Sr-deficient to avoid $SrCO_3$ formation, however, TiO_2 can be used without any problems. When measuring in CO_2 atmosphere the main species are K^+ and HCO_3^-. No loss of conductivity was observed for 10 wt% K_2CO_3 immobilized in TiO_2 when changing the atmosphere from N_2 to CO_2.

Chapter 6

Summary and Concluding Remarks

The purpose of this thesis has been to explore the potential of immobilized K_2CO_3 (aq) as a possible electrolyte for co-electrolysis of CO_2 and water at approx. 200 °C. This has been done by exploring the properties of pure K_2CO_3 (aq) and immobilized K_2CO_3 (aq) as well as the properties of the matrix materials $SrTiO_3$ and TiO_2.

The conductivity of 5-30 wt% K_2CO_3 (aq) at ambient temperature has been measured and found to fit well with literature values. The conductivity is very temperature sensitive as even an increase of a few degrees causes an increase in conductivity. Since the boiling point of water increases with increased pressure and salt concentration, it is possible to measure the conductivity of K_2CO_3 (aq) at elevated temperatures if the solution is pressurized. The conductivity is above 0.1 S/cm for all measured concentrations above 60 °C. The conductivity of K_2CO_3 (aq) can be measured up to approx. 150 °C without any problems. Above this temperature precipitation can occur for concentrations of 20 wt% K_2CO_3 (aq) or more, which causes a decrease in conductivity. Calculated phase diagrams confirm that precipitation should

be taking place. The activation energy was found to be in the range 0.14-0.17 eV and did not appear to be very concentration dependent.

For practical applications aqueous K_2CO_3 is difficult to handle but immobilization is a promising option for easier handling. It is important that the materials used for immobilization are not electronically conducting but porous, durable and easy to fabricate. Small pores are also preferable as it increases the capillary forces, thus binding the solution stronger in the matrix. Two different materials were used for immobilization of K_2CO_3 (aq): $SrTiO_3$ and TiO_2. Both matrix materials were found to fulfill the material requirements and immobilized K_2CO_3 (aq) solutions without any problems.

However, water management has been a key issue for immobilized K_2CO_3 (aq) at elevated temperature and pressure. Drying of samples at elevated temperatures and pressures was observed for K_2CO_3 (aq) immobilized in both $SrTiO_3$ and TiO_2. Calculations were made using FactSage[68] in order to help understand and solve the problem. The water partial pressure increases with temperature and it was found that the amount of steam at elevated temperatures could not be neglected and thus loss of water from the electrolyte needs to be avoided. A reservoir with a slightly lower K_2CO_3 (aq) concentration than the electrolyte was initially put in the bottom of the autoclave to prevent any drying of the samples. However, both the experimental results and the FactSage calculations showed that this was not preventing the problem. It was found that the water partial pressure only changed a little with K_2CO_3 (aq) concentration and the driving force for evaporating water from the reservoir instead of the sample was, therefore, not very strong. To decrease the water management issue the reservoir was changed to pure water and the volume of the autoclave was decreased using ceramic beads and by increasing the reservoir volume. Furthermore, the evaporation area (surface area) was increased by only partly covering the ceramic beads. Changing the reservoir to pure water should in theory result in flooding of the sample at equilibrium but this was not observed in any tests. However, this needs to be considered further e.g. while conducting long-term measurements. The measurements became more stable after the above mentioned setup changes. It could, how-

ever, be seen that the conductivity difference between the different concentrations appeared to decrease at elevated temperatures and when ramping down in temperature. A solution for longterm testing would be having a setup with a flow where an adjustable amount of steam can be added.

The microstructure of the $SrTiO_3$ and TiO_2 matrices were very different. The pore size was much smaller in $SrTiO_3$ than in TiO_2. At ambient conditions the conductivity only appeared to be dependent on the open porosity of the matrix. The conductivity could be fitted with Archie's law with a cementation exponent of 1.6. In order to optimize the matrix structure further, open porosities above 50% could be targeted and achieved using pore formers.

The conductivity of 5-30 wt% K_2CO_3 (aq) immobilized in $SrTiO_3$ was investigated as function of temperature and pressure. It was found that the conductivity increased with both concentration and temperature. However, above 90-120 °C the conductivity often became unstable due to the previously described water management issues (drying out). The conductivity was found to be above 0.1 S/cm for all measured concentrations at temperatures above 115 °C. The activation energy was found to be in the range 0.11-0.22 eV, which is similar to the activation energy found for pure K_2CO_3 (aq).

When conducting measurements on K_2CO_3 (aq) immobilized in $SrTiO_3$ in CO_2 atmosphere it was found that unwanted $SrCO_3$ formation occurred. $SrCO_3$ is an insulator and furthermore, the formation appeared to mainly take place at the surface of the electrodes of the cell/pellet, thereby blocking them. Even with the $SrCO_3$ formation it was possible to measure in CO_2 atmosphere, the conductivity just appeared to be limited. The $SrCO_3$ formation was caused by the $SrTiO_3$ having an unfortunate excess of SrO due to it not being completely stoichiometric. It was, however, found that using Sr-deficient $SrTiO_3$ would eliminate this problem. In this study, TiO_2 has been investigated as an alternative to $SrTiO_3$, as TiO_2 show no unwanted reactions in CO_2 atmosphere.

The conductivity of 5-20 wt% K_2CO_3 (aq) immobilized in TiO_2 was also mea-

sured. As with $SrTiO_3$, it was found that the conductivity increased with both concentration and temperature. The conductivity was found to be lower when using TiO_2 for immobilization compared to $SrTiO_3$, especially at elevated temperatures and higher K_2CO_3 (aq) concentrations. However, this difference is most likely attributed the differences in microstructure, and not caused by using different materials.The activation energy was found to be in range 0.13-0.15 eV, which is in the same range as the activation energy found for pure K_2CO_3 (aq) solution and K_2CO_3 (aq) immobilized in $SrTiO_3$, 0.14-0.17 eV and 0.11-0.22 eV, respectively. A TiO_2 pellet with 10 wt% K_2CO_3 (aq) was tested in both N_2 and CO_2. No significant conductivity difference was found between the two measurements. However, calculations by FactSage show that a change in aqueous species occurs when the atmosphere is changed from N_2 to CO_2, as CO_3^{2-} is to a large extend converted to HCO_3^-.

Several different electrode materials have been used for the conductivity measurements such as Pt, Ag, Cu and STN. No difference was found on the conductivity when comparing Pt and Ag+STN (10 wt%) electrodes. It was found that TiO_2 was the best matrix material for Ag electrodes as the chance of delamination was very little.

Overall, immobilized K_2CO_3 (aq) shows good promise as a potential electrolyte for co-electrolysis of CO_2 and water at 200 °C. A conductivity of above 0.1 S/cm at 200 °C can be achieved in N_2 atmosphere using both TiO_2 and $SrTiO_3$ for the immobilization if the concentration of K_2CO_3 (aq) is 5 wt% or more. TiO_2 can be used in CO_2 atmosphere and the conductivity of 10 wt% K_2CO_3 (aq) immobilized in TiO_2 appears to be the same in CO_2 atmosphere as in N_2 atmosphere. Further tests of especially electrodes and catalysts are necessary to make a full working cell.

Chapter 7

Future Work

The work presented in this thesis mainly focus on the electrolyte part of a future cell for co-electrolysis of CO_2 and water. However, initial studies on cell performance have also been performed on a symmetrical cell consisting of a TiO_2 pellet with 10 wt% immobilized K_2CO_3 (aq) and Ag electrodes, see Appendix E.

Several things can be done to continue the work presented in this thesis. Changing the setup so it has gas flow would be a great improvement. It would, however, also require that the gas is humidified, otherwise the cell would quickly dry out. Humidification can be done by passing the inlet gas through an aqueous solution (or water) or by having a catalytic burner that can produce steam. As the water partial pressure changes with temperature, pressure and K_2CO_3 (aq) concentration the added amount of steam must be varied. By having a setup with gas flow long-term testing should be possible as well as stability tests. It would also be possible to use higher concentrations of K_2CO_3 (aq) in CO_2 atmosphere since a gas flow would make it possible to start the test without CO_2 and only add it at elevated temperatures

where higher concentrations of K_2CO_3 (aq) can be used without precipitation occurring. A setup with gas flow would also make it possible to see how the gas composition affects the conductivity and cell performance. Furthermore, a gas flow would make it possible to detect products formed during operation of the cell. Only short tests of performance can be made in a closed setup for safety reason due to the risk of performing water splitting. This will lead to formation of H_2 and O_2 gas in an explosive mixture.

Fabricating matrices with a higher porosity should lead to significantly higher electrolyte conductivities according to the results presented in Section 5.3.2. The porosity can be increased by using for example pore formers.

In order to test full cells further development of the electrodes is necessary as well as finding suitable catalysts that will promote the desired reactions. Full cells (non-symmetrical) have to be fabricated to prove that co-electrolysis with immobilized K_2CO_3 (aq) as the electrolyte is possible. For testing full cells a two atmosphere setup would be desirable so the products formed on each side of the cell can be determined as well as the amount of gas that crosses over.

Testing other aqueous electrolytes could also be interesting and by choosing materials with different cat- and anions it should be possible to learn more about the conductivity contribution from the different ions. Furthermore, trying other matrix materials, such as Sr-deficient $SrTiO_3$, Al_2O_3 and e.g. polymers, would be of interest. This could increase the potential of immobilized electrolytes further as well as increase the amount of possible applications.

Bibliography

[1] Balat, M. *International Journal of Hydrogen Energy* **2008**, *33*, 4013–4029.

[2] REN21, *Renewables 2012, Global Status Report 2012*; 2012; Available: www.ren21.net.

[3] Apak, S.; Atay, E.; Tuncer, G. *International Journal of Hydrogen Energy* **2012**, *37*, 5481–5497.

[4] The Danish Government, *Energy Strategy 2050*; 2011.

[5] Ahmed, N. A.; Miyatake, M.; Al-Othman, A. *Energy Conversion and Management* **2008**, *49*, 2711–2719.

[6] Ursua, A.; Gandia, L. M.; Sanchis, P. *Proceedings of the IEEE* **2012**, *100*, 410–426.

[7] Singhal, S. *Solid State Ionics* **2000**, *135*, 305–313.

[8] Ebbesen, S. D.; Mogensen, M. *Journal of Power Sources* **2009**, *193*, 349–358.

[9] Graves, C.; Ebbesen, S. D.; Mogensen, M.; Lackner, K. S. *Renewable and Sustainable Energy Reviews* **2011**, *15*, 1–23.

[10] Grigoriev, S.; Porembsky, V.; Fateev, V. *International Journal of Hydrogen Energy* **2006**, *31*, 171–175.

[11] Marini, S.; Salvi, P.; Nelli, P.; Pesenti, R.; Villa, M.; Berrettoni, M.; Zangari, G.; Kiros, Y. *Electrochimica Acta* **2012**, *82*, 384–391.

[12] Haynes, W. M., Ed. *CRC Handbook of Chemistry and Physics*, 92nd ed.; CRC Press/Taylor and Francis: Boca Raton, FL.

[13] Bialik, M.; Sedin, P.; Theliander, H. *Industrial & Engineering Chemistry Research* **2008**, *47*, 1283–1287.

[14] Meranda, D.; Furter, W. F. *Journal of Chemical & Engineering Data* **1977**, *22*, 315–317.

[15] Kulkarni, A.; Giddey, S. *Journal of Solid State Electrochemistry* **2012**, *16*, 3123–3146.

[16] Krull, F.; Fritzmann, C.; Melin, T. *Journal of Membrane Science* **2008**, *325*, 509–519.

[17] Baltus, R. E.; Counce, R. M.; Culbertson, B. H.; Luo, H.; DePaoli, D. W.; Dai, S.; Duckworth, D. C. *Separation Science and Technology* **2005**, *40*, 525–541.

[18] Archie, G. E. *Transactions of the AIME* **1942**, *146*, 54–62.

[19] Ahmed, S.; Aitani, A.; Rahman, F.; Al-Dawood, A.; Al-Muhaish, F. *Applied Catalysis A: General* **2009**, *359*, 1–24.

[20] Denton, J.; Gascoyne, J. M.; Potter, R. J. Catalytically active gas diffusion electrodes comprising nonwoven fibrous structure. 1997; US 6010606.

[21] Holtappels, P.; Sorof, C.; Verbraeken, M. C.; Rambert, S.; Vogt, U. *Fuel Cells* **2006**, *6*, 113–116.

[22] Hori, Y. In *Modern Aspects of Electrochemistry*; Vayenas, C. G., White, R. E., Gamboa-Aldeco, M. E., Eds.; Modern Aspects of Electrochemistry 42; Springer New York: New York, NY, 2008; Chapter 3, pp 89–189.

[23] Hori, Y.; Kikuchi, K.; Suzuki, S. *Chemistry Letters* **1985**, 1695–1698.

[24] Olah, G. A.; Prakash, G. K. S. Recycling of Carbon Dioxide into Methyl Alcohol and Related Oxygenates or Hydrocarbons. 1998; WO 9850974A1.

[25] Gattrell, M.; Gupta, N.; Co, a. *Journal of Electroanalytical Chemistry* **2006**, *594*, 1–19.

[26] Centi, G.; Perathoner, S.; Winè, G.; Gangeri, M. *Green Chemistry* **2007**, *9*, 671.

[27] Sigma-Aldrich. http://www.sigmaaldrich.com.

[28] Allebrod, F.; Chatzichristodoulou, C.; Mollerup, P. L.; Mogensen, M. B. *International Journal of Hydrogen Energy* **2012**, *37*, 16505–16514.

[29] Tricoli, V.; Carretta, N.; Bartolozzi, M. *Journal of The Electrochemical Society* **2000**, *147*, 1286.

[30] Dimitrova, P.; Friedrich, K.; Stimming, U.; Vogt, B. *Solid State Ionics* **2002**, *150*, 115–122.

[31] Singhal, S.; Kendall, K. *High-temperature Solid Oxide Fuel Cells: Fundamentals, Design and Applications*; Elsevier Science, 2003; Chapter 4.

[32] Jacobson, A. J. *Chemistry of Materials* **2010**, *22*, 660–674.

[33] Minh, N. Q. *Journal of the American Ceramic Society* **1993**, *76*, 563–588.

[34] Misra, S. *AIP Conference Proceedings* **2012**, *1461*, 379–382.

[35] Maurice, J.-L.; Carrétéro, C.; Casanove, M.-J.; Bouzehouane, K.; Guyard, S.; Larquet, E.; Contour, J.-P. *physica status solidi (a)* **2006**, *203*, 2209–2214.

[36] Mohammed Hussain, A.; Høgh, J. V.; Jacobsen, T.; Bonanos, N. *International Journal of Hydrogen Energy* **2012**, *37*, 4309–4318.

[37] Blennow, P.; Hansen, K. K.; Wallenberg, L. R.; Mogensen, M. *Journal of the European Ceramic Society* **2007**, *27*, 3609–3612.

[38] Inframat Advanced Materials, USA. 2010; http://www.advancedmaterials.us/3822-ON1.htm.

[39] Blennow, P.; Hagen, A.; Hansen, K. K.; Wallenberg, L. R.; Mogensen, M. *Solid State Ionics* **2008**, *179*, 2047–2058.

[40] Lowell, S.; Shields, J. E.; Thomas, M. A.; Thommes, M. *Characterization of Porous Solids and Powders: Surface Area, Pore Size and Density*, 4th ed.; Springer New York, 2004.

[41] Gurovich, B. M.; Frolova, T. V.; Mezheritskii, S. M. *Zhurnal Prikladnoi Khimii* **1983**, *56*, 2612–2614.

[42] Bandi, A.; Specht, M.; Weimer, T.; Schaber, K. *Energy Conversion and Management* **1995**, *36*, 899–902.

[43] Hori, Y.; Wakebe, H.; Tsukamoto, T.; Koga, O. *Electrochimica Acta* **1994**, *39*, 1833–1839.

[44] Chaplin, R.; Wragg, A. *Journal of Applied Electrochemistry* **2003**, *33*, 1107–1123.

[45] Cook, R. L. *Journal of The Electrochemical Society* **1990**, *137*, 607.

[46] Mahmood, M. N.; Masheder, D.; Harty, C. J. *Journal of Applied Electrochemistry* **1987**, *17*, 1159–1170.

[47] Mahmood, M. N.; Masheder, D.; Harty, C. J. *Journal of Applied Electrochemistry* **1987**, *17*, 1223–1227.

[48] Savinova, E. R.; Yashnik, S. A.; Savinov, E. N.; Parmon, V. N. *Reaction Kinetics & Catalysis Letters* **1992**, *46*, 249–254.

[49] Hara, K. *Journal of The Electrochemical Society* **1994**, *141*, 2097.

[50] Hara, K.; Kudo, A.; Sakata, T. *Journal of Electroanalytical Chemistry* **1995**, *391*, 141–147.

[51] Smart, L. E.; Moore, E. A. *Solid State Chemistry: An Introduction*, 3rd ed.; CRC Press, 2005.

[52] West, A. R. *Basic Solid State Chemistry*, 2nd ed.; Wiley, 1999.

[53] Goodhew, P. J.; Humphreys, J.; Beanland, R. *Electron Microscopy and Analysis*, 3rd ed.; Taylor & Francis Ltd, 2001.

[54] Ackermann, J. *Manual for the SUPRA (VP) and ULTRA Scanning Electron Microscopes*; 2005.

[55] Pashley, R.; Karaman, M. *Applied Colloid and Surface Chemistry*; John Wiley & Sons, 2004.

[56] Marmur, A. *Langmuir* **2003**, *19*, 8343–8348.

[57] Pement, F. W.; Wilson, I. L. W.; Aspden, R. G. *Materials Performance* **1980**, *19*, 43–49.

[58] Takemura, K.; Shibazaki, T.; Hashimoto, H.; Ushiku, M.; Kudo, H. Metallic material suitable for containers exposed to CO, CO2, H2, and steam. 1997.

[59] Craig, B. D., Anderson, D. S., Eds. *Handbook of Corrosion Data*, 2nd ed.; ASM International, 1995.

[60] Apelblat, A. *The Journal of Chemical Thermodynamics* **1992**, *24*, 619–626.

[61] Balej, J. *International Journal of Hydrogen Energy* **1985**, *10*, 233–243.

[62] Landviser. http://www.landviser.net/content/four-electrode-probe.

[63] van der Pauw, L. J. *Philips Res. Repts.* **1958**, *13*, 1–9.

[64] Moron, Z. *Measurement* **2003**, *33*, 281–290.

[65] Bonanos, N. *Journal of Physics and Chemistry of Solids* **1993**, *54*, 867–870.

[66] Orazem, M. E.; Tribollet, B. *Electrochemical Impedance Spectroscopy*; John Wiley & Sons, 2008.

[67] Gamry Potentiostats. http://www.gamry.com/products/potentiostats/.

[68] FactSage version 5.5. 2010.

[69] Bruggemam, D. A. G. *Annalen der Physik* **1935**, *24*, 636–679.

[70] Landauer, R. Electrical conductivity in inhomogeneous media. 1978; http://link.aip.org/link/APCPCS/v40/i1/p2/s1&Agg=doi.

[71] Washburn, E. W., Ed. *International Critical Tables of Numerical Data, Physics, Chemistry and Technology (1st Electronic Edition)*; Knovel, 2003; Chapter VI, pp 229–256.

[72] Barsoukov, E., Macdonald, J. R., Eds. *Impedance Spectroscopy: Theory, Experiment, and Applications*, 2nd ed.; John Wiley & Sons: Hoboken, NJ, 2005; p 243.

[73] Corey, V. *Physical Review* **1943**, *64*, 350–357.

[74] Melinder, A. k. Thermophysical Properties of Aqueous Solutions Used as Secondary Working Fluids. Doctoral Thesis, KTH, 2007.

[75] Vlaev, L. T.; Genieva, S. D.; Tavlieva, M. P. *Journal of Structural Chemistry* **2003**, *44*, 995–1000.

[76] Minh, N. Q.; Takahashi, T. *Science and Technology of Ceramic Fuel Cells*; Elsevier, 1995.

[77] Azad, S.; Engelhard, M. H.; Wang, L.-Q. *The journal of physical chemistry. B* **2005**, *109*, 10327–31.

[78] Voigts, F.; Argirusis, C.; Maus-Friedrichs, W. *Surface and Interface Analysis* **2012**, *44*, 301–307.

[79] Tammeveski, L.; Erikson, H.; Sarapuu, A.; Kozlova, J.; Ritslaid, P.; Sammelselg, V.; Tammeveski, K. *Electrochemistry Communications* **2012**, *20*, 15–18.

[80] Miyauchi, M.; Nakajima, A.; Fujishima, A.; Hashimoto, K.; Watanabe, T. *Chemistry of Materials* **2000**, *12*, 3–5.

[81] Lee, C.-S.; Kim, J.; Son, J. Y.; Maeng, W. J.; Jo, D.-H.; Choi, W.; Kim, H. *Journal of The Electrochemical Society* **2009**, *156*, D188.

[82] Toyoda, T.; Yabe, M. *Journal of Physics D: Applied Physics* **1983**, *16*, L251–L255.

[83] Diebold, U. *Applied Physics A: Materials Science & Processing* **2003**, *76*, 681–687.

[84] Heifets, E.; Piskunov, S.; Kotomin, E.; Zhukovskii, Y.; Ellis, D. *Physical Review B* **2007**, *75*, 115417.

[85] Schufle, J.; Yu, N.-T. *Journal of Colloid and Interface Science* **1968**, *26*, 395–406.

[86] Pashley, R. M.; Rzechowicz, M.; Pashley, L. R.; Francis, M. J. *The journal of physical chemistry. B* **2005**, *109*, 1231–8.

[87] Stroemich, C.; Sumbar, E.; Vermeulen, F.; Chute, F. *IEEE Transactions on Geoscience and Remote Sensing* **1992**, *30*, 911–917.

Appendices

Appendix A

Phase Diagrams

A.1 CO_2 Phase Diagrams

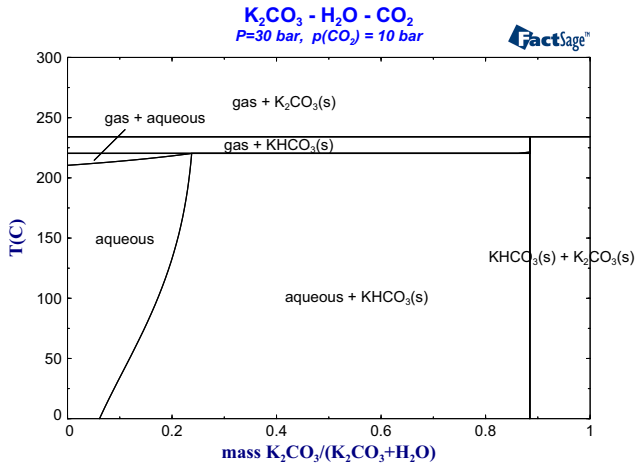

Figure A.1: Calculated phase diagram for K_2CO_3 and H_2O at 0-300 °C at a total pressure of 30 bar with 10 bar of CO_2. The phase diagram has been calculated using FactSage.[68]

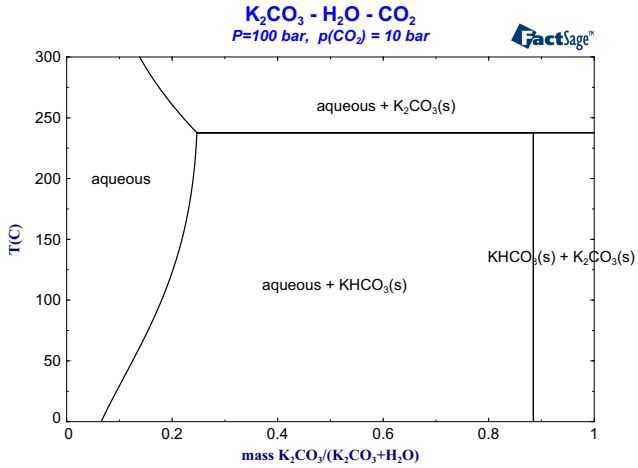

Figure A.2: Calculated phase diagram for K_2CO_3 and H_2O at 0-300 °C at a total pressure of 100 bar with 10 bar of CO_2. The phase diagram has been calculated using FactSage.[68]

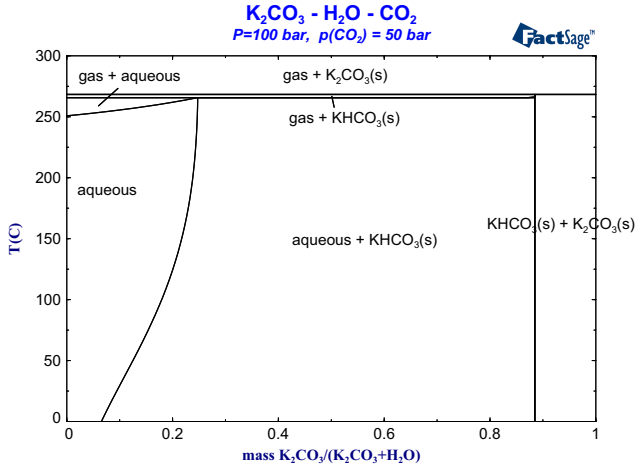

Figure A.3: Calculated phase diagram for K_2CO_3 and H_2O at 0-300 °C at a total pressure of 100 bar with 50 bar of CO_2. The phase diagram has been calculated using FactSage.[68]

Appendix B

XRPD Diffractograms after Calcinations

B.1 $SrTiO_3$ from GNP

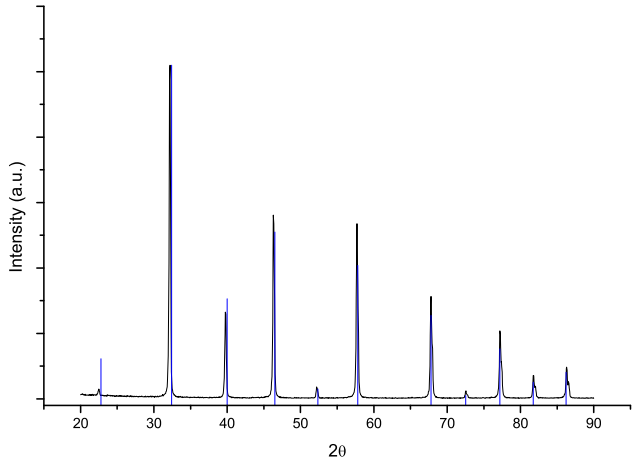

Figure B.1: XRPD diffractogram of $SrTiO_3$ made with the GNP calcined at 350 °C. The blue lines indicate $SrTiO_3$ peaks.

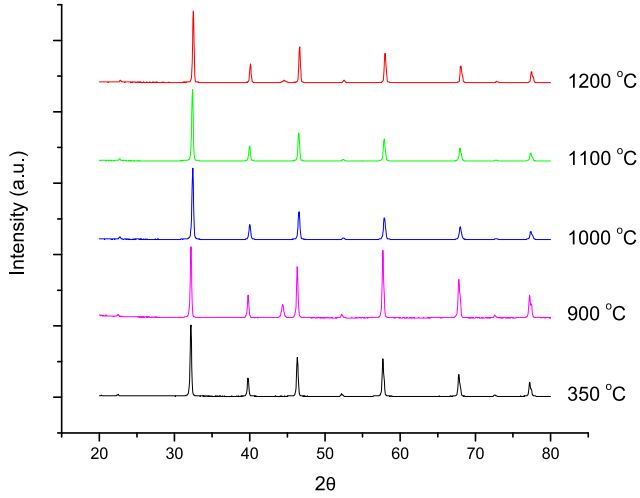

Figure B.2: XRPD diffractograms of $SrTiO_3$ made with the GNP calcined at 350–1200 °C. The extra peak at 44° (2θ) at 900 and 1200 °C is due to diffraction from the sample holder.

Appendix C

XRPD after Test in CO_2

C.1 Sr-deficient $SrTiO_3$

C.2 $Sr_{0.94}Ti_{0.9}Nb_{0.1}O_3$

C.3 $SrTiO_3$ Not Soaked in K_2CO_3 (aq)

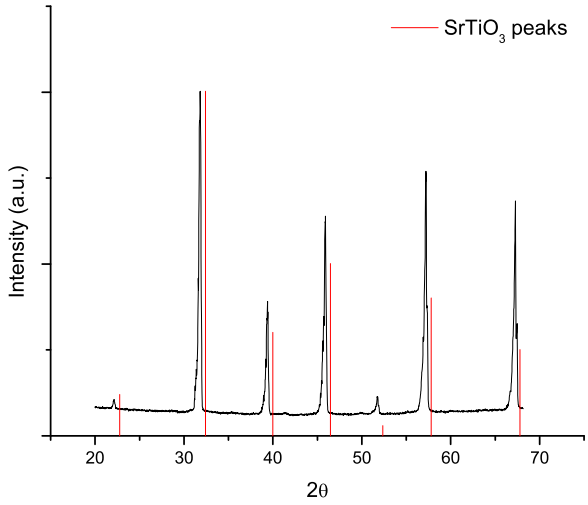

Figure C.1: XRPD diffractogram of $Sr_{0.95}TiO_3$ after test in CO_2. The sample was rinsed several times with water to remove the K_2CO_3 (aq) before the XRPD measurement. The peaks for $SrTiO_3$ are shown. The peaks are slightly shifted due to the sample not being properly aligned during the measurement.

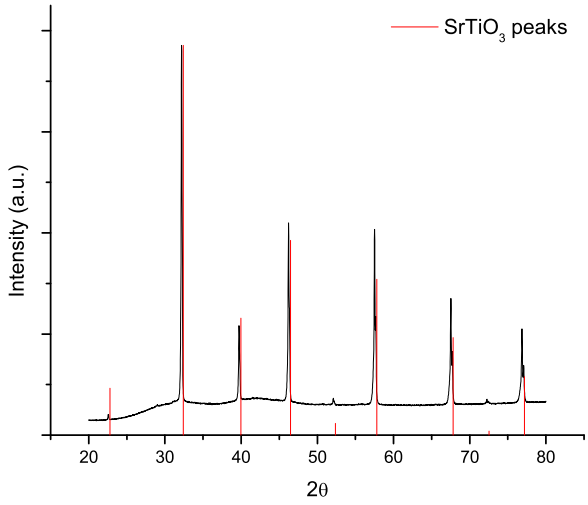

Figure C.2: XRPD diffractogram of $Sr_{0.95}TiO_3$ after test in CO_2. The sample was rinsed several times with water to remove the K_2CO_3 (aq) before the XRPD measurement. The peaks for $SrTiO_3$ are shown.

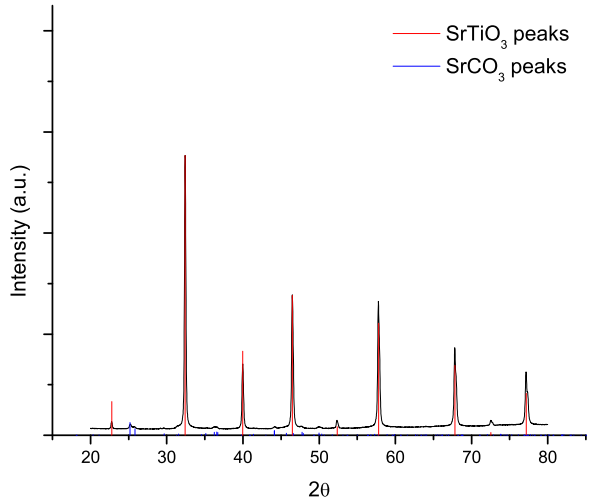

Figure C.3: XRPD diffractogram of $SrTiO_3$ after test in CO_2, the sample was not soaked in K_2CO_3(aq) before the test. The sample was rinsed several times with water to remove the K_2CO_3 (aq) before the XRPD measurement. The peaks for $SrTiO_3$ and $SrCO_3$ are shown.

Appendix D

Additional Conductivity Results

D.1 Conductivity of 5-20 wt% K_2CO_3 (aq) immobilized in TiO_2

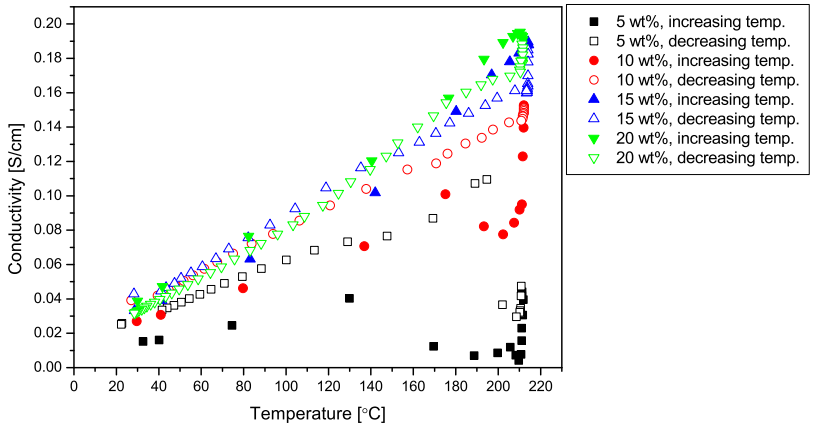

Figure D.1: Conductivity of 5-20 wt% K_2CO_3 (aq) immobilized in TiO_2 from ambient temperature to approx. 215 °C. Data for both increasing and decreasing temperature is shown. All measurements were performed on the same pellet. All measurements were performed with an initial pressure of 30 bar and the pressure was allowed to increase with temperature.

Appendix E

Initial Studies of Cell Performance

A symmetrical cell consisting of a TiO_2 pellet with 10 wt% immobilized K_2CO_3 (aq) and Ag electrodes has been tested in both N_2 atmosphere and in synthetic air (21% O_2, 79% N_2). Figure E.1 and E.2 show how the polarized impendance measurement change with the atmosphere. In N_2 atmosphere it is impossible to tell the electrode resistance as the nyquist curve never bends down within the measured frequency range. In synthetic air the electrode resistance appears to be around 10-12 $\Omega \cdot cm^2$. It can also be seen that the measurement in synthetic air is not stable as the nyquist curve makes a sharp bend at low frequencies. Figure E.3 and E.4 show how the impedance spectra of the cell is affected by the polarization. The measurements before and after polarization show that it is necessary to apply a current to get the reaction to run.

Figure E.5 shows cyclic voltammograms (CV) measured during the tests. The measurement in N_2 atmosphere was made at 191 °C and the measurement in synthetic air was made at 204 °C. In both cases 3 cycles were made. It can clearly be seen that the cell behavies different in the two different atmo-

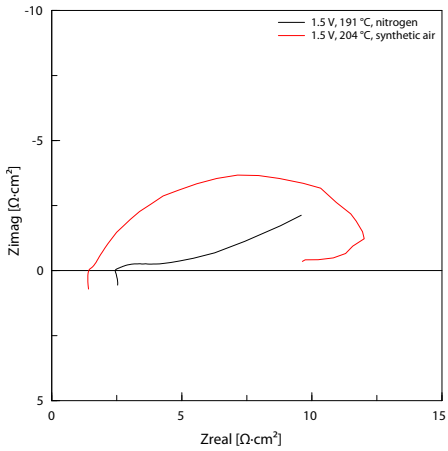

Figure E.1: Nyquist plot of polarized impedance measurement obtained in N_2 atmosphere and in synthetic air. The applied cell potential was 1.5 V. The same cell has been used for the two test. The impedance spectra have been obtained at 191 °C in N_2 atmoshpere and at 204 °C in synthetic air.

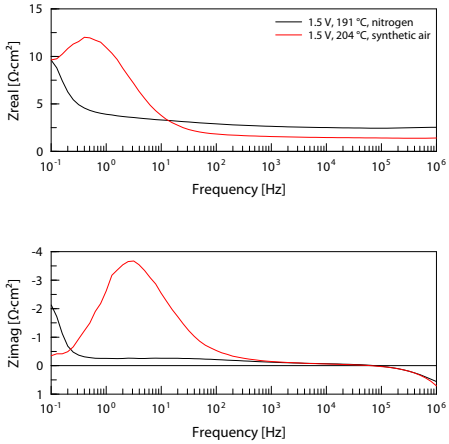

Figure E.2: Bode plot of polarized impedance measurement obtained in N_2 atmosphere and in synthetic air. The applied cell potential was 1.5 V. The same cell has been used for the two test. The impedance spectra have been obtained at 191 °C in N_2 atmoshpere and at 204 °C in synthetic air.

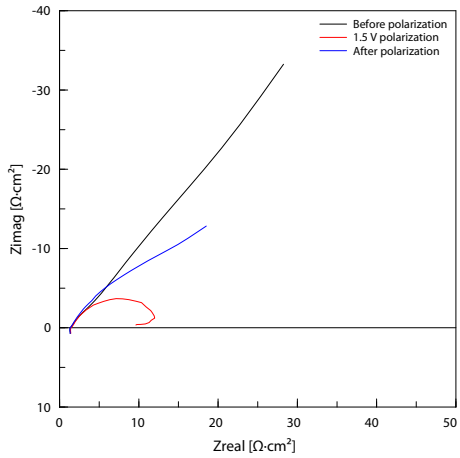

Figure E.3: Nyquist plot of impedance measurement before, during and after polarization. The applied cell potential was 1.5 V. The measurements were performed at 204 °C in synthetic air.

spheres. The performance in synthetic air is much better and peaks at 180 mA/cm^2 at 1.5 V.

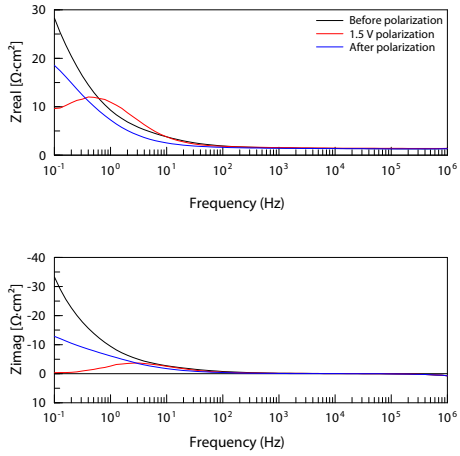

Figure E.4: Bode plot of impedance measurement before, during and after polarization. The applied cell potential was 1.5 V. The measurements were performed at 204 °C in synthetic air.

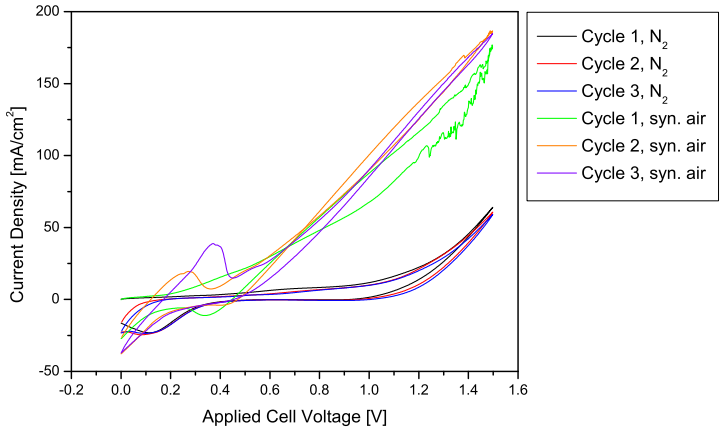

Figure E.5: Cyclic voltammogram (CV) obtained during measurements on a symmetrical cell consisting of a TiO_2 pellet with 10 wt% immobilized K_2CO_3 (aq) and Ag electrodes. Measurements were performed in both N_2 atmosphere and synthetic air. Three cycles were made in each atmosphere; they were measured at 191 °C in N_2 atmosphere and 204 °C in synthetic air. The sweep rate was 50 mV/s and the step size 2 mV.